ERDC TR-24-4

U.S. ARMY

US Army Corps of Engineers®

ERDC

US Army Futures Command and the Assistant Secretary for the Army Acquisition, Logistics, and Technology Basic and Applied Research Programs

A Comprehensive Approach to Data Collection, Management, and Visualization for Terrain Characterization in Cold Regions

W. Brad Baxter, Amanda J. Barker, Samuel A. Beal, Lauren V. Bosche, Ryan R. Busby, Zoe R. Courville, Eli J. Deeb, Stacey J. Doherty, Thomas A. Douglas, Arthur B. Gelvin, Robert M. Jones, Taylor D. Sullivan, Dragos A. Vas, and Robyn A. Barbato

February 2024

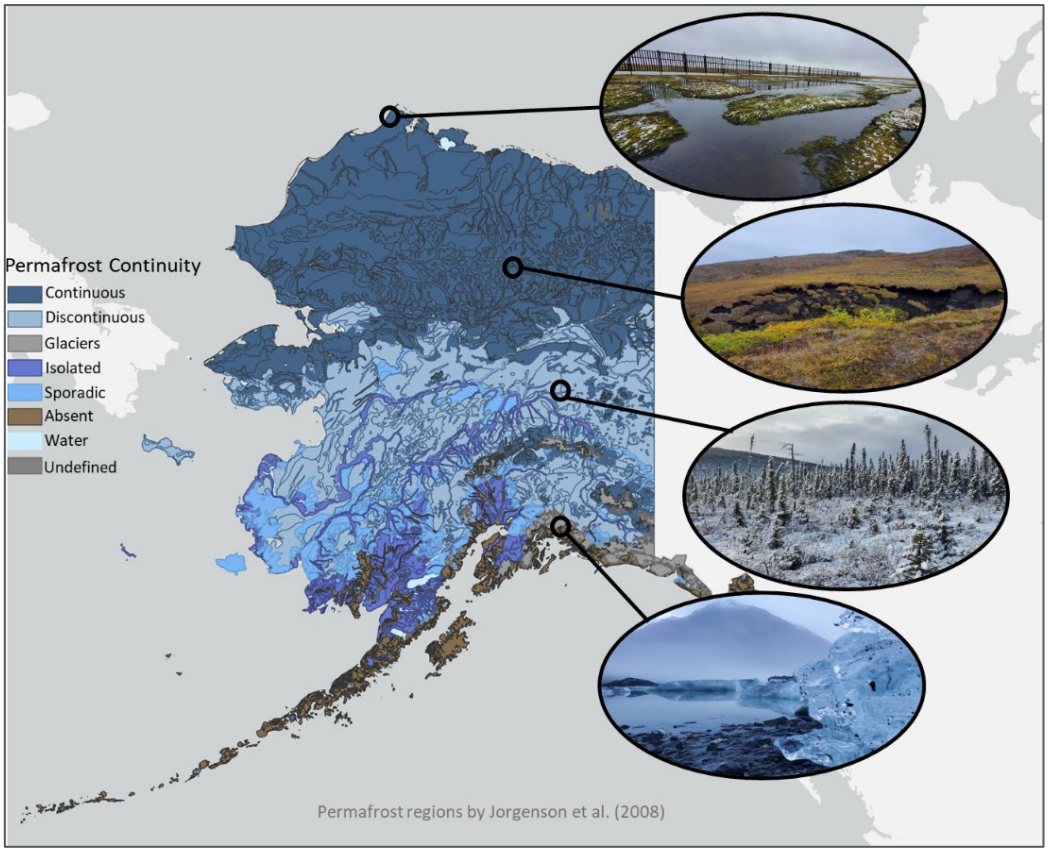

Engineer Research and Development Center

The US Army Engineer Research and Development Center (ERDC) solves the nation's toughest engineering and environmental challenges. ERDC develops innovative solutions in civil and military engineering, geospatial sciences, water resources, and environmental sciences for the Army, the Department of Defense, civilian agencies, and our nation's public good. Find out more at www.erdc.usace.army.mil.

To search for other technical reports published by ERDC, visit the ERDC online library at https://erdclibrary.on.worldcat.org/discovery.

US Army Futures Command and the
Assistant Secretary for the Army Acquisition,
Logistics, and Technology Basic and Applied
Research Programs

ERDC TR-24-4
February 2024

A Comprehensive Approach to Data Collection, Management, and Visualization for Terrain Characterization in Cold Regions

W. Brad Baxter, Amanda J. Barker, Samuel A. Beal, Lauren V. Bosche, Zoe R. Courville, Eli J. Deeb, Stacey J. Doherty, Thomas A. Douglas, Arthur B. Gelvin, Robert M. Jones, Taylor D. Sullivan, Dragos A. Vas, and Robyn A. Barbato

US Army Engineer Research and Development Center (ERDC)
Cold Regions Research and Engineering Laboratory (CRREL)
72 Lyme Road
Hanover, NH 03755-1290

Ryan R. Busby

US Army Engineer Research and Development Center (ERDC)
Construction Engineering Research Laboratory (CERL)
2902 Newmark Drive
Champaign, IL 61824

Final Report

Prepared for US Army Futures Command
The Assistant Secretary for the Army Acquisition, Logistics, and Technology
Basic and Applied Research Programs
Vicksburg, MS 39180

Under MIPR 0642384626

Abstract

As global focus shifts to northern latitudes for their enhanced access to newly viable resources, US Army operational readiness in these extreme environments is increasingly important. Rapid and accurate intelligence on the conditions influencing operations in these regions is essential to mission success and warfighter safety. Arctic and boreal environments are highly heterogeneous, including changing extents of frozen versus thawing ground, snow, and ice that affect ground trafficability and visibility, terrain physics, and physicochemical properties of water and soil. Furthermore, projected climatic warming in these regions makes the timing of seasonal transitions increasingly uncertain. Broad coverage of long-term datasets is critical for assessing spatial and temporal variability in these northern environments at the landscape-scale. However, decadal measurements are difficult to acquire, manage, and visualize in the field setting. Here, we present a synopsis of data collection, management, and visualization for long-term permafrost, snow, vegetation, geophysics, and biogeochemical data from Alaska and review related literature. We also synthesize short-term data from various permafrost affected sites in the US and northern Europe to further assess the state of northern landscapes. Altogether, this work provides a comprehensive approach for high-latitude field site management to accurately inform mission-related operations in extreme northern environments.

Contents

Figures and Tables

Figures

Tables

Preface

This study was conducted for US Army Futures Command, the Assistant Secretary for the Army Acquisition, Logistics, and Technology Basic and Applied Research Programs, under MIPR 0642384626. The technical monitor was Dr. Elizabeth Ferguson, Environmental Laboratory.

The work was performed by the Biogeochemical Sciences Branch, Engineering Resources Branch, the Terrestrial and Cryospheric Sciences Branch, the Signature Physics Branch, and the Lidar and Wetlands Group of the Remote Sensing/GIS Center of Expertise US Army Engineer Research and Development Center–Cold Regions Research and Engineering Laboratory (ERDC-CRREL). At the time of publication, Mr. Nathan J. Lamie, Dr. Melisa Nallar, Dr. John. W. Weatherly, and Mr. Paul M. Kutia were branch chiefs, respectively, and Dr. Elias J. Deeb was group leader; and Dr. Orian Z. Welling was division chief. The acting deputy director of ERDC-CRREL was Ms. Kelly M. Swiderski and the acting director was Dr. Ivan P. Beckman. The work was also performed by the Training Lands and Heritage Branch, ERDC-Construction Engineering Research Laboratory (CERL). At the time of publication, Ms. Angela Rhodes was branch chief; and Dr. George Calfas was division chief. The deputy director of ERDC-CERL was Ms. Michelle Hanson and the director was Dr. Andy Nelson.

We acknowledge numerous organizations that provided supplemental data to the effort, including the National Science Foundation Long Term Ecological Research Network, the Circumpolar Active Layer Monitoring Network, the Toolik Field Station Environmental Data Center, the Finnish Meteorological Institute, the Swedish Polar Research Secretariat and Abisko Scientific Research Station, the Bureau of Land Management, and the Natural Resources Conservation Service.

COL Christian Patterson was commander of ERDC, and Dr. David W. Pittman was the director.

This page intentionally left blank.

1 Introduction

The amplified impacts of climate change on northern latitudes are attracting global interest to these regions for their enhanced access and newly viable resources, making US Army operational readiness in these environments increasingly important. In response, the Army issued its strategy "Regaining Arctic Dominance" in 2021 recognizing the importance of terrain analysis in cold regions. Due to the complexity of northern landscapes and the dynamic nature of Arctic and boreal ecosystems, comprehensive terrain analysis at the landscape scale is necessary to sufficiently assess the regional conditions that influence large-scale force maneuverability and function. A spatially contiguous network of long-term datasets is needed to recognize the physiographic and climatic variability experienced at various spatial and temporal scales across northern cold regions. These landscape-scale, long-term datasets provide integral information for accurately informing operations planning and execution by providing the data necessary for illustrating trends and isolating controls that inform modeling projections. However, collecting and maintaining large datasets poses a series of inherent challenges and can prove especially complicated in extreme northern environments.

This report synthesizes numerous methods for characterizing northern terrain conditions and reviews related literature to serve as a general framework for the collection and management of vital datasets for investigating cold regions. We present a collection of measurements spanning various Arctic and boreal environments in Alaska, Finland, and Sweden. These datasets include decades of sampling and collection efforts from numerous research groups and integrate approximately 700,000 individual observations and measurements on cryospheric and biogeochemical features that influence terrain conditions and their spatial and temporal change. The primary datasets incorporate thaw depths, seasonally thawed active layer thickness measurements, soil temperatures, ground-penetrating radar surveys, microbial community analyses, geochemical analyses, snowpack depths, localized meteorological data, and repeat ground-based light detection and ranging (lidar) scans. The compilation of long-term datasets from the respective study locations addresses numerous physical and biogeochemical phenomena, including heterogeneity in permafrost, ground ice, and snow conditions across space and time, chemical and biological characterization of terrain states, and landscape-scale change

over multiyear study periods. The methodology, analyses, and data reported here can serve as a basis for future analysis of terrain controls to inform models and projections in high-latitude cold regions.

1.1 Background

1.1.1 Data Collection for Cold Region Terrain Characterization

Surface conditions in northern landscapes are significantly influenced by underlying permafrost characteristics, ice, biology, and snow. Soil moisture content, structural stability, and surface elevation change may vary markedly by permafrost ice content and top-down thaw extent, each of which may independently vary on an annual and seasonal basis. During fall freeze up and spring melt, the surface conditions of snow, ice, or frozen versus unfrozen soil can change in a matter of hours to days. These variations can lead to surface irregularity caused by the presence of wetlands, thaw subsidence, thermokarst lakes, thaw slumps, frost heaves, hummocky terrain, and other permafrost degradational features. Additionally, seasonal freeze and thaw cycles can result in significant frost heave and surface change. Much of this irregularity relates to ground ice content, ecotype, and soil hydrological processes that are confined within the seasonally thawed active layer. Active layer dimensions can therefore highly influence surface conditions and alter microtopography, making the active layer a critical parameter for evaluation in terrain analysis (Shur et al. 2005; Bockheim and Hinkel 2005).

In addition to influencing terrain conditions and trafficability, thawed permafrost zones serve as biogeochemical hotspots amidst the otherwise frozen matrix of permafrost soils, and are important regions for organic carbon cycling, greenhouse gas production, and mineral weathering and transport (Barker et al. 2014; Doherty et al. 2020; Barbato et al. 2022; Barker et al. 2023 in press; Baker et al. 2023). Newly thawed soils expose labile carbon to microbial activity, resulting in the oxidation of soil organic carbon (SOC), a major factor in the global carbon budget (Douglas et al. 2014; Ping et al. 2015). Permafrost soils are thought to contain double the amount of carbon that is currently in the Earth's atmosphere (Schuur et al. 2015), making the fate of this carbon upon thaw an important subject of study. A large volume of SOC is stored at depth in the permafrost of Alaska's North Slope (Figure 1) (Hugelius et al. 2013; 2014) and as it thaws, deeper SOC stores are subjected to microbial decomposition and subsequent greenhouse gas emissions (i.e., carbon dioxide and methane)

(Ernakovich et al. 2022). Repeat measurements of permafrost thaw extent and active layer conditions are therefore of high importance both for evaluating northern terrain trafficability and suitability, and also understanding the setting for permafrost carbon feedback.

Figure 1. Map of soil organic carbon (kg/m²) at (*a*) 30 cm and (*b*) 100 cm depth in the soil profile for Alaska. (Map adapted from dataset by Hugelius et al. 2013, https://doi.org/10.5194/essd-5-393-2013. Creative Commons 4.0.)

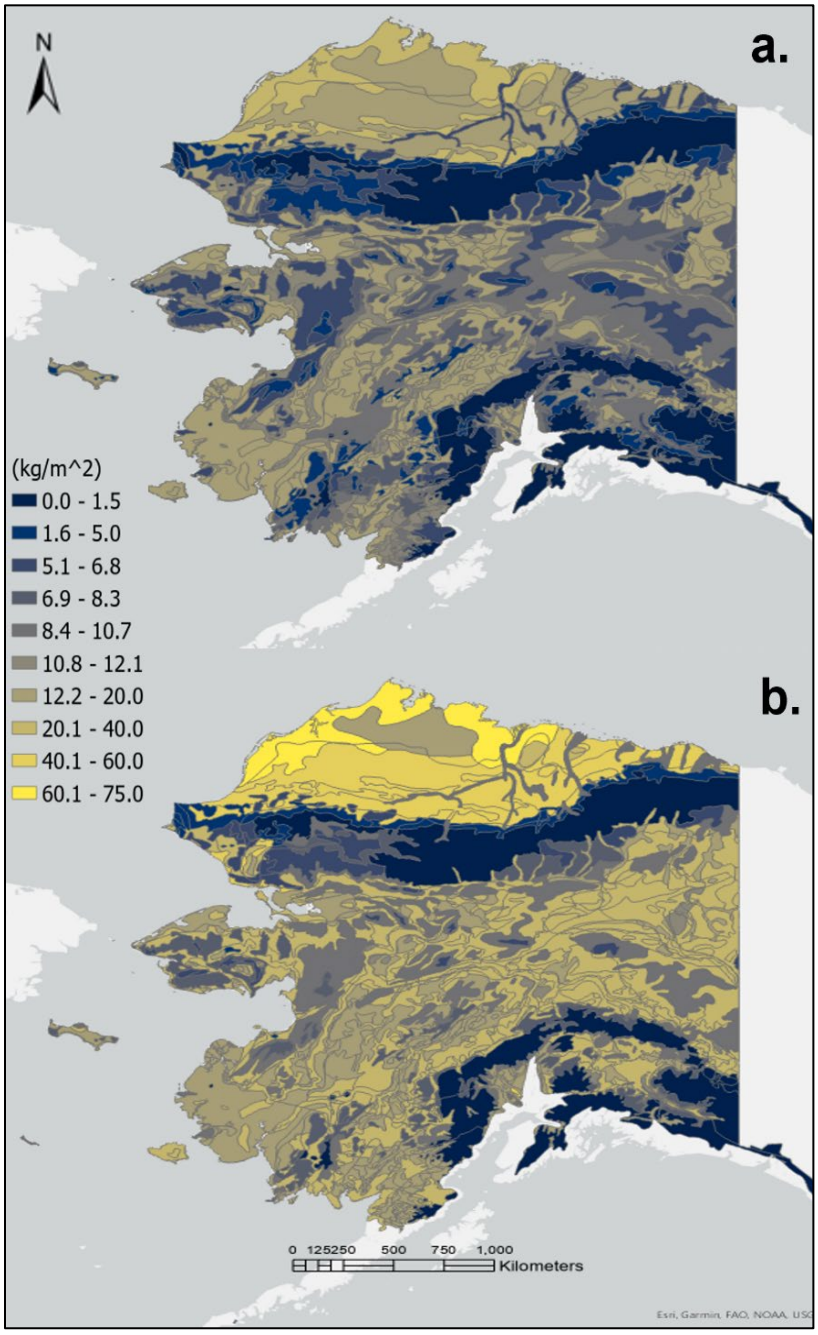

A common metric for monitoring the status and change of seasonal thaw extent is repeat evaluation of the active layer thickness (ALT) across space and time. ALT is commonly measured by manually probing thaw depths in late fall when thaw has reached a near maximum extent. These probe-derived depths can compare with geophysical surveys of ALT to expand the spatial coverage of ALT data. Additionally, since ALT is related to soil type and surface vegetation, ALT measured in situ may be upscaled based on notable landscape controls such as the biophysical settings, providing for large-scale characterization of ALT (Zhang et al. 2021). Repeat measurements of ALT through time illustrate change and can inform terrain models that rely on active layer controls on various surface parameters. More recently, various remote detection methods have emerged for assessing ALT (i.e., Schaefer et al. 2015; Parsekian et al. 2021) but are beyond the current scope of this report.

While ALT is integral for assessing the state of near-surface permafrost, conditions within the active layer such as soil temperature and moisture content also influence chemical reaction rates and microbial activity, making these parameters important considerations in evaluating biogeochemical processes (Barbato et al. 2015). Soil temperature and moisture content are readily measured with various in situ instrumentation techniques including buried temperature sensors and conductivity probes. In addition, soil sampling from active layer materials allows for chemical and microbial analysis, which can each be indicative of various soil thermal and chemical conditions and processes.

Soil composition and thermal state are also related to vegetation structure on the landscape. Vegetation surveys are critical for proper terrain assessment as root structure can directly influence the engineering properties of the soil matrix including particle cohesion, slope shear strength and stability, and compressibility (Waldron 1977; Tosi 2007). Additionally, vegetation composition defines ecotypes which can be indicative of underlying soil and snow conditions and their changes over time, and vegetation itself can create serious challenges in surface maneuverability. Vegetation surveys for root strength are key in assessing plant influence on soil strength and are performed at the point scale by generating random survey locations in the sites of interest. Root strength samples are then taken from a fixed plot at each location of interest. Species types are determined, and soil strength is quantified from representative root samples within each survey plot. Larger scale surveys

of vegetation cover often rely on multispectral remote sensing techniques and image classification to map land cover types. These results can then compare with other landscape parameters such as ALT or snow depth to extrapolate these variables to greater spatial scales by their relationship to observable vegetation cover (Zhang et al. 2021).

The final landscape parameter reviewed in this report is snowpack. Snow accumulation and snowpack thickness may directly inhibit surface transport during winter months, but also relates to surface moisture conditions during the successive melt season and can influence underlying soil thermal properties. Therefore, snowpack conditions are important considerations for all-season operations. Additionally, snow depths and snow densities may be used in forecasting water supply and projecting water resource availability following the melt season. Snow depths and density are commonly monitored with permanent or semipermanent meteorological stations and repeat field-based measurements. Upscaling of in situ snow depth measurements may also be performed based on present biophysical controls (Douglas and Zhang 2021). The detection of snow depths and water equivalents with remote sensing techniques is also increasingly employed but is improved by calibration with ground-based measurements.

1.1.2 Data Management

Data from various retrieval platforms and collaborative efforts assume multiple file types and require various management systems with ample storage capacity. External drives are useful for physically backing large quantities of data and provide a means for file compilation and organization. In consequence of multiple data sources, inconsistencies in data presentation and descriptions are common amidst compiled datasets. These inconsistencies are readily resolved by establishing data standards that apply for all files in a dataset, such as parameters and identifiers that must be included for each measurement and applying these standards to secondary data files. The raw and edited files can then be stored and shared in cloud-based networks such as a network shared drive for real-time updates and sharing across collaborators.

1.1.3 Data Visualization in Geographic Information Systems (GIS)

Geospatial representation of environmental data is key in identifying spatial relationships and trends across regions. Geographic information systems (GIS) are commonly used to display spatial datasets as map

layers, known as feature classes, that contain discrete elements with attribute information. Map feature classes are often stored as shapefiles that associate objects (data points) with coordinates and stores their information in attribute tables. These shapefiles can be edited, shared, and accessed from multiple GIS platforms.

Various developers provide GIS software and services with capabilities that have evolved to grant users many tools and options for creating, editing, and sharing spatial data. Common GIS software include QGIS® and Esri ArcGIS® products, each offering a multitude of mapping and data visualization capabilities. QGIS is an open-source GIS platform that supports various spatial data functionalities and formats. The Esri ArcGIS (2022) suite includes desktop mapping applications, an online platform for mapping and managing feature classes across multiple devices and users, and various mobile apps that allow users to access and edit spatial data from mobile devices while on or offline. This offline functionality allows for field-based mapping that couples digital object descriptions with GPS location, making spatial data convenient for sharing and eliminating the need to digitize field notes and GPS coordinates. Given its various capabilities, GIS have become instrumental for visualizing and managing spatial datasets in environmental studies.

1.1.4 Site Physiography and History

1.1.4.1 Interior Alaska

This study includes measurements from four long-term research sites in Interior Alaska (Table 1, Figure 2, and Figure 3) including the ERDC-Cold Regions Research and Engineering Laboratory (CRREL) Permafrost Tunnel Research Facility, ERDC-CRREL Farmer's Loop Permafrost Experimental Station, the State of Alaska Department of Natural Resources Creamer's Field Migratory Waterfowl Refuge, and the US National Science Foundation's Long Term Ecological Research (LTER) Alaska Peatland Experiment (APEX) research site (each are detailed below).

Alaska's interior is framed by the Alaska Range to the south, the Mackenzie Mountains to the east, and the Brooks Range to the north, which serve as orographic barriers to coastal moisture sources and contribute to a continental interior climate. The subarctic latitude of the region leads to low sun angles during winter months with day lengths near Fairbanks, Alaska, reaching below 4 hours on the December solstice, and

near constant sunlight during the summer months reaching near 22 hours of daylight on the June solstice (Hinzman et al. 2006). The mean annual temperature is −2.4°C and mean annual precipitation is 330 mm (Jorgenson et al. 2020), with snowfall accounting for 40%–45% of annual precipitation (Liston and Hiemstra 2011).* The region is underlain by discontinuous permafrost (Figure 2), with permafrost soils primarily confined to north-aspect slopes, lowlands, and localized areas where snowpack or insulative vegetation support ice. The permafrost of the interior study sites is generally syngenetic, organic carbon rich Yedoma with high ice content and silty texture owing to a largely loess (eolian silt) parent (Péwé 1975; Hamilton et al. 1988). Vertical continuity in permafrost of this region can reach 60 m depth with varying active layer thicknesses (Shur and Jorgenson 2007; Douglas et al. 2021), and where present, permafrost acts as a confining layer to groundwater infiltration causing many perched surface waters in permafrost-affected lowlands. The region falls within the boreal (taiga) biome, but the range in soil conditions supports a diverse collection of ecotypes including black spruce forest, mixed deciduous forest, tussock tundra, and various wetland types (Douglas and Zhang, 2021).

Table 1. Location and biophysical setting of core study sites.

Interior Alaska					
Site Name	Latitude	Longitude	Elev. (m)	Biome	Permafrost
Permafrost Tunnel	64.9514838°N	147.6209214°W	244	Boreal Forest	Discontinuous
Farmer's Loop	64.8752564°N	147.6736551°W	145	Boreal Forest	Discontinuous
Creamer's Field	64.8632479°N	147.7342481°W	135	Boreal Forest	Discontinuous
APEX Bonanza Creek	64.7000433°N	148.3037300°W	120	Boreal Forest	Discontinuous
North Slope Alaska					
Site Name	Latitude	Longitude	Elev. (m)	Biome	Permafrost
Imnavait Creek	68.6104465°N	149.3154900°W	896	Arctic tundra	Continuous
Happy Valley	69.1491667°N	148.8327778°W	290	Arctic tundra	Continuous
Utqiaġvik	71.2919976°N	156.7849005°W	3	Arctic tundra	Continuous
Northern Europe					
Site Name	Latitude	Longitude	Elev. (m)	Biome	Permafrost
Sodankylä, Finland	67.3669009°N	26.6289743°E	174	Boreal Forest	Sporadic
Abisko, Sweden	68.3544132°N	18.8157511°E	372	Boreal Forest	Discontinuous

* For a full list of the spelled-out forms of the units of measure used in this document and their conversions, please refer to *US Government Publishing Office Style Manual*, 31st ed. (Washington, DC: US Government Publishing Office, 2016), 248–52 and 345–47, https://www.govinfo.gov/content/pkg/GPO-STYLEMANUAL-2016/pdf/GPO-STYLEMANUAL-2016.pdf.

Figure 2. Map of Alaska study sites distributed across the discontinuous permafrost region in Alaska's interior and the continuous permafrost region on Alaska's North Slope. Individual sites labeled are (*1*) Utqiaġvik, (*2*) Happy Valley, (*3*) Toolik Lake, (*4*) Imnavait Creek, (*5*) the Permafrost Tunnel, (*6*) Creamer's Field and Farmer's Loop, and (*7*) Bonanza Creek / Alaska Peatland Experiment (APEX). (Permafrost continuity defined by Jorgenson et al. 2008.)

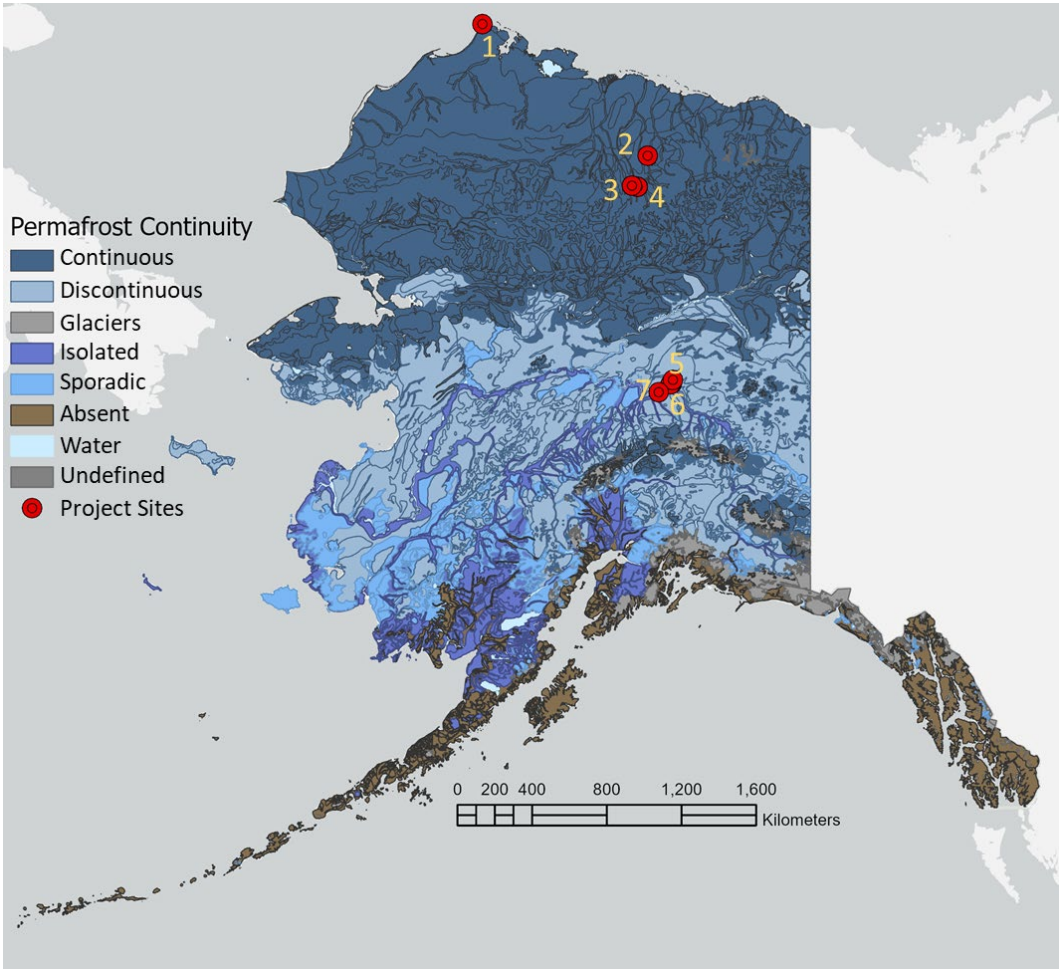

Figure 3. Map of all study sites in Northern Europe (*top*) and Alaska (*bottom*).

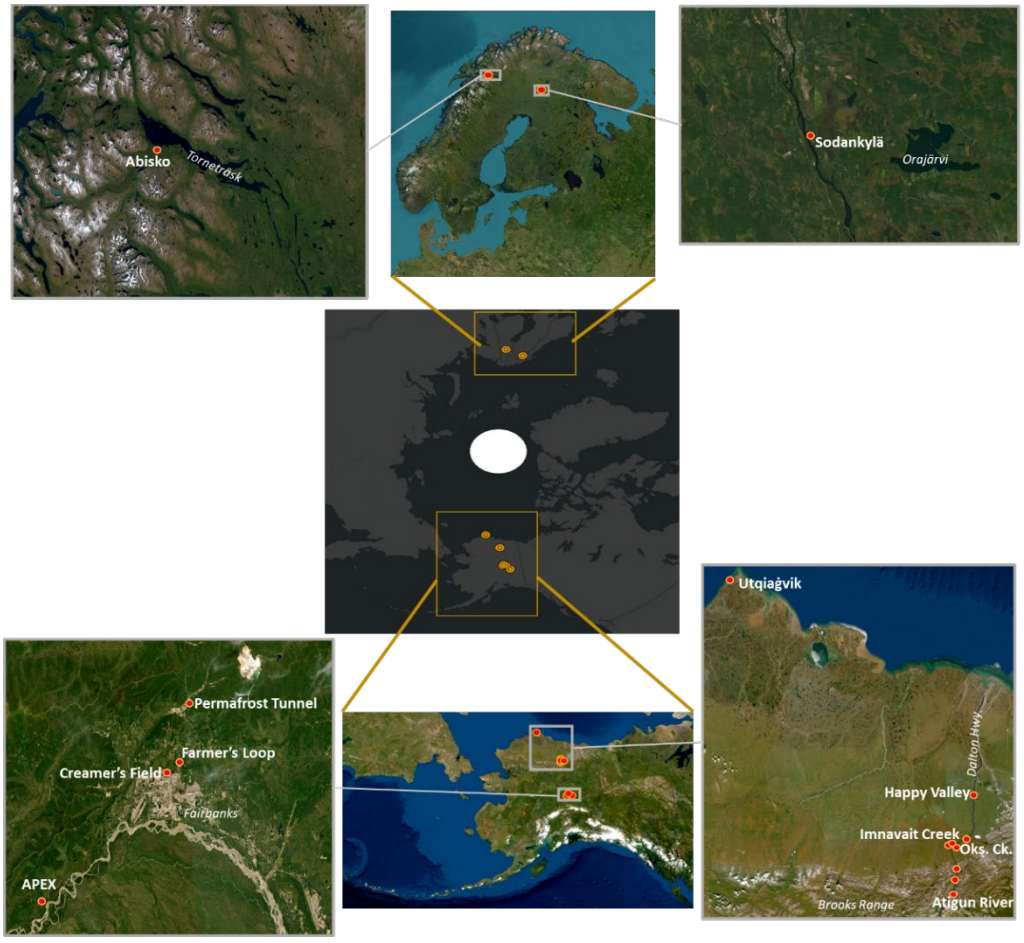

1.1.4.2 The Permafrost Tunnel Research Facility

The Permafrost Tunnel Research Facility (Permafrost Tunnel, hereafter) is owned and managed by CRREL on US Army land near the town of Fox, Alaska (Figure 3). The Permafrost Tunnel was excavated in the 1960s into a northwest-aspect hill and passes through mainly syngenetic permafrost, exposing a stratigraphic sequence containing Late Pleistocene eolian silts defined as the Goldstream Formation (Péwé 1975), underlain by reworked Fox Gravel (Péwé 1975; Hamilton et al. 1988; Kanevskiy et al. 2008; Douglas et al. 2011). Loess largely sources from glacial catchments of the Alaska Range and fluvial silt bars to the south, while the Fox Gravel is thought to issue from local bedrock parent material. Numerous ice wedges, segregation ice lenses, riparian vegetation remains, and Pleistocene megafaunal bones are found in the tunnel deposits. Growing atop these deposits at the ground surface is black spruce (*Picea mariana*) forest which supports an understory of shrubs *Salix*, *Rhododendron,* and *Vaccinium,* lichen (*Cladonia*), and mosses (*Sphagnum*).

1.1.4.3 Farmer's Loop Permafrost Experimental Station

The Farmer's Loop Permafrost Experimental Station (Farmer's Loop) is operated by CRREL on Army land near the city of Fairbanks, Alaska (Figure 3). The 1 km² site was established in 1945 and has supported numerous geophysical, geotechnical, and engineering studies on permafrost (Douglas et al. 2008). The property features low-relief topography (Zhang et al. 2021) and vegetation cover is predominantly spruce (*Picea spp.*) forest with some mixed *Betula* canopy and a low shrub (*Vaccinium*) understory with moss (*Sphagnum*) substrate (Anderson et al. 2019).

1.1.4.4 Creamer's Field Migratory Waterfowl Refuge

Creamer's Field is a historical agriculture site in Fairbanks, Alaska (Figure 3), that began operation as a dairy in the early 1900s. The cleared fields are now recognized and maintained as a National Wildlife Refuge for migratory waterfowl (Alaska.gov, n.d.). Boreal forest and wetlands frame the edges of the agricultural fields making the site a convenient location for comparing land cover controls on permafrost and snow characteristics. Vegetation structure in the undeveloped acres mainly consists of deciduous stands, mixed coniferous–deciduous (*Picea*, *Larix*, and *Betula*) forest, and shrubland with sedge tussocks.

1.1.4.5 Alaska Peatland Experiment (APEX)/Bonanza Creek Site

The APEX site is an extensively studied fen located in the Tanana River floodplain near the Bonanza Creek Experimental Forest southwest of Fairbanks, Alaska. APEX is a long-term peatland manipulation program that has involved multiple studies on boreal wetland carbon dynamics and microbial respiration (i.e., Turetsky et al. 2008; Fan et al. 2013; Anderson et al. 2019). The fen has produced a 1 m thick peat layer in contact with mineral soil below. Vegetation cover at the site transitions from black spruce (*P. mariana*) forest to diverse communities of peat mosses (*Sphagnum*) and emergent vascular species (*Carex* and *Equisetum*) (Turetsky et al. 2008).

1.1.4.6 The North Slope of Alaska

Alaska's North Slope refers to the land area north of the Brooks Range, a vast expanse of Arctic tundra incorporating the Arctic Foothills and Arctic Coastal Plain physiographic provinces. This report draws on data acquired from various locations across the North Slope (Table 1 and Figure 3),

including numerous sites along the Dalton Highway and near the village of Utqiaġvik (Figure 3). The region experiences extreme seasonal ranges in temperature and sunlight hours and is underlain by continuous permafrost (Figure 2) reaching approximately 250 m depth in the foothills (Jorgenson et al. 2008) and up to 400 m depth on the northern coastal plain near Utqiaġvik (Jorgenson et al. 2008; Arp et al. 2011). Permafrost soils throughout the region exhibit many signs of freezing including cryoturbation, frost boils, frost heaves, polygons, and other patterned ground (Ping et al. 1998). Similarly, the effects of soil freezing are expressed in landscape features, creating palsas and other peat formations in the low Arctic, peat mounds, pingos, thermokarst lakes, and ice wedge polygons throughout the Arctic Coastal Plain, and extensive tussock microtopography throughout the region. The underlying geomorphology transitions from sloping deglaciated and unglaciated catchments in the foothills to low-relief deltaic and floodplain flats across the coastal plain (Ping et al. 1998; Wang et al. 2019). Together, the diverse spatial distribution of these features makes the North Slope terrain highly heterogeneous and important to characterize at high spatial resolution.

Dominant land cover on the North Slope includes moist acidic and nonacidic tundra, dry tundra, scrublands, and wetlands (Wang et al. 2019). Permafrost soil parent material on the North Slope is generally unconsolidated surficial deposits eroded from the passive margin sequence that was uplifted to form the Brooks Range and delivered north via alluvial, colluvial, and eolian processes (Wang et al. 2019). The Arctic Foothills are mantled by loess and glacial drift of the late Sagavanirktok advance and Itkillik phases of Pleistocene glaciation in the Brooks Range (Ping et al. 1998; Wang et al. 2019). The coastal plain consists of similar deposits with textures fining towards the coast, but also features marine sediments sourced from multiple marine transgressions and regressions (Sellmann 1975).

1.1.4.7 Northern Europe

An international scope is necessary to understand regional differences in cold-region terrain and climate zones across the Global North. This report features two primary study sites in northern Europe (Table 1 and Figure 3) including the Abisko Valley in the county of Norrbotten, Sweden, and the municipality of Sodankylä in Lapland, Finland.

The Abisko Valley has been researched for over a century following the establishment of the Abisko Scientific Research Station in 1912, which is managed by the Swedish Polar Research Secretariat. Many long-term datasets are available for the site such as ALT, which have been recorded since 1978 (Jonasson et al. 2012), and are accessible from INTERACT GIS (https://www.interact-gis.org/). The valley features an apparent glacial overprint and soils are developed from glaciofluvial deposits, with peat occurring in localized depressions (Berglund et al. 1996). Due to Abisko's leeward position in a rain shadow, the climate undergoes strong orographic influence and generally receives less annual precipitation than the oceanic and continental climates of the surrounding areas (Kohler et al. 2006; Berglund et al. 1996). Meteorological instrumentation at the research station has recorded a mean annual precipitation for the region of approximately 310 mm and annual mean temperature of 0.7°C since record began in 1913 (Kohler et al. 2006). Vegetation cover follows the elevational gradient of the valley, ranging from alpine areas in the uplands to boreal forest in the lowlands containing mainly spruce (*Picea*), pine (*Pinus*), birch (*Betula*), various *Populus*, alder (*Alnus*), and willow (*Salix*) species (Berglund et al. 1996).

The Finnish Meteorological Institute site in Sodankylä, Finland, sits near the margins of northern Finland's periglacial area (as defined by the 0°C limit of the late 1990s) in the Lapland region (Kejonen, 1997). Mean annual precipitation is 539 mm and mean annual temperature is 0.2°C (Finnish Meteorological Institute, 2023). Soils in the Sodankylä area have a sandy texture and support lichens (*Cladina* and *Cladonia*), mosses (*Dicranum* and *Hylocomium*), and shrubs (*Empetrum* and *Vaccinium*) with tree cover dominated by Scots pine (*Pinus sylvestris*, Köster et al. 2013).

1.2 Objectives

This study presents a comprehensive synthesis of the field techniques and data management tools used by two US Army Corps of Engineers Research and Development Center (ERDC) labs: the CRREL and the Construction Engineering Research Laboratory (CERL). Further data were acquired from collaborators and other long-term monitoring efforts to provide a reference methodology for cold regions research. This report therefore can serve as an outline and description of the types of data useful for characterizing cold region terrain conditions and the associated collection, management, and visualization methodology. The basis for an extensive long-term monitoring

dataset is provided here with repeat snow, vegetation, lidar, geophysical, and biogeochemical measurements collected from across the boreal Northern Hemisphere.

1.3 Approach

Site selection was informed by review of existing databases and sites with existing instrumentation that support histories of long-term collection programs. New sites were visited early in the study to install continuous measurement instrumentation such as soil temperature and moisture sensors, and various meteorological instruments. Upon site visitation, thaw depth measurements were taken manually, and where performed, non-destructive, catchment-scale probing of subsurface characteristics was carried out with geophysical techniques. This information was used to indicate frost table depths, thaw features, and where geophysics were surveyed, changes in soil media. Vegetation surveys were conducted to classify climatic and soil conditions at sites and to provide validation for future object-based land cover determinations. Soils were sampled for microbial and geochemical analyses throughout the growing season. Snow thickness and density were continuously monitored in winter months with meteorological instrumentation at study sites or measured manually at the end of the winter season to represent total accumulation. Repeat measurements would be conducted in the following years, and data continuously processed and visualized throughout the project duration. Statistical analyses of data were applied to reveal relationships between the acquired data and potential controls, and machine learning techniques were used to project the observed data to larger scales. Geospatial data were visualized and analyzed throughout the process with GIS.

2 Methods

2.1 Satellite Imagery

Satellite-based imagery can provide repeat, large-scale coverage of spectral information at multiple wavelengths that are useful for characterizing various terrain characteristics. Imagery can be a powerful resource for identifying and monitoring permafrost-affected landscapes as the subsurface processes associated with permafrost relate to identifiable surface characteristics (Philipp et al. 2021). Furthermore, satellite systems with along-track stereos sensors enable the generation of surface models to assess vegetation and snow cover (Kääb 2008). In this study, DigitalGlobe satellites were tasked through the Army Geospatial Center to acquire high resolution WorldView imagery in stereo for field sites in Alaska, Finland, and Sweden. DigitalGlobe was chosen for its tasking capability to specify acquisition times, the temporal resolution and optical stereo of retrievals, and the advanced spatial resolution of the WorldView satellite constellation. Imagery acquired with WorldView-2 yields 0.46 m spatial resolution in panchromatic bands and 1.84 m in eight-band multispectral while WorldView-3 provides 0.31 m panchromatic and 1.24 eight-band multispectral resolutions.

Imagery collection windows were maintained from June 2021 into April 2022. WorldView imagery was tasked throughout this timeframe to capture seasonal variations including peak vegetation productivity in August 2021, the leaf-free period in September and October 2021, peak snow coverage in March 2022, and the spring snowmelt in April 2022 (Figure 4). Specific platform coverage for each field site is shown in Table 2.

Table 2. DigitalGlobe tasked satellite imagery and associated field sites.

Collection Site	Satellite	Acquisition Date
Finnish Meteorological Institute	WV-2	8/2/2021
Happy Valley	WV-3	9/4/2021
Bonanza Creek	WV-2	10/5/2021
Imnavait Creek	WV-2	10/8/2021
Finnish Meteorological Institute	WV-2	3/3/2022
Abisko Scientific Research Station	WV-3	3/13/2022
Abisko Scientific Research Station	WV-2	3/18/2022
Permafrost Tunnel	WV-3	4/4/2022
Farmer's Loop	WV-4	4/5/2022
Creamer's Field	WV-3	4/4/2022

Figure 4. WorldView-3 imagery view of the Bonanza Creek / APEX study area and adjacent Tanana River. (Image used with permission from ©2021 Maxar.)

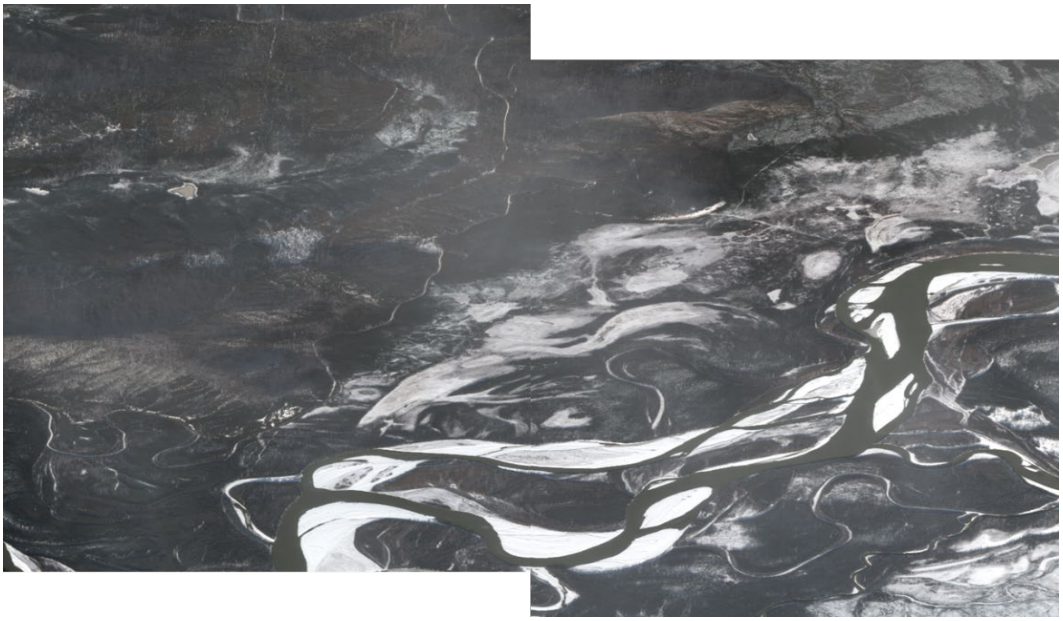

2.2 Permafrost

2.2.1 Active Layer Thickness

ALT in the CRREL sites was manually probed at 1 to 4 m spacing along defined survey transects with permanently fixed end markers on an annual basis. Thaw depths were measured and recorded late in the thaw season following the thaw probing procedures described in Douglas et al. (2016). Land cover observations were recorded for the extent of each survey transects to allow for comparisons of ALT with land cover type. Active layer was not measured where survey points had been eroded away or intersected with deep water. ALT in the Circumpolar Active Layer Monitoring (CALM) sites was manually probed following similar methods, although the measurement points were guided by an array of 11 × 11 grid nodes evenly distributed within a 1 km^2 grid (Brown et al. 2000; Shiklomanov et al. 2010).

2.2.2 Soil Temperatures

Continuous measurement of depth-specific soil temperatures was completed with instrumentation of HOBO® U23 Pro v2 two-channel temperature loggers (Onset, Bourne, Massachusetts) buried at regular depths throughout the soil profile. For sensor deployment, a 0.75 cm diameter hole was excavated to the desired depth using a slide hammer

and rod, and temperature sensors protected in plastic sleeves were then installed through the hole.

2.3 Soil and Porewater Geochemistry

Soil samples were either collected by excavating soil pits or collecting cores using a Snow Ice and Permafrost Research Establishment (SIPRE) coring barrel coupled to a powerhead. Soil pits were excavated in locations that contained rocks or pebbles greater than 5 cm, as this coarser substrate may damage SIPRE coring equipment. Photos of a soil core and an excavated soil pit are shown in Figure 5. Soil pits were opened by first temporarily removing the vegetative mat and storing it aside. Narrow spade shovels were used to remove thawed active layer material when sampling in summer months and a jackhammer was used to excavate frozen active layer in frost-supporting months. In summer months, a jackhammer was used as necessary when permafrost was reached within the 1 m target depth. Soil pits and cores were subsampled at 20 cm depth increments. Soil samples were thawed (if frozen) and dried at 60°C in a convection oven. The subset of samples allocated for Fe* speciation were immediately stored frozen at −4°C and remained frozen until analysis. Samples were analyzed for pH, major ions, trace elements, iron speciation, carbon, nitrogen, and organic content.

Figure 5. Images showing excavated soil core from Storflaket Mire, Sweden (*left*), and soil pit from Imnavait Creek, Alaska (*right*), each differentiating sampling locations in vegetation, active layer, and permafrost.

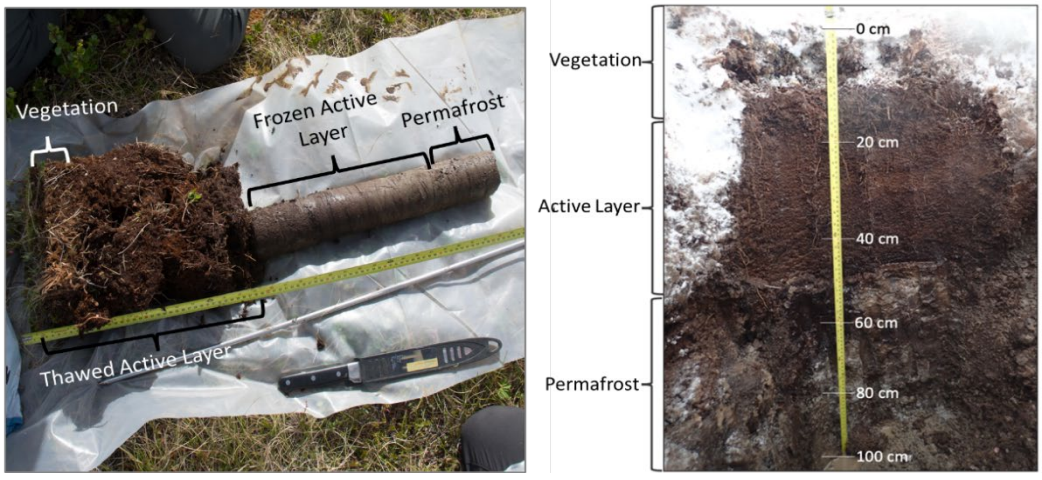

* For a full list of the spelled-out forms of the chemical elements used in this document, please refer to *US Government Publishing Office Style Manual*, 31st ed. (Washington, DC: US Government Publishing Office, 2016), 265, https://www.govinfo.gov/content/pkg/GPO-STYLEMANUAL-2016/pdf/GPO-STYLEMANUAL-2016.pdf.

Porewater samples were collected from subsections of the soil pit or SIPRE core by squeezing the soil fraction and collecting the porewater in centrifuge tubes, filtering the liquid to less than 0.45-micron filter size using a nylon membrane filter. Porewater samples for trace metal analysis were acidified with 6 mol/L ultrapure nitric acid (0.1 mL per 100 mL sample) and stored in a refrigerator at 4°C until analysis. Porewater samples were analyzed via ion chromatography for major ions, inductively coupled plasma-mass spectrometry for trace metals, and ultraviolet spectrophotometry for Fe speciation.

2.4 Soil Microbiology

Soil microbial communities mediate many biogeochemical processes and are an important factor to include in terrain characterization, particularly for forecasting landscape-level shifts. Microbial community characterization through DNA high throughput sequencing was performed at discrete sampling events across the field sites. A subset of soil samples was collected for microbial analysis from the soil pit or soil cores. Soil samples were generally collected from depths spanning surface soil to permafrost, depending on field site location. Samples were taken in triplicate or quadruplicate using ultraclean sampling methods and wearing Tyvek suits and N-95 face masks (see Figure 6). Tyvek suits and masks were not worn when sampling more microbially abundant surface soils.

Figure 6. Images showing soil collection for microbial community analysis (*top left* and *right*) and the supplies used to ensure sterile sample collection (*bottom left*).

The collection tools were first cleaned with 70% ethanol or 70% isopropanol, followed by DNAse, and then RNAse solutions. Kimwipes were used for applying solution to the tools and wiping away excess. Soil samples were placed into Whirl-Pak bags and stored under –10°C or colder until analysis. Samples collected for DNA sequencing were stored at –80°C.

2.5 Vegetation

2.5.1 Root Strength

Surveys on root strength and vegetation cover were performed in boreal forest sites to evaluate their influence on soil strength, compressibility, and cohesion. The locations of study plots were generated randomly then used to navigate to each site. The plot centers were marked and used as the starting point for measuring 7.3 m axes passing from the center to each cardinal direction, dividing each plot into 4 equal-area quadrants. 35 random shear vane samples were collected from each quadrant at 10 cm depth using an H-4227 Field Shear Vane (Humboldt Manufacturing, Elgin, Illinois). A 25.4 mm × 50.8 mm tip was used where this 10 cm depth incorporated organic-rich soils and the standard 20 mm × 40 mm tip was used for mineral soils. The number and species of coniferous and deciduous trees with a diameter at breast height greater than 10 cm was recorded for each quadrant. Percent cover of graminoid and moss was measured in a 0.25 m^2 quadrat to the nearest 5% across five random locations within each quadrant. Lastly, the depth to mineral soil was measured once for each quadrant, and frost table depths were manually probed in five random locations in each quadrant.

Root samples were tested for tensile strength in the lab. Samples were washed to remove soil material while preserving the maximum root mass. Roots with no major defects were subsampled and measured for diameter at three different sites with a caliper. The diameter for the subsample was averaged and roots were trimmed to 15–30 times the average diameter following Genet et al. (2005). Root samples were then glued to steel eye nuts with the gauge and thread opening of eye nuts relating to root diameter. Once glued and cooled, root samples were stored in plastic wrap under refrigeration until testing to reduce cellulose degradation (Alam et al. 2018).

Tensile strength tests were conducted using the MTS T-Slot Universal Testing Machine in Newmark Structural Engineering Laboratory at the

University of Illinois at Urbana-Champaign. Root samples were connected at the top to load cells, actuator, and crosshead via a threaded connecting link and eyebolt. The bottom was similarly connected to a base plate anchored to a T-slot table. The tensile strength was tested by elevating the actuator at a constant rate of 1 mm/min until failure. The maximum tensile force of the sample was then recorded in output files.

2.5.2 Vegetation Cover

Vegetation surveys were tailored in respect to the measurements or sampling performed at each site. Basic vegetation surveys were performed along repeat thaw probing and snow depth transects to identify the dominant ecotype (i.e., mixed taiga, coniferous taiga, deciduous forest, wetland, shrubland, sedge tundra, etc.). For sites instrumented for soil respiration and sampled for microbiology, vegetation structure was recorded in greater detail. A 1 m × 1 m plot was centered on the sampling site, then surveyed for substrate (i.e., mosses, lichens, bare soil, etc.), understory, and canopy species and percent coverage where applicable. For root sampling sites, the procedure is described in Section 2.5.1.

2.5.3 Root Strength Statistical Analysis

A simple univariate linear regression model was fit to each predictor variable regressed on the shear vane values. Next, spatial correlation among plots was tested using Moran's I (Gittleman and Kot 1990). The null hypothesis was no spatial correlation; test statistics with p-values < 0.05 were regarded as evidence of spatial correlation. For predictor variables that did not exhibit spatial correlation, the nonspatial simple linear regression was used and tested against a null model that did not include the predictors using the Anova function in the R (R Development Core Team 2021) package car (Fox 2019). If Moran's I detected evidence of spatial correlation, a spatial regression model as implemented in the R package spaMM (Rousset and Ferdy 2014) was applied and the spatial coordinates Matern covariance function (Stein 1999) were included. A likelihood ratio test was used to compare the spatial model fit against a null model that only included the spatial coordinates as random effects using the likelihood ratio test (LRT) function in the R package spaMM.

2.6 Snow Surveys

Snow characteristics, namely snowpack depth and density, are essential considerations in terrain conditions as well as climate research and freshwater resource management. The following subsections explore the main methods used to conduct snow depth and density measurements.

2.6.1 Snow Depth Measurement

Numerous methods have emerged for measuring snow depth, including manual methods, electronic instrumentation, and remote sensing techniques. Manual measurements involve probing the snowpack with either a graduated avalanche probe or other measuring device, or automated depth-measurement probes such as a Magnaprobe (SnowHydro LL, Fairbanks, Alaska). Electronic snow depth sensors, such as ultrasonic sensors, (e.g., SR50 by Campbell Scientific, Logan, Utah, measure two-way travel times of sound waves to quantify snow depths in real time. Remote sensing techniques, such as airborne radar or satellite-based sensors, offer spatially continuous measurements of snow depth over large areas. In this study, the CRREL team applied Magnaprobes for repeat measurements of snow depth along defined transects in the Alaska field areas.

The Magnaprobe has two main components, a 153 cm steel rod equipped with a sliding plastic disc, and a backpack-mounted data logger with GPS unit (Sturm and Holmgren, 2018). Magnaprobes were selected for their capability to automatically assign geographic positioning to snow depth measurements. However, a tendency to over-estimate snow depths was recognized due to consistent penetration of the probe into frozen moss beneath the snowpack, or air pockets where snow is suspended over yielding vegetation. This was accounted for by taking control measurements for a subset of Magnaprobe measurements at each site and comparing actual snow depths to measured depths to assess error.

Control measurements were taken using either a 2-m engineering folding ruler (e.g., Rhino Engineer's Folding Ruler by US Tape, Pennsburg, Pennsylvania), a snow depth probe by Snowmetrics (Fort Collins, Colorado), or a commercial avalanche probe (e.g., QuickDraw Pro Probe 240 by Black Diamond Equipment, Ltd). With these tools, snow depth measurements were made by inserting the ruler or probe vertically into the snow surface until reaching refusal by the ground surface, validating

that refusal was met at the ground surface by digging away snow, and recording the depth in cm and geographic coordinates into a field notebook, handheld GPS unit, or mobile device.

2.6.2 Snow Density Measurement

Snow density is typically measured by weighing a known volume of snow with a mobile scale in the field in order to capture unaltered snow properties. In this study, two volume extraction devices were applied according to snow conditions. A cylindrical tube of known volume (Snowmetrics, Fort Collins, Colorado) was favored in shallow snowpack and wedge cutters shaped as triangular prisms of known volume (Snowmetrics, Fort Collins, Colorado) were used in deeper snowpack. Each method involves inserting the volume extractor laterally into a freshly excavated snow-pit wall exposure, extracting a sample of known volume, and weighing the sample with a scale. Given sufficient snow depth (20 cm or more), density measurements were made using either a 100 cm^3 or 250 cm^3 wedge cutter sampled from a snow pit wall that exposes the stratigraphic layers. Preferably, density sampling was performed on a north-facing wall of a snow pit to reduce melt of the excavated snow layers prior to sampling. In this study, snow pits were dug in a 1 m × 1 m perimeter and snow density measurements were duplicated every 10 cm depth in the snowpack starting from the surface and ending at the ground contact. The density of snow is calculated from the mass divided by the known volume of the sampling device.

2.7 Terrestrial Lidar

2.7.1 Field Collection

Lidar surveys are used worldwide to develop high-resolution scans of surface elevation and other surface features. Repeat Lidar is a proven method for widespread identification of hot spots in surface change and has become increasingly applied for change detection in permafrost regions (Avian et al. 2008; Barnhart and Crosby 2013; Jones et al. 2013; Kociuba et al. 2014; Marx et al. 2017; Anders et al. 2020; Douglas et al. 2021). Terrestrial laser scanning (TLS) and aerial laser scanning (ALS) involve the collection of lidar point cloud data for a surface and can provide high-resolution elevation data to allow for differencing of the derived digital elevation models (DEMs) or point clouds to illustrate surface change. In boreal forest areas, the portability of TLS systems and

use of multi-return lidar allows for ground surface measurements beneath dense forest canopies.

TLS surveys were performed above the Permafrost Tunnel throughout the thaw seasons of 2017 and 2018. Scans were focused on two thaw features where noticeable surface erosion has ensued, a larger erosion feature (Site A) located at 64.9495327°N, 147.6173131°W and a smaller erosion feature (Site B) located at 64.9504113°N, 147.6162452°W. Elevation data were collected with a Leica C10 ScanStation (Leica, St Gallen, Switzerland) with an estimated 100 m range in clear line of sight conditions. Geographic positions of scans were referenced with a Trimble R8 GNSS base station (Trimble, Westminster, Colorado) that broadcasted corrections to a Trimble R8 rover, providing an internal GPS data file for post-processing the survey data.

A real-time kinematic (RTK) survey style was applied to allow for corrections of multipath errors and atmospheric effects. Individual TLS scan lines were positioned to create maximum overlap and coverage of a continuous area once all scans were combined. Each scan was taken at a 360° horizontal and 270° vertical sweep arc. This scan geometry collected point returns from multiple surfaces and subsequent RGB color images were taken for the scanned area if light conditions were suitable. Scans were performed at intermediate resolution producing a 10 cm gap between adjacent points at a 100 m radius from the instrument. For each scan, four to six Leica high-definition survey (HDS) targets were distributed throughout the scan area to serve as tie points for georeferencing the scans. The location of each target was surveyed with a Trimble DGPS R8 rover in RTK mode. Each scan was acquired by the same individual researcher, therefore minimizing scan incoherence caused by contrasting subjectivity of multiple operators (Anders et al. 2020).

Each elevation point was produced in x, y, z format of Easting, Northing, and Elevation. These points were projected to WGS84, Universal Transverse Mercator (UTM) Zone 6N. North American Vertical Datum of 1988 (NAVD88) was used as the vertical projection calculated based on GEOID12B and is reported using the Orthographic elevation values. Each data point is associated with an intensity value (i), a measure of the return strength of the laser beam, and a color value (RGB) which was assigned from panoramic photos collected from an internal camera. The final data format produced values in (E, N, z, I, r, g, and b) for each data point.

2.7.2 Data Processing

Location data for the survey points were processed using Trimble Business Center, where the base station's internal GPS file is sent to the Online Positioning User Service (OPUS) operated by NOAA's National Geodetic Survey. This tool automatically processes the internal file to compute global positions within centimeters of accuracy and allows for further refinement of locations acquired for the HDS targets.

Lidar point cloud data were processed in Leica Geosystems Cyclone software using the REGISTER module to align the point clouds from scans captured in different positions and the Survey module for performing measurements on laser scan data. First, raw data were imported to Cyclone, point clouds were unified and images were blended, then ModelSpaces was created to begin modeling. Each file created by the scanner, including the point cloud, images, target scans, and all other data associated with scanner placement, was stored in a ScanWorld folder. Within each ScanWorld, a coordinate system was established based on the array of targets that were scanned, and registration mean absolute error (RMAE) or errors for each constraint, such as a target, were calculated simultaneously. Constraints on the coordinate system with error values greater than 6 mm were disabled and the registration was recalculated to produce a new set of errors for each constraint. The process was repeated until a low RMAE was achieved, allowing for an error range of 0.002 m to 0.011 m for the output dataset. The project-centric coordinate system was referenced to a global coordinate system using information from the HDS targets, where the quality of the targets survey affects overall RMAE of the project (0.01 m to 0.13 m). Upon registration of the ScanWorlds files, minor edits were made to the output point cloud, including removal of extraneous points caused by the sun, the top handle of the scanner, and from midair objects. The processed point cloud was then exported and converted to a .las file for manipulation in geospatial software.

2.8 Geophysics

Geophysical methods offer an efficient, noninvasive means for probing permafrost continuity and other cryospheric characteristics (such as snow depth and stratigraphy) that are fundamental for characterizing cold regions. Ground-penetrating radar (GPR) is an electromagnetic geophysical technique well suited for permafrost investigations as the transmitted radio waves are sensitive to contrasts in dielectric

permittivity, an electromagnetic property that varies with soil type, soil water content, and water phase (Neal 2004). Therefore, GPR can detect material interfaces with differing physical properties within a substrate, such as the frost front, and can be used to map ALT in permafrost environments (Schaefer et al. 2015; Parsekian et al. 2021). In this study, GPR data were collected on 3 August 2022, in Abisko, Sweden.

GPR surveys were collected using a 400 MHz antenna manufactured by Geophysical Survey System, Inc. (Nashua, New Hampshire) in bistatic transmitter/receiver geometry. A GSSI instrument console was used to record and measure the travel time of radar waves transmitted from the antenna at ground surface, to reflection from the top of permafrost underfoot (Arcone and Delaney 1982). Positioning information for the antenna was continuously retrieved from a handheld GPS mounted to the antenna platform that was pulled manually in a sled at approximately 0.5 m/s. The GPS linked location information to each measured radar response, known as a trace.

GPR instrument settings were adjusted to suit the survey substrate. Radar wave velocity through the survey media can then be calculated by comparing two-way travel times with frost probing depths recorded at 2 m increments along the GPR transect. In this study, the radar velocities were assumed, as radar wave speed in seasonally frozen soils range from those of ice to those of liquid water and depend on a number of pedophysical parameters (Arcone and Delaney, 1982; Bakian-Dogaheh et al. 2019). Table 3 lists radar wave velocities for common survey media. The travel times associated with radar reflection at the frost table were approximated from the assumed velocity and were manually picked to represent the frost table depth along the transect at the time of survey.

Table 3. Radar wave velocities for common high-latitude soil constituents.

Material	Permittivity	Wave Velocity (m/ns)
Liquid water	80	0.03
Ice	4	0.15
Soil	15	0.08

For the Abisko site, a radar wave speed of 0.07 m/ns was used based upon a 0.75 m thaw depth revealed by SIPRE coring and a 21 ns two-way travel time for the thawed near-surface velocity. A basic processing sequence was applied to raw data in ReflexW (Sandmeier 2016) software using minimal

steps: subtraction of the mean for each trace to eliminate instrument noise, start time correction to zero to eliminate empty data times, horizontal distance correction using a trace interpolation from the GPS data and averaging traces every 0.1 m, manual linear and exponential gain function beginning after 7 ns, time cut below 70 ns to eliminate returns below the investigation depth, and topographic correction using local digital elevational data. The collection of radar traces for a survey transect are displayed as radargrams, each containing horizontal lines with color indicating the amplitude of the reflection (based on two-way travel time) to appear as cross-sectional approximations of subsurface reflections.

In other studies, the CRREL team has applied GPR alongside electrical resistivity tomography (ERT) as an additional tool to parse liquid from solid water phases in the substrate (Barker et al. 2023 in press), and the method will be briefly mentioned here. ERT operates with a lower frequency electrical field to determine resistivity of the subsurface (Parsekian et al. 2014). Resistivity was measured with ERT to supplement the frost table depths inferred with GPR to better inform interpretations on active layer dimensions and the presence of thaw bulbs or cryopegs that remain liquid at subzero temperatures. Therefore, ERT in Barker et al. (2023 in press) was surveyed in overlap with GPR transects to allow comparison of the separate datasets for similar areas. A SuperSting R8 system (Advanced Geosciences, Inc.) with 84 electrodes was used applying a dipole-dipole geometry to measure resistivity profiles. Electrode spacing was determined based on transect length, but was generally held as 1 m to 2 m. A quasi-Newton optimization technique (Loke and Barker 1996) was applied to invert resistivity data for modeling profiles in RES2DINV (Geotomo software).

2.9 Machine Learning

Machine learning algorithms model and project results for unknown tasks or objects based on known training data and can be tailored for upscaling environmental data measured in situ. Typically, a relationship between an object of interest (dependent variable) and an object readily observed at large scales (independent variable) is established, then the large-scale coverage of the independent variable and its known relationship with the dependent variable is used to extrapolate dependent values to larger scales than feasibly observed. In high latitude studies, this technique is particularly useful for upscaling localized point measurements of

monitoring data such as ALT and snow depth to the landscape scale. Since many in situ measurements are time and labor intensive, upscaling allows for greater spatial coverage than realistically accomplished in the field, making spatial variations more apparent.

Both ALT (Zhang et al. 2021) and snow depth (Douglas and Zhang, 2021) demonstrate significant relationships with the ecotype in which they occur. Therefore, machine learning algorithms can be applied to determine ALT and snow depth based on the ecotype present, which is readily classified at large scales with remotely sensed imagery. The following subsection summarizes the object-based machine learning ensembles tested for cold-regions applications in former studies (Douglas and Zhang, 2021; Zhang et al. 2021). Due to similarities in the methods for upscaling ALT and snow depth, repeat measurements of thaw and snow depths, are collectively referred to in the following section as “in situ measurements”.

In situ measurements were upscaled using hyperspectral classifications in an object-based learning algorithm that consults the relationships between ecotypes and the observed measurements (developed in Zhang et al. 2021; Douglas and Zhang 2021) (summarized in Figure 7). Hyperspectral imagery was collected during the most cloud-free periods of the growing season for each study site, reducing cloud interception of channel wavelengths and ensuring a strong representation of ecotypes. Any water bodies and impervious road surfaces in the imagery were masked before ALT processing. Thaw depths were manually recorded following the thaw probing procedures outlined in Douglas et al. (2016) during late fall (generally October) when thaw reaches its maximum depth and best represents the active layer thickness. Snow depths were measured late in the snowpack season along repeat transects with Magnaprobe (SnowHydro, Fairbanks Alaska) measurements taken at 1 m to 2 m spacing (Douglas and Zhang 2021). For snow surveys, lidar data was obtained where available.

Upon imagery and measurement acquisition, the high dimensionality of the hyperspectral imagery was reduced with Minimum Noise Fraction (Green et al. 1988). This produced eigenimages that were further analyzed on the basis of visual appearance and their eigenvalues. Image segmentation was then performed using multiresolution segmentation in eCognition (Trimble 2014) to produce image objects in preparation for Object-Based Image Analysis (OBIA). Image objects were defined based on color and geometry

for ALT, or geometry and size for snow depth, and the mean and standard deviation of these features were used as model predictors. In situ measurements were spatially matched with image objects to synchronize the field and hyperspectral data, giving the model context for upscaling measurements to un-surveyed areas based on their ecotype. Objects containing multiple measurements were assigned the average of their measurements. For snow surveys, lidar statistical descriptors of canopy heights and terrain for image objects were merged with spectral information where lidar coverage was available. Endmember scenarios for ALT and snow depth (minimums and maximums for the period of record) were matched with image objects to accommodate variability.

An ensemble of regression algorithms was incorporated into the models, including two machine learning algorithms; Support Vector Machine (SVM) and Random Forest (RF); and the conventional Multiple Linear Regression (MLR). Each were administered through Waikato Environment for Knowledge Analysis (open-source software, Hall et al. 2009). The respective algorithms were selected by approach to regression and were leveraged together to produce multiple predictions. The respective outputs were integrated by weighting based on their coefficient of determination (r) values following Zhang et al. (2021) and the combining scheme in Zhang et al. (2018). The resulting ensemble predictions were validated for accuracy using a combination of the product r value, mean errors, and by comparing model predictions with the independent in situ datasets. Further details on the selected algorithms and model validations are discussed in Zhang et al. (2021) and Douglas and Zhang (2021). Similar machine learning approaches can be applied to upscale other environmental data provided a clear linkage with a readily obtainable, large-scale predictor dataset such as hyperspectral imagery.

Figure 7. Simplified workflow for applying hyperspectral imagery to upscale point measurements. (Methodology data from Zhang et al. 2021; image by authors.)

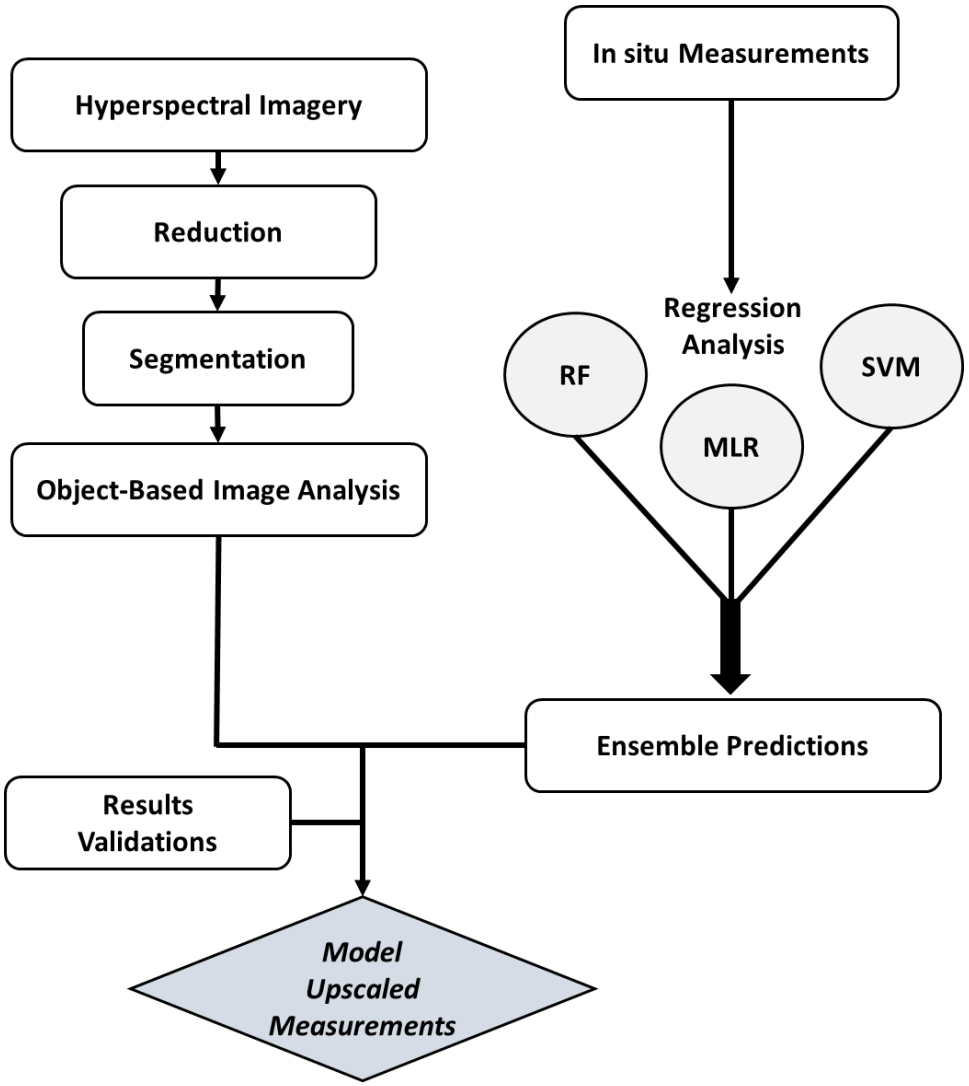

2.10 Data Management

The compilation of cryological, meteorological, hydrological, and biogeochemical data in this study culminate in a large composite dataset involving numerous file formats and sources. Data were initially backed on hard drives and stored locally on computers or external drives before being backed on a shared server. Attributes across the various datasets were considered to inform data standards that would guide all tabular storage and representation. These standards include site identifiers, geographic coordinates, collection date, subject of observation (e.g., snow depth), descriptions, and measurements or observations of the subject. Raw data files were then compiled and used to create tables that conform

to the noted standards. The raw files and edited files were uploaded to a cloud-based drive and shared amongst collaborators.

Tabular geospatial data were archived in comma separated files (.csv) or spreadsheets (.xlsx) that associate data points with coordinate information. These files were ingested into a geospatial environment via Python (Van Rossum and Drake 2009) scripting for efficient conversion of multiple files. The code converted .csv files and spreadsheet data into the appropriate layer files in QGIS. Alternatively, .csv files were imported to ArcGIS Pro and converted to shapefiles.

2.11 Data Visualization from Field to Feature

Geospatial visualization of data is important for illustrating distributional trends in observed variables and in assessing potential geographical controls on observed phenomena. This study applied QGIS® and multiple Esri® ArcGIS products as known platforms for visualizing spatial data, but also as effective means for digitally collecting, storing, analyzing, and sharing spatial data.

Field-based measurements exported from various acquisition platforms were converted to vector layers in Esri shapefile format in ArcGIS Pro® by inputting the geographical coordinates of observations and fixed acquisition platforms as x, y data, or by creating a point feature class and adding the sites by their geographical coordinates. Other field measurements or observations were directly recorded in the shapefile format to simultaneously map and collect data by using the field-based mapping functionality of ArcGIS Field Maps®. Editable shapefiles were created in ArcGIS Online® (AGOL) to serve as templates for intended datasets, including fillable forms with user-specified prompts to guide field observations. These editable layers were synced for offline access and loaded into the Field Maps web app, to be accessed in the field via the Field Maps mobile app. This allowed operators to view existing data layers while offline in the field and to collect new data points or information in the editable shapefiles. Upon completing field collection in the Field Maps app, edits were synced to AGOL where collaborators could access the updated shapefiles. Figure 8 demonstrates typical workflows for transferring data as shapefiles across desktop, offline, and online platforms for data visualization, editing, and sharing.

Figure 8. Simplified workflow for managing and editing shapefiles across desktop (ArcGIS Pro®), cloud (ArcGIS Online® [AGOL]), and mobile (ArcGIS Field Maps®) geospatial visualization platforms.

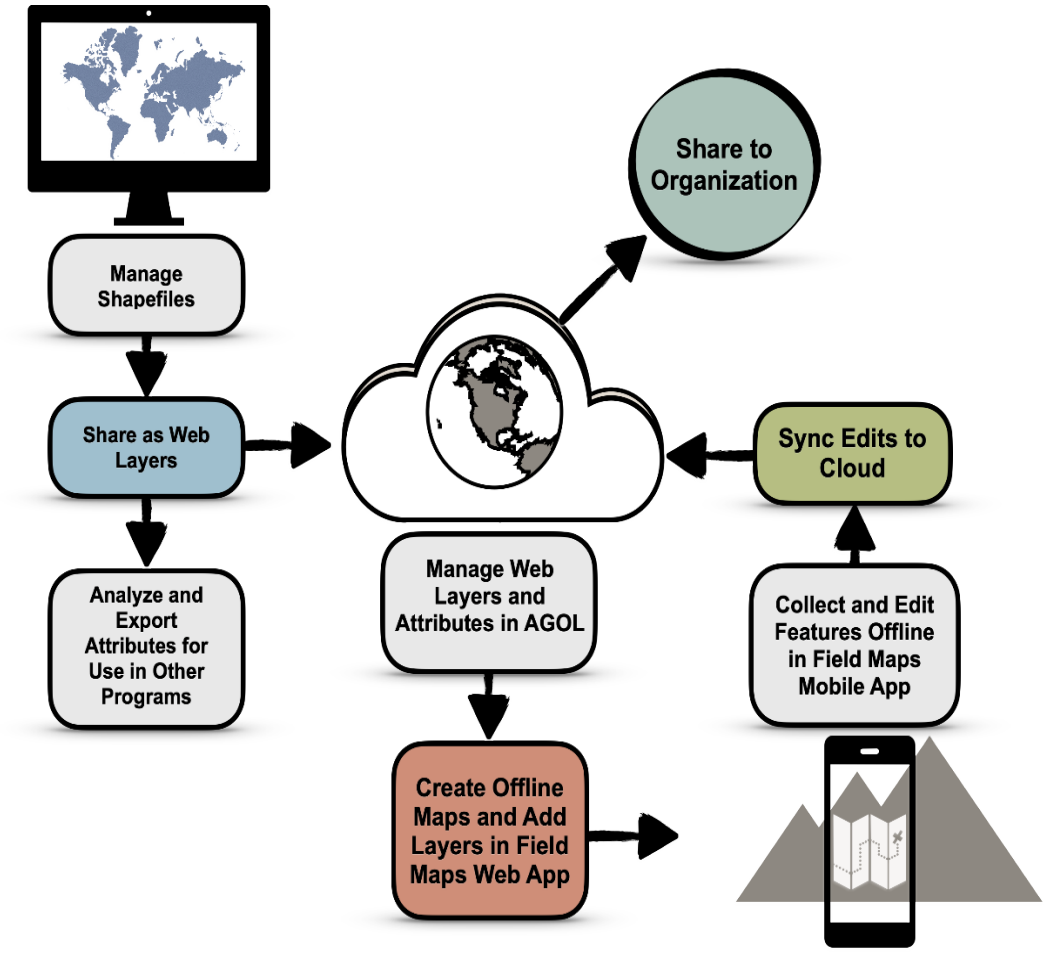

3 Results and Discussion

3.1 Long-Term Trends in Permafrost Landscape Properties

Repeat measurements of ALT provide critical insight into permafrost change over time. Several long-term monitoring efforts provide site-specific ALT for various locations throughout Alaska, allowing for comparisons across major climatic, physiographic, and ecological zones. The following sections address spatial and temporal trends in the repeat ALT recorded for CRREL sites in Interior Alaska, compared with grid-based ALT recorded on Alaska's north slope by the CALM program (Brown et al. 2000; Shiklomanov et al. 2010). These results demonstrate variability in top-down thaw extent and progression across sites with contrasting soil thermal properties and land cover.

3.1.1 Discontinuous Permafrost Region–Interior Alaska

Interior Alaska lies within the discontinuous permafrost region (Figure 2) as defined by Jorgenson et al. (2008), where mean annual permafrost temperatures at 1.2 m depth range from –2.60°C to –0.05°C and are actively increasing (Douglas et al. 2021). Repeat measurements along four main transects in Interior Alaska represent ALT in multiple ecotypes of the taiga biome: conifer (*P. mariana*) forest above the Permafrost Tunnel; mixed conifer forest (*Picea glauca* and *P. mariana*), tussock tundra, and wetlands at Farmer's Loop; mixed conifer-deciduous boreal forest (*P. glauca, P. mariana*, and *Betula papyrifera*), wetland, and sedge tussock in Creamer's Field. Each survey transect was visited late in the thaw season from 2013 through 2020. Two locations along the ALT transect at the Permafrost Tunnel eroded away by 2017, decreasing *n* from 2017 to 2020 by two measurements. The collection of ALT for each site displays overall trends in the culmination of top-down thaw over 10 years of monitoring.

Figure 9 and Figure 10 display ALT by ecotype across the Interior Alaska transects. Across all sites it is apparent that the top of near-surface permafrost is migrating downward as the permafrost degrades. Additionally, the lateral thaw of permafrost at some locations has resulted in decreased continuity of permafrost across the ground surface, since winter freeze back is typically no greater than approximately 1 m. Mean ALT for the CRREL transects in Interior Alaska shown in Figure 11, panel a display a general deepening trend and downward thaw propagation over time from an intersite mean of 58 m to 82 cm from 2013 to 2022

respectively. The Creamer's Field transect demonstrated the highest percentage of increase over this 9-year period of 56%. The lowest increase occurred at the Farmer's Loop sites, where transect B achieved 34% and transect A 31% of increase. For Interior sites collectively, average ALT increased at an annual rate of 4 cm/yr from 2013 to 2022, although the change was not uniform throughout the period of observation. The highest rate of ALT increase across sites occurred from 2013 to 2014, when average ALT increased by 16 cm.

Spatial trends in ALT have been associated with ecotype or vegetation cover in many permafrost-affected regions, including the North Slope of Alaska (Nelson et al. 1997; 1998), Northwest Territories, Canada (Fisher et al. 2016), the Qinghai-Tibet Plateau (Wang et al. 2010; 2018), and maritime Antarctica (Guglielmin et al. 2012; Almeida et al. 2014). For the Interior Alaska sites in this study, the deepest ALT occurred in disturbed areas, averaging 103 cm, which is expected (Brown et al. 2015; Zhang et al. 2021). Among natural land cover types, ALT is greatest in wetlands where the average is 100 cm, followed by mixed taiga forest at 85 cm, and tussock tundra at 68 cm. Spruce dominated forest with moss and lichen understory is generally underlain by the lowest ALT of 65 cm on average. These results generally support the land cover-to-ALT relationships discussed for the same transects in Zhang et al. (2021), but the additional ALT measured over 2021 and 2022 reveal an increased mean ALT in disturbed sites from those summarized in 2021. The relationships between ALT and ecotype presented in this study continue to support the potential for the influence of land cover on soil thermal properties to serve as a strong spatial control on ALT (Fisher et al. 2016). Namely, ALT is least beneath moss and lichen substrates, likely in response to their insulative capacity as a soil-air buffer and the surface cooling effect of nonvascular evaporation during the snow-free season (Heijmans et al. 2004; Loranty et al. 2018). As discussed in Zhang et al. (2021), ALT in wetlands is likely greatest due to enhancement from conductive heat transfer through ponded surface water.

Figure 9. Field-measured active layer thickness (ALT) along Farmer's Loop transects *a* ("Fla", *top*) and *b* ("FLb", *bottom*), passing through mixed taiga, wetlands, tussock tundra, and moss spruce forest ("spruce forest").

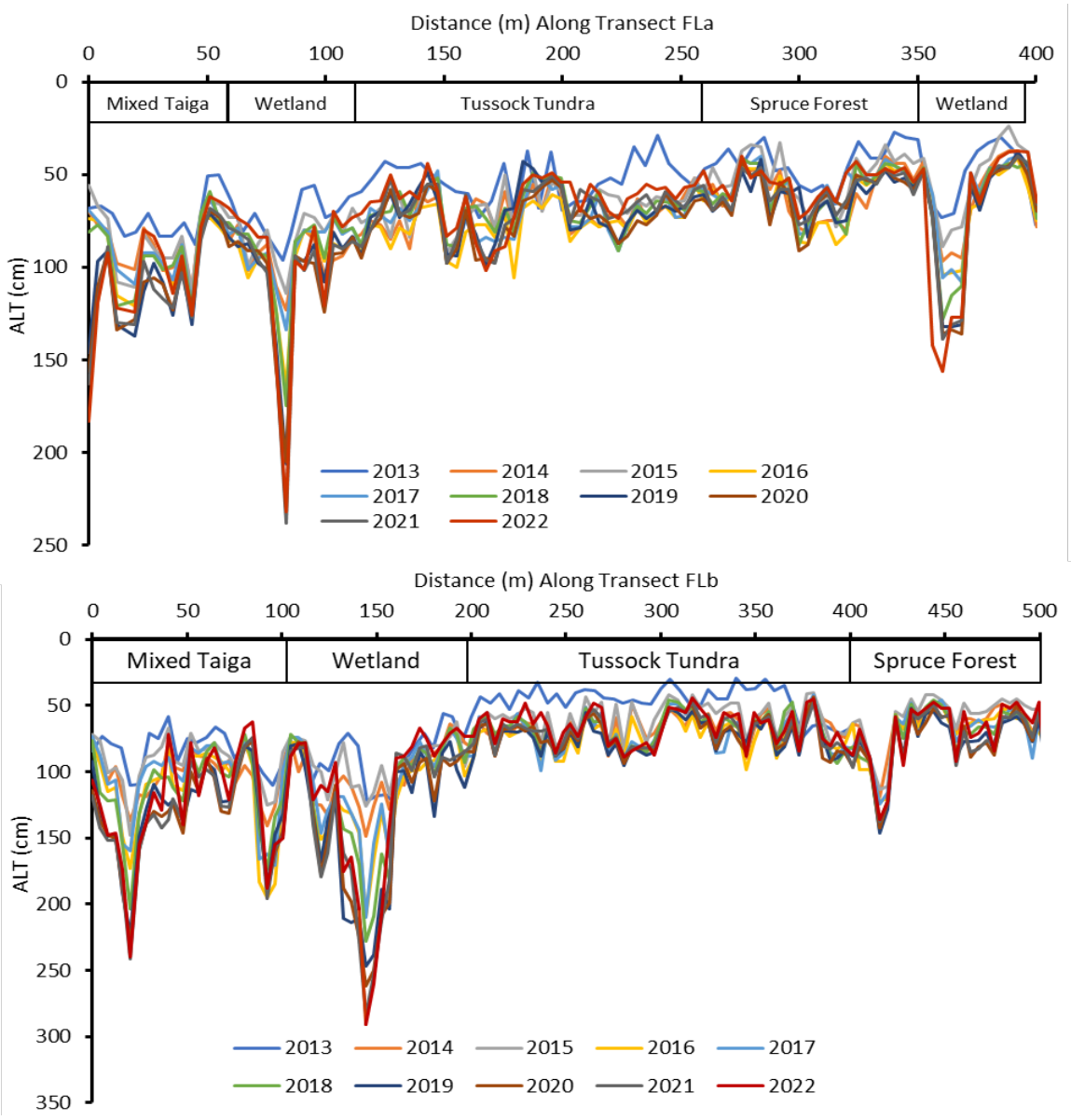

Figure 10. Field-measured ALT along transects at the Permafrost Tunnel ("PT", *top*) and Creamer's Field ("CF", *bottom*), passing through mixed taiga, wetlands, tussock tundra, and moss spruce forest. *Red arrows* indicate high disturbance.

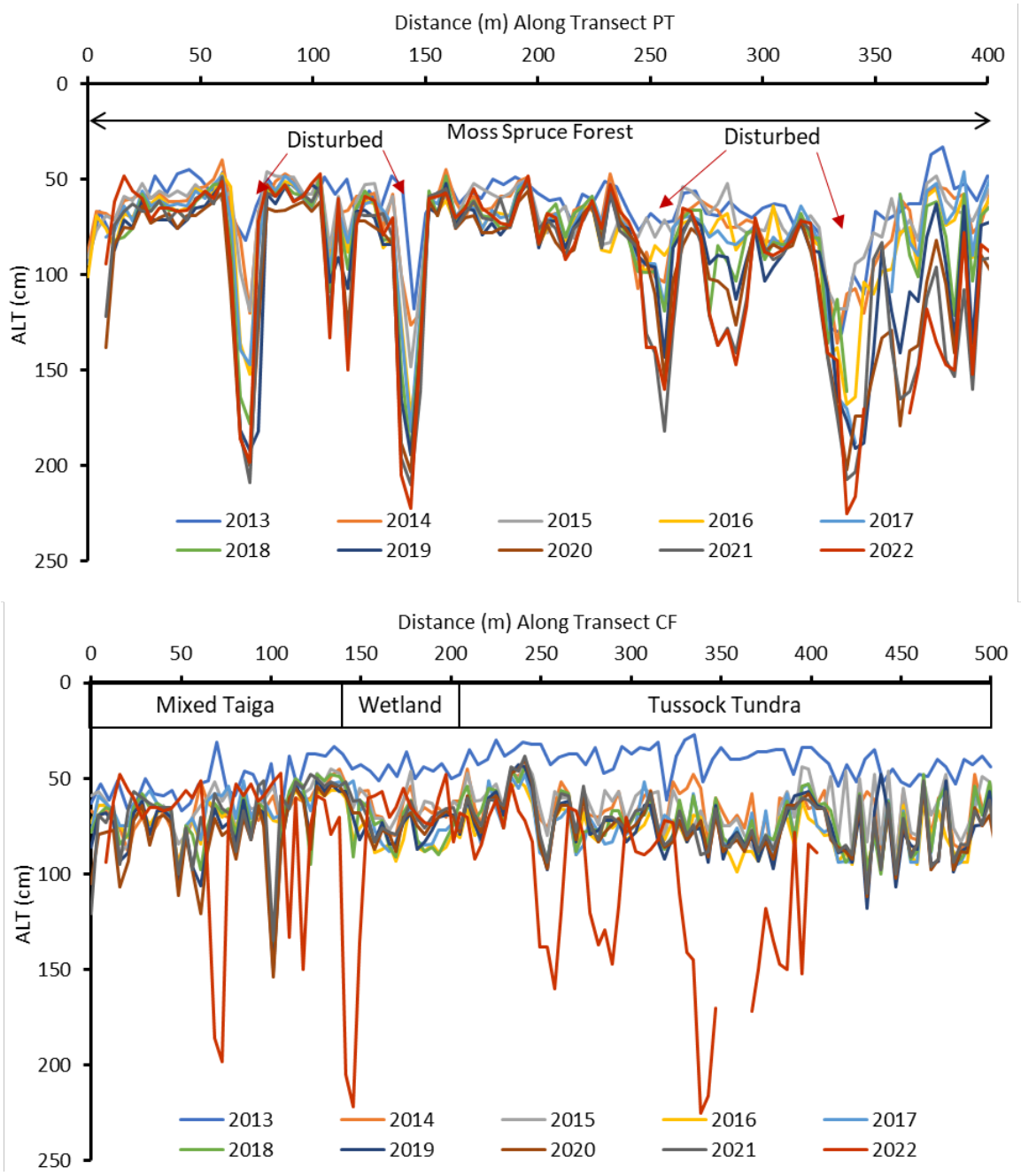

At the local scale, monitoring of soil temperatures at each of these sites display a warming trend at depth with buried sensors exceeding 0°C by 2019 or earlier in each site. Soils at 1.5 m depth in Farmer's Loop reached 0°C in the summer of 2017 (Figure 11*d*), and above-freezing temperatures reached depths as low as 1.8 m above the Permafrost Tunnel in the summer of 2021 (Figure 11*c*). In Creamer's Field, soils at 1.24 m depth ceased to freeze by 2016 and have remained unfrozen since (Figure 11*b*).

The general trends in average ALT over time tend to covary among all three sites (Figure 11*a*) demonstrating consistency in temporal controls on ALT at the regional scale. Various environmental forcings have been related to temporal controls on regional ALT such as air temperature, summer precipitation, and snow conditions (Shiklomanov et al. 2010; Loranty et al. 2018). In particular, sensible heat transfer by summer precipitation was attributed to interannual increases in ALT at these study sites by Douglas et al. (2020), with the relative degree of influence dependent on insulative properties of overlying vegetation. These meteorological conditions are plotted for the study period in Figure 12. Considering these temporal controls, projected increases in summer temperatures and precipitation at boreal latitudes (Serreze et al. 2011; Stocker et al. 2013; Zhang et al. 2013) will likely lead to the continued increase of ALT in the future. The magnitude of ALT change will likely express differently by location however, following the spatial controls on ALT mentioned above.

The notable changes in mean ALT for Interior Alaska sites represent the long-term permafrost state for the discontinuous region. Changes in ALT are less apparent in the Alaskan Arctic, where permafrost temperatures are the lowest among the study sites.

Figure 11. Mean ALT and soil temperatures for Interior Alaska sites, including (*a*) annual entire-transect mean ALT for each Cold Regions Research and Engineering Lab (CRREL) site, and soil temperatures for actively thawing sites at (*b*) Creamer's Field, (*c*) the Permafrost Tunnel, and (*d*) Farmer's Loop. Soils at each site reach 0°C or higher at depths greater than 1 m by 2021.

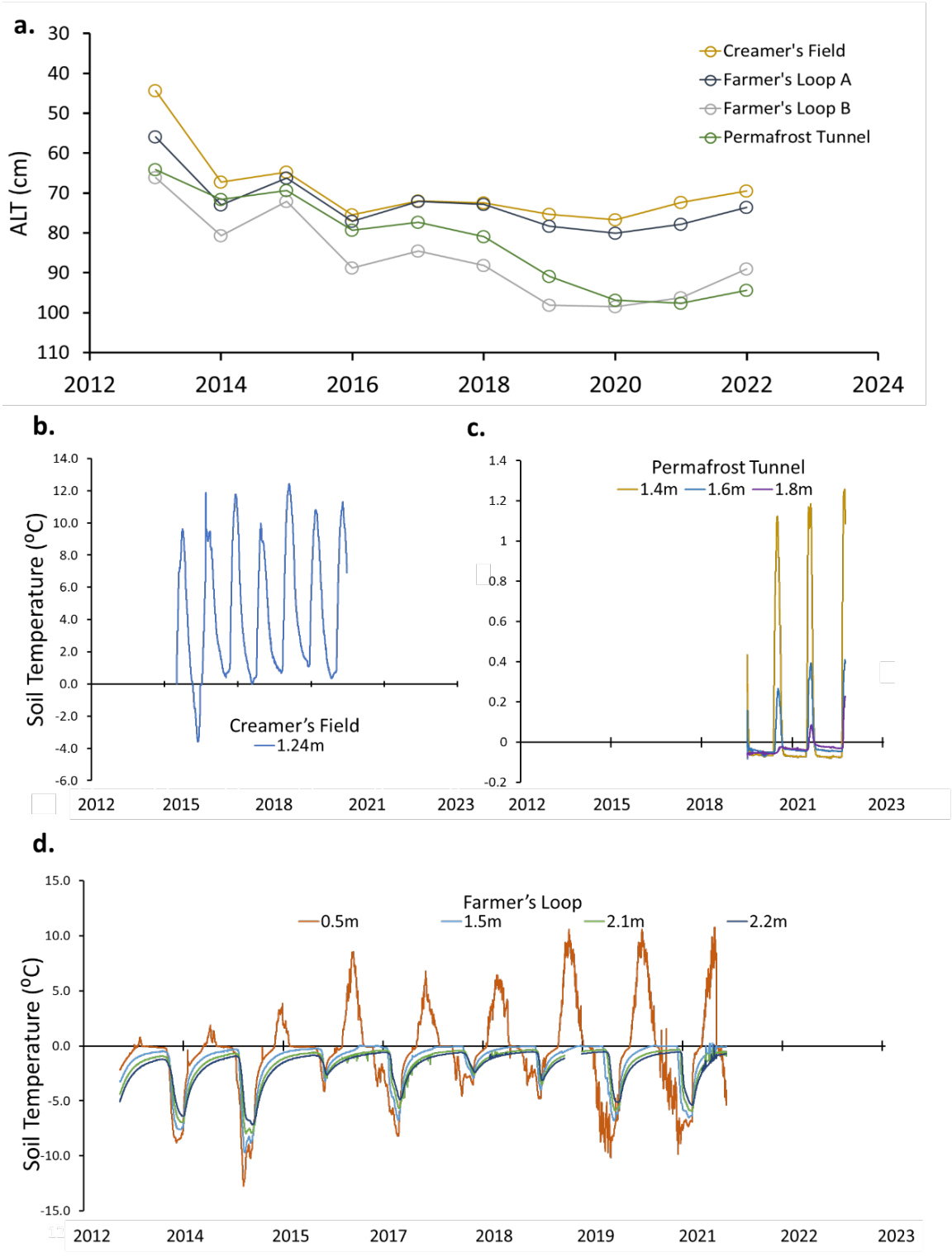

Figure 12. Annual total precipitation and mean temperature for Fairbanks, Alaska (Alaska Climate Research Center 2023), for the period of ALT record.

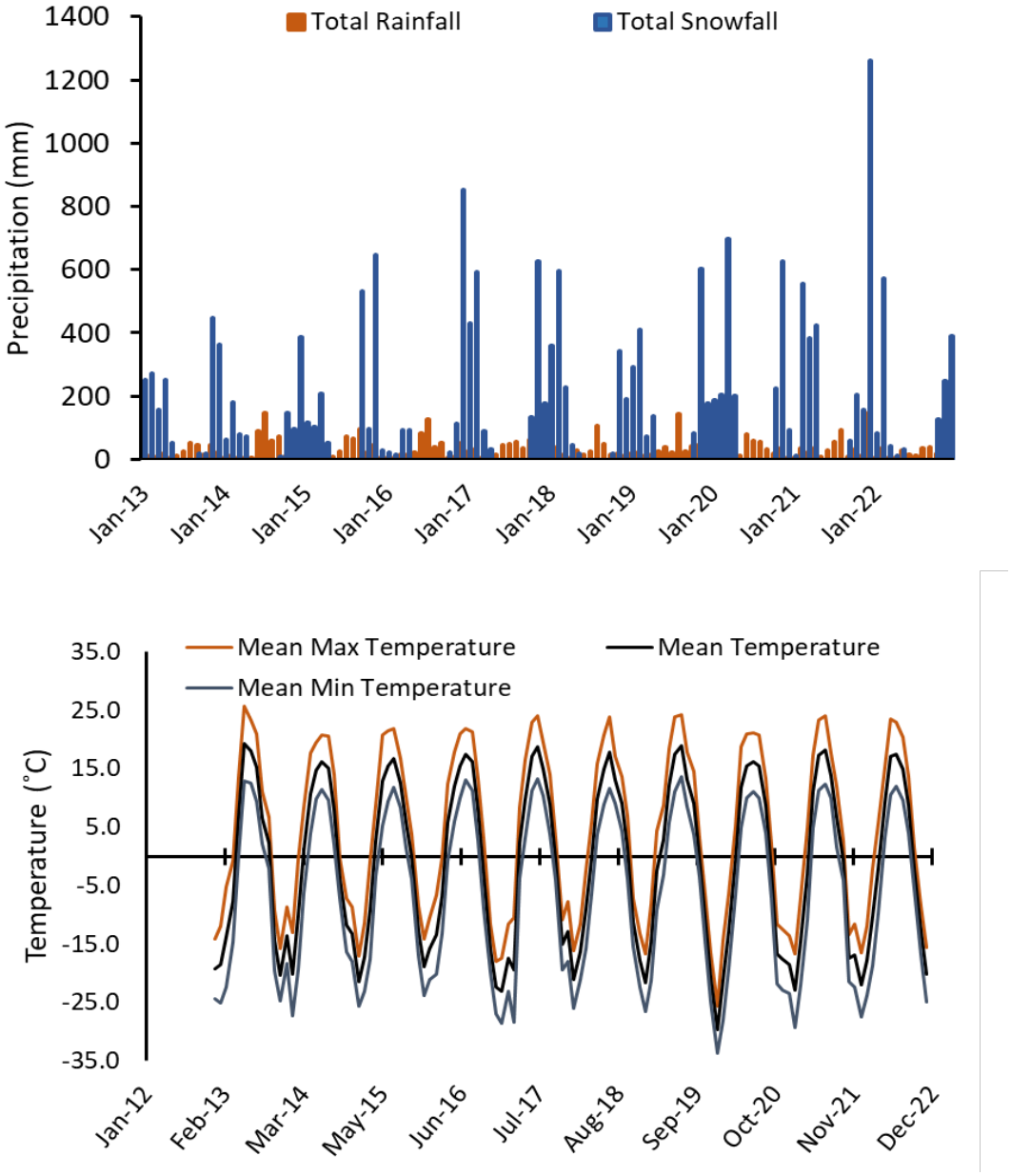

3.1.2 Continuous Permafrost Region - North Slope of Alaska

While the deepening trend in ALT for Interior Alaska from 2013 to 2022 illustrates change in the discontinuous permafrost region, ALT from sites on Alaska's North Slope represent change in lower temperature (–2°C mean at 1 m depth, Toolik Field Station) permafrost of the continuous permafrost region. Long-term ALT monitored by the CALM program was retrieved for a total of 8 sites to represent active layer changes in both the Arctic Foothills of the Brooks Range (Figure 13*a*), and the Arctic Coastal Plain (Figure 13*b*).

Figure 13. ALT averaged along transects for circumpolar active layer monitoring (CALM) sites in the Arctic Foothills (*a*) and Arctic Coastal Plain (*b*). *Dashed lines* represent trendlines for each data series.

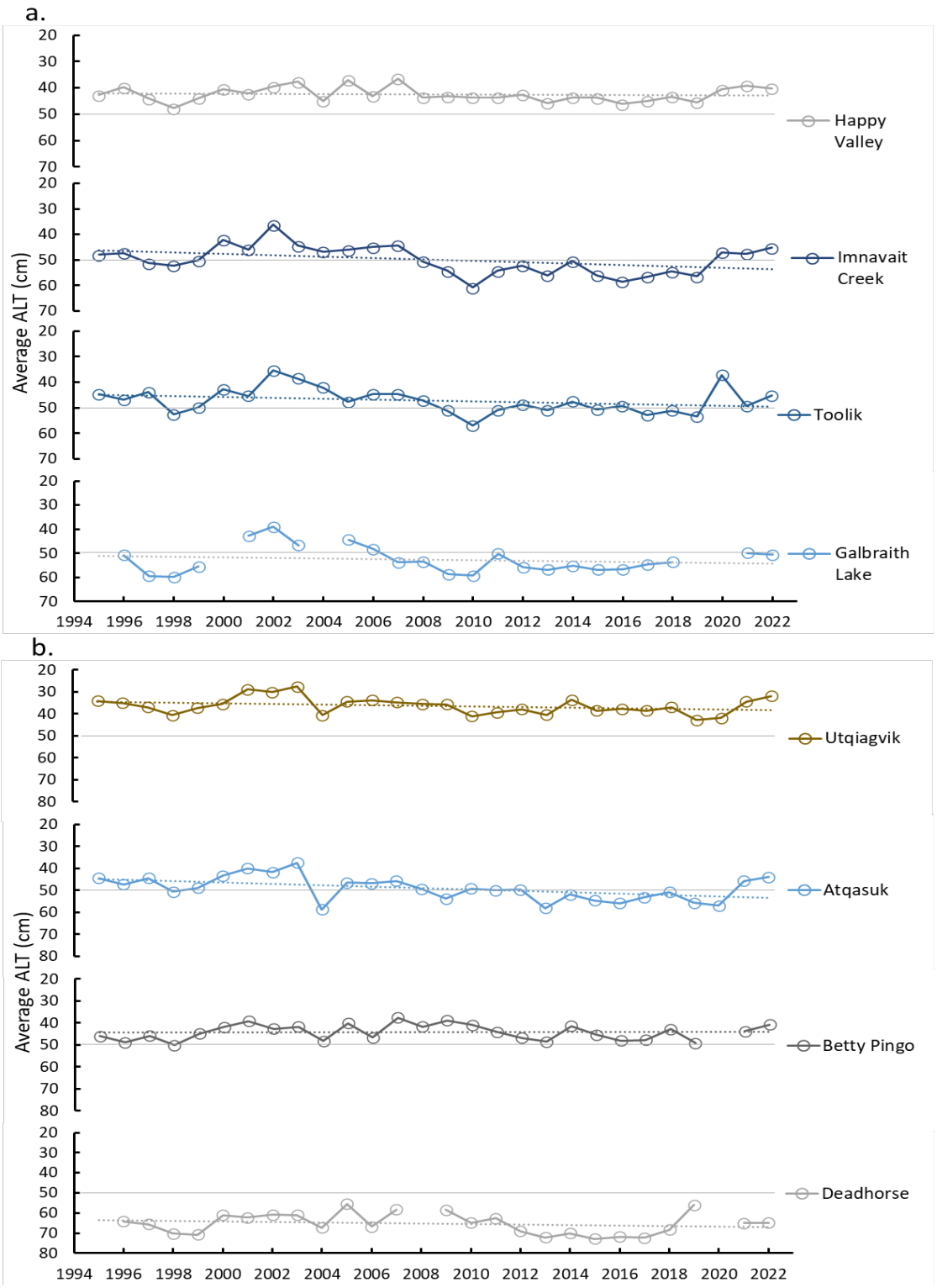

While ecotype appeared to strongly influence small-scale spatial variability in ALT for the Interior sites, ecotypes differ minimally between moist or dry sedge or shrub tundra across Foothills sites. However, ALT generally decreases with increasing distance north from the Brooks Range, with greatest overall values near Galbraith Lake, where annual mean ALT averaged at 53 cm from 1995 to 2022 (n = 23). Annual mean ALT averaged 47 cm at Toolik Lake (n = 56) and 50 cm at Imnavait Creek (n = 84) but only reached 42 cm at Happy Valley (n = 56) in the transition to the Coastal Plain. The gradient in average ALT across these sites may partially relate to the effect of increasing latitude on insolation, but other factors are evidently involved as mean ALT in Coastal Plain sites does not conform to a northward thinning gradient (Deadhorse average 65 cm, Atqasuk at 49 cm, etc.). Shiklomanov et al. (2010) evaluated the relationships between CALM-measured ALT and detailed landscape observations for Utqiaġvik on the Coastal Plain using variograms, and related ALT spatial variability with sediment texture and organic layer thickness. Therefore, the gradient of decreasing ALT with increased distance from the range front may relate to surficial geology whereas increasing distance from glacial catchments of the range results in fining texture class, which leads to lower conductivity when wet and slower thaw propagation in these areas. Precipitation patterns related to the orographic influence of the Brooks Range may play an additional role.

Despite the spatial differences in mean ALT across the sites, the temporal variability in ALT at each follows a similar pattern over the 27-year period. Temporal controls on North Slope ALT have been commonly studied and are generally attributed to soil moisture content and the geological and meteorological conditions that influence it (Hinkel and Nelson 2003; Shiklomanov et al. 2010; Luo et al. 2016), as well as influences on soil thermal properties such as air temperature and snowpack thickness (Hinkel and Nelson, 2003; Shiklomanov et al. 2010; Luo et al. 2016). Consistent with these observations, the combination of low annual temperatures and consistent snowfall in 2002 correlates with the lowest ALT values across Foothills sites (Figure 14).

Beyond interannual variability, longer-term change in ALT from 1995 to 2022 is minimal in this region. For instance, Galbraith Lake and Toolik Lake exhibit 0% change while Imnavait Creek and Happy Valley show small ALT decreases of 6%. The mean interannual change in ALT is 0 cm across these sites with a maximum thickening of 12 cm from 2020 to

2021 and maximum thinning of 16 cm from 2019 to 2020 at Toolik caused by a decreased ALT in 2020 that was not experienced elsewhere. The greatest perturbation to the stability in ALT across the region was a decrease in 2002 of 2 to 10 cm across the sites. The potential driver for this decrease is minimal top-down thaw caused by low summer temperatures in 2002 (Figure 14).

Figure 14. ALT averaged along transects for CALM sites in the Arctic Foothills of Alaska's north slope. Climate data for Chandalar Shelf (Alaska Climate Research Center 2023).

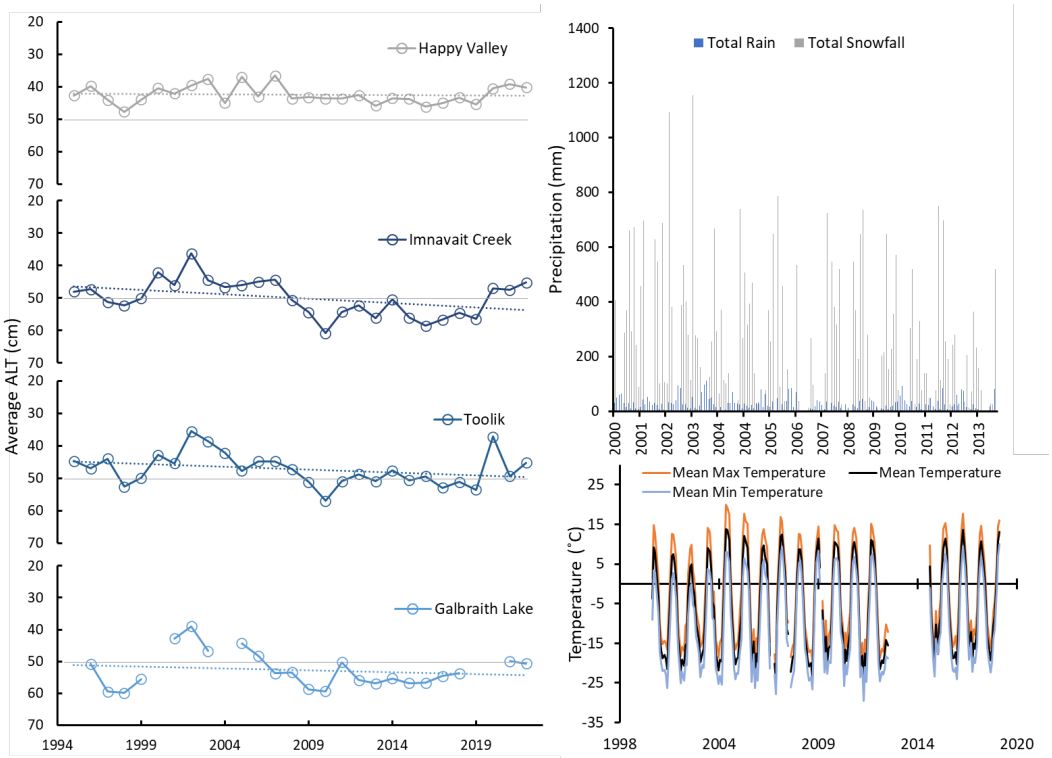

Mean ALT at sites on the Arctic Coastal Plain generally display low variability from 1995 to 2022 with the average ALT range of 17 cm for all sites (Figure 15). Interannual change averages at 0 cm for each of the 4 sites but exhibits the highest range in Atqasuk where ALT decreased 12 cm from 2004 to 2005 but increased 21 cm from 2003 to 2004, likely due to changes in surface conditions as snowfall was variable during this period. Temporal change over this period diverges by region whereas the time-series curves for Utqiaġvik and Atqasuk in the central Arctic share similar shapes, each differing from the temporal patterns of Deadhorse and Betty Pingo to the east. Comparisons of climatological data from NOAA Co-op meteorological sites (WRCC 2023) reveal similar mean annual temperatures for Utqiaġvik (–10°C) and Kuparuk (–11°C) but higher total snowfall throughout the year in Utqiaġvik as a potential mechanism.

Although ALT shows less of an apparent trend on the North Slope than in the Interior, subsidence records suggest that thaw in the last decade has potentially reached ice-rich layers at the top of permafrost for North Slope sites (Shiklomanov et al. 2010). Furthermore, the lack of ALT increase on North Slope soils may base from consolidation of active layer soils following thaw (Streletskiy et al. 2017), and it is likely that ground subsidence could lead to stable ALT measurements while the top of near-surface permafrost migrated downward (Shiklomanov et al. 2013).

Figure 15. ALT averaged along transects for CALM sites on the Arctic Coastal Plain of Alaska's north slope. NOAA Cooperative Observer Program meteorological data from Desert Research Institute Western Regional Climate Center (2023).

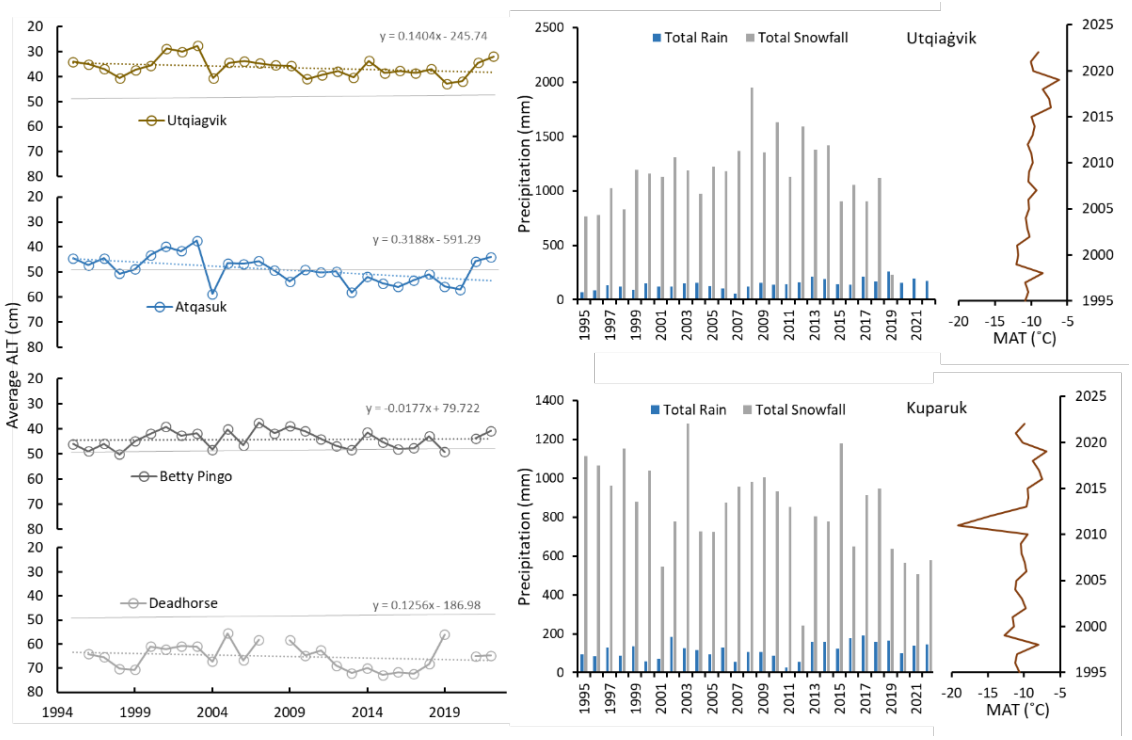

The overall low variability in ALT of North Slope sites compared to Interior sites represents different vertical extents of downward thaw propagation between the continuous and discontinuous permafrost regions, with nuances excluded by the ALT metric mentioned above. The repeat ALT measurements discussed in this section offer broadly spatially extensive coverage of active layer information but can be expanded further with machine learning approaches (see Zhang et al. 2021), or when coupled with geophysical techniques. The following section explores GPR applications for frost table detection in yet another permafrost setting, that of the Abisko Valley, Sweden, where soil temperatures are greater than Interior Alaska and permafrost is distributed more sparsely.

3.1.3 Geophysical Survey of Permafrost Distribution in Sweden

Permafrost in Abisko, Sweden, is comparatively warmer (near 0°C at 5 m depth) than the previously discussed sites of the Interior and North Slope of Alaska and has undergone much degradation and thaw in recent decades (Johansson et al. 2011). Locating the permafrost distribution and depth in the Abisko region may therefore provide an analog of permafrost distribution and conditions for Alaska in the near future. The capacity of GPR for noninvasively probing water phase contacts along the permafrost freezing front offers the capability for mapping frost table depth, or lack thereof, at the catchment scale and was applied in Abisko for this purpose.

The GPR traces either showed strong reflections at a subterranean interface between materials of contrasting permittivity, or were attenuated by excess surface moisture where present (Figure 17). The noted interface reflection may be sensitive to a number of stratigraphic contacts including (1) the organic-mineral soil contact with contrasting water content and therefore dielectric permittivity, (2) the redox boundary of soil minerals with differing porewater saturation and conductivities, (3) the groundwater table, and (4) the top of permafrost interface. The last interpretation is favored here, as the trace reflections tend to occur beneath topographic highs, suggesting potential frost mounds (surface elevated by ice content of soil beneath) or areas unaffected by thaw subsidence. Furthermore, the detected signal reflection consistently occurred at around 20 ns to 30 ns travel time, which roughly translates to 0.5 m to 1 m depth, comparable to ALT measured in the early 2000s for nearby Heliport, Kursflaket, and Mellanflaket, mires of around 50 cm to 80 cm (Åkerman and Johansson 2008). Despite the likely degradation since these reports, the ALT by Åkerman and Johansson and depth of GPR reflections from this study compare well since GPR surveys were collected in early August, likely before the thaw front reached its maximum extent for 2022. Alternatively, the detection of a shallow water table is possible, although groundwater in permafrost catchments is assumed to exist perched on the frost table (i.e., suprapermafrost baseflow) (Bense et al. 2009), making a detection of the water table roughly indicative of permafrost depth. Evaluation of the potential for the noted soil unit contacts to express in the GPR signal requires further testing and validation.

Based on the interpretation of strong signal reflections on a frost table, the collection of survey transects together show the presence or absence of permafrost detections in the study area (Figure 16 and Figure 17). As mentioned, the trace reflections of a potential frost table are limited to

topographically higher areas such as the northern 25 m of Transect 3 (A to A′) and the northern 25 m of Transect 2 (B to B′), where the GPR survey transitioned from an elevated mound near the station (A and B′), down to a saturated low area (A′ and B). The lack of potential frost table detections in the low, poorly drained area to the south of the station are either caused by signal attenuation in a more highly saturated soil medium, the absence of a frost table in this area, or some combination of the two possibilities.

Figure 16. *Top*, map of ground-penetrating radar (GPR) survey transects T1–5 near the Abisko Scientific Research Station in Abisko, Sweden. *White arrows* indicate the direction of GPR travel along each transect. *Bottom*, depths of GPR picks representing potential permafrost.

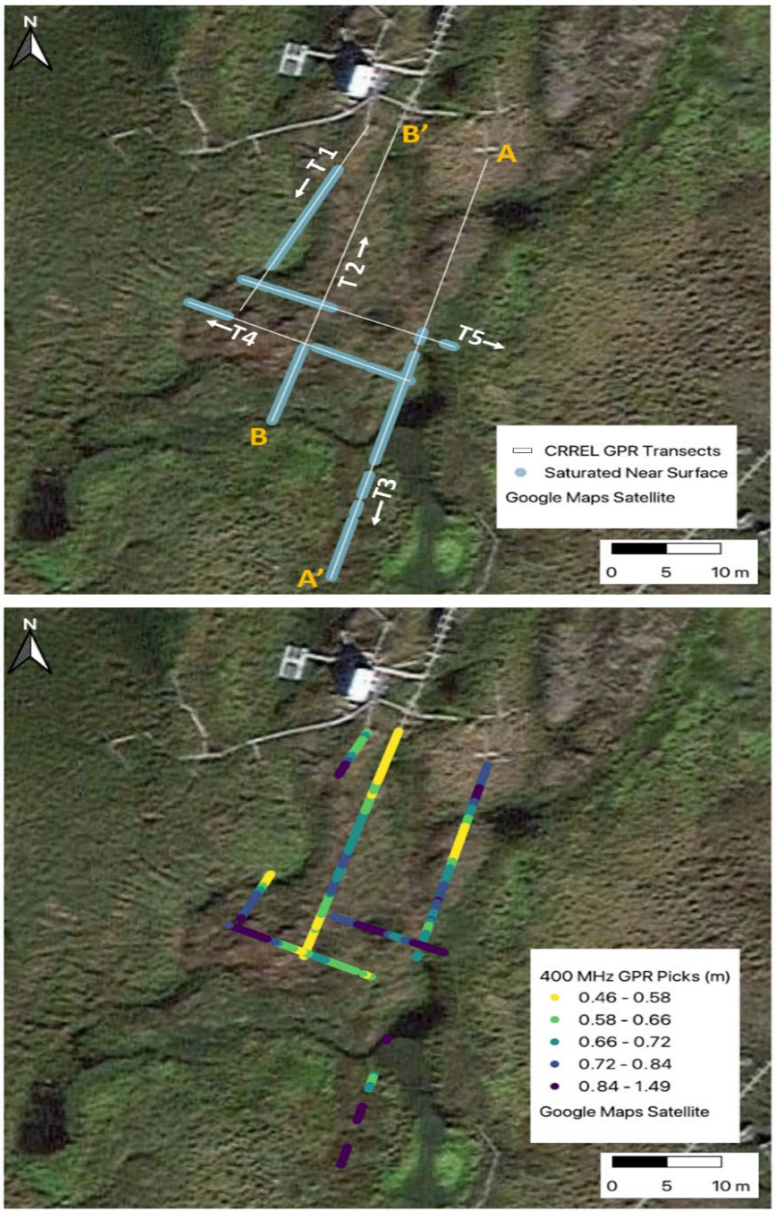

Figure 17. Annotated radargrams from transects 3 (*a*) and 2 (*b*) demonstrating example traces indicating a reflection on potential frost tables or attenuation of the radar signal due to saturated or nearly saturated conditions.

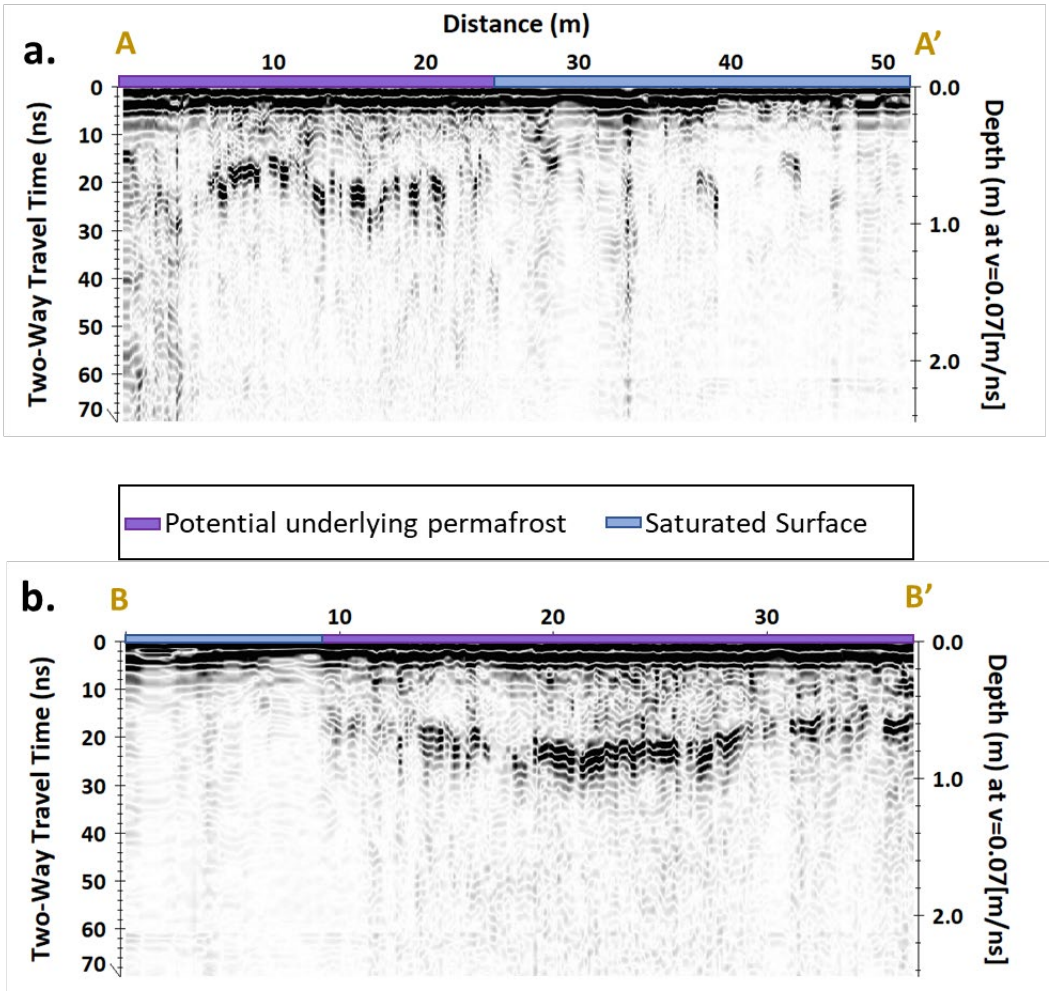

Further field validation in the Abisko field area is required to resolve ALT from GPR, because minimal calibration data were available from the time of GPR survey for evaluating the trace interpretations discussed. Manual frost probe depths taken regularly along the GPR scan paths can be used to validate whether the depth of major reflections or absence thereof cooccur with probe refusal at a frost table. In lack of this information, other causes for the radar reflection such as the organic-mineral soil interface, soil redox boundary, or the water table cannot be excluded, and further lab testing is necessary to measure the local effect of soil organic-mineral and redox boundaries on GPR signals.

Continued measurements of ALT, whether attained by manual thaw probing or GPR, will provide a consistent means for characterizing change

in permafrost depth into the future. Other techniques have developed for characterizing ALT over broad spatial scales, including use of machine learning to upscale manual ALT measurements based on biophysical controls. For an example of the application of this technique for Interior Alaska, please see Zhang et al. (2021). While ALT is a critical parameter for characterizing temporal and spatial trends in top-down permafrost thaw, ALT alone fails to represent localized effects of permafrost degradation. For instance, repeat ALT may overlook hot spots of surface change caused by thermokarst features, and fails to highlight localized biogeochemical processes and biophysical conditions in permafrost. The following section explores the application of repeat lidar for imaging surface expressions of permafrost thaw for Interior Alaska and explores various other short-term investigations of local character in permafrost-affected areas.

3.2 Short-Term Investigations in Permafrost Regions

3.2.1 Surface Change Hot Spots Viewed with Ground-Based Lidar

Repeat annual measurements of landscape-scale changes across a terrain can inform model predictions that readily assess terrain conditions. For these measurements, lidar can be extremely useful as it allows for high-resolution comparisons of ground surface elevation to illustrate zones of increased change, such as thermokarst hot spots and other degradational features, and can be employed in ground or aerial-based platforms (Kokelj and Jorgenson 2013; Rowland and Coon 2015; Douglas et al. 2016). In this study, a raster-based differencing of TLS-derived DEMs is explored to demonstrate the capability of lidar systems for change detection in permafrost terrain, where thaw-induced ground subsidence (sinking) or freeze-induced heave (rising) can commonly occur (see Barnhart and Crosby 2013; Marx et al. 2017; Anders et al. 2020 for demonstrations of point-cloud differencing in similar applications).

Differencing of TLS-derived DEMs acquired at Site A above the Permafrost Tunnel on August 2017 from that acquired on June 2017 (difference = June 2017 – August 2017) demonstrates a mean surface change of 8 cm increase (–0.08 differencing result, std. = 14 cm) over the 2017 thaw season (Figure 18). The mean heave detected largely correlates with areas outside of a thaw trough feature centered in the scan zone while positive differencing values suggestive of subsidence are mainly focused along the trough (Figure 18). The detected mean heave versus subsidence may be attributed to surface water pooling from snowmelt and summer

precipitation or expansion of the moss substrate through water absorption by the time of scan acquisition in August. Alternatively, summer heave has been observed elsewhere and is thought to occur by downward transport of water in the thawed active layer to frozen sub-adjacent active layer or the top of permafrost (Mackay 1983), although observations on this mechanism of heave suggest it is generally more subtle than that detected at the Permafrost Tunnel. False heave caused by differences in scanning position or incidence angle between scans (Marx et al. 2017) is recognized as a possibility, although scan position and incidence angle were held constant for each acquisition.

The maximum detected decreases of around 1 m occurred sporadically along the trench and most likely indicate locations of surface erosion or mass wasting, such as slumping. Difference values along the trough feature mainly indicate 0 cm to 50 cm of decrease. If interpreted as thaw-induced subsidence, these rates far exceed that detected by TLS in Arctic Canada of under 10 cm (Marx et al. 2017), although the scan location in the Northwest Territories features colder permafrost than the actively degrading ice-rich yedoma found above the Permafrost Tunnel (Péwé, 1975; Hamilton et al. 1988). Furthermore, the potential subsidence values at Site A are lower than that observed elsewhere (2 m–6 m) in Interior Alaska (Osterkamp et al. 2000). The detected differences may then be attributed to loss of excess ground ice (Shur et al. 2005), or localized erosion induced by thaw, but the influence from instrument effects caused by the differencing process should not be excluded (Marx et al. 2017; Anders et al. 2020).

Figure 18. Terrestrial Laser Scanning (TLS)–derived digital elevation model (DEM) and DEM difference maps for Site A above the Permafrost Tunnel. Positive values indicate thaw subsidence, and negative values indicate heave.

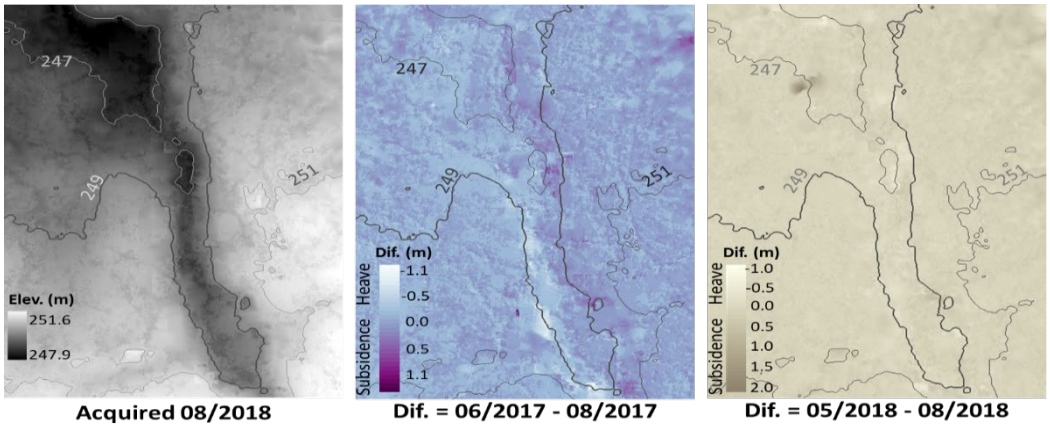

Acquired 08/2018 Dif. = 06/2017 - 08/2017 Dif. = 05/2018 - 08/2018

Differencing of the DEMs scanned May 2018–August 2018 demonstrates a mean surface change of 6 cm decrease (0.06 differencing result, std. = 12 cm) over the 2018 thaw season in contrast to 2017. However, the mean is affected by an artificial "hot spot" of 2 m subsidence that is noticeable along the thaw trench where occlusion likely resulted from a thick accumulation of deadfall under a section of drunken forest. The absence of this artefact in the 2017 scan is likely due to increased stacking of deadfall from 2017 to 2018. An artificial heave effect caused by surface water pooling may be similar for the thaw season of 2018, as summer precipitation and snowpack the preceding winter are comparable to that of 2017. Detected differences along the thaw trough display greater subsidence or loss to erosion in 2017 than that of 2018 and generally featured approximately 50 cm to 1 m of decrease in 2017 versus approximately 0 cm to 50 cm of decrease in 2018. This level of interannual variability may be expected due to differences in various physical conditions from year to year (Shiklomanov et al. 2010; Bartsch et al. 2019; Douglas et al. 2020).

For each scan at Site A, anomalous difference values were detected along the northwest periphery of the scan area where such changes are unlikely, suggesting those values were an artefact of decreased point cloud density at the limit of the scan range. These anomalies were excluded to remove their influence on the whole-scan statistics. Other effects caused by vegetation interference or occlusion may affect differencing results (Cifuentes et al. 2014; Fan et al. 2014; Anderson et al. 2018), although these effects are mitigated by the applied methodology of scanning from multiple positions and a consistent, low incidence angle (Marx et al. 2017).

At Site B, scans were performed later into the thaw season and the May 2018–October 2018 difference raster (Figure 19) produced a mean value of –12 cm (std. = 10 cm), or mean surface heave. Overall, subsidence values of around 50 cm are comparable to that of Site A. However, unlike Site A, these subsidence values were less confined to the trough feature and seem more distributed across the scan area. This may be a result of scan timing and downward thaw propagation, with thaw reaching ice-rich permafrost (Shur et al. 2005; Zwieback and Meyer 2021) by the later scanning date of October at Site B, resulting in greater widespread subsidence than that achieved outside of the trough feature in August at Site A.

Figure 19. TLS-derived DEM and DEM difference map for Site B above the Permafrost Tunnel. Positive values indicate thaw subsidence, and negative values indicate heave.

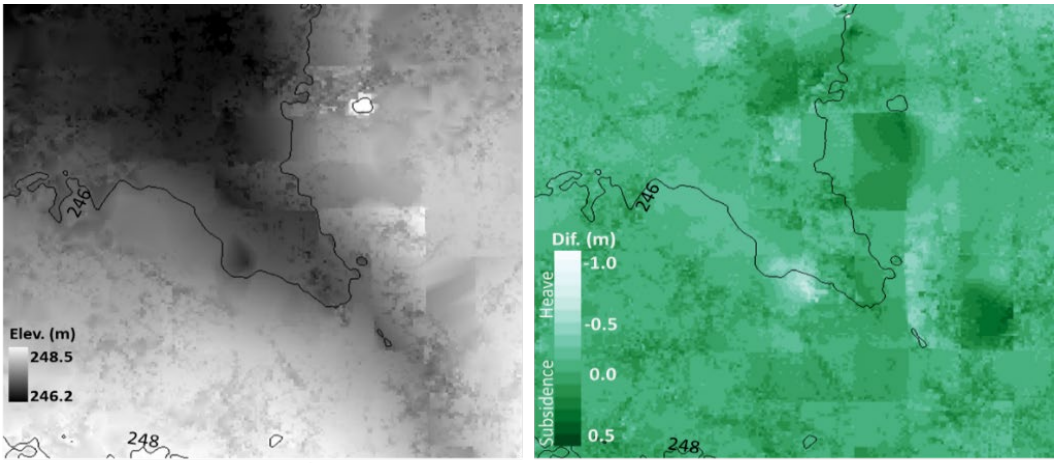

Overall, the raster-based difference maps demonstrate substantial detections of elevation differences above the Permafrost Tunnel at the seasonal scale, especially along the "hot spot" trough feature at Site A. The difference results outside of this hot spot suggest a combination of heave and subsidence values, which may partially represent differential thaw settlement (Streletskiy et al. 2017), or some degree of surface water pooling effects. Differencing over greater time scales is likely to illustrate more drastic surface changes along the thaw features as erosion continues with permafrost degradation. The application of a raster differencing used in this study is susceptible to sampling and occlusion effects as mentioned, and point-cloud differencing is increasingly applied. Marx et al. (2017) report that plausible refinement of subsidence at the millimeter scale is achievable when a point cloud difference is applied correctly. Therefore, application of point-based differencing (Eitel et al. 2016) on future scans may yield refined deformation rates above the Permafrost Tunnel.

3.2.2 Permafrost Geochemistry

Geochemical cycling and elemental transport in permafrost is heavily impacted by vertical thaw extent, as the majority of subsurface water flow occurs within the active layer (McNamara et al. 1997) where mineral weathering and mobilization of trace elements may occur (Barker et al. 2014). Likewise, elemental distributions in permafrost soils and surface waters may be suggestive of active layer processes and thaw status, and may indicate the potential for trace metal transport to surface waters. To visualize the mobility of trace metals in soils above the Permafrost Tunnel,

trace metal concentrations were quantified for bulk soils subsampled from a 100 cm SIPRE core (Figure 20). Concentrations were highest in Fe, Al, and Mg and generally decrease downcore with the most abrupt change occurring from 31 to 74 cm. Much lower concentrations were observed for Ba, Cr, Cu, Ni, Mn, and Zn, each showing a minor increase with depth before reaching 31 cm, from where concentrations begin to decrease with depth for each element.

The core was collected on 7 May 2018 when seasonal thaw extent was minimal. These concentrations therefore likely represent the vertical distribution of trace metals from the time freezing ensued the previous fall. At that time, top-down thaw would have reached its maximum extent, allowing for liquid water passage through the full active layer thickness. The concentrations of most metals were enriched near 50 to 75 cm depths, likely indicating the active zone for water transport perched above the top of permafrost, and below the top-down freezing front. Downward leaching of metallic minerals and metal complexes with increasing moisture conditions may occur as the active layer thaws, leading to the accumulation of this illuvium above the frost table, below which further downward leaching is impeded. One exception to this general distribution trend is manganese, with enriched values at the ground surface. Manganese is known to accumulate in surface soils as a result of plant uptake and release at the end of the growing season (Li et al. 2021).

Figure 20. Soil concentrations of chromium (Cr), copper (Cu), nickel (Ni), zinc (Zn), manganese (Mn), barium (Ba), aluminum (Al), iron (Fe), and magnesium (Mg) sampled from a permafrost core taken above the Permafrost Tunnel.

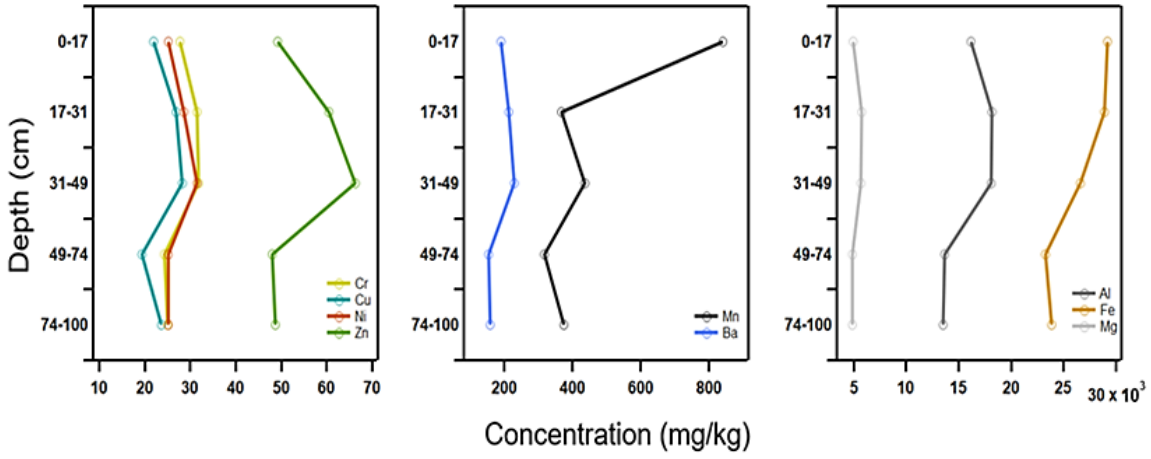

The distribution of metals along a common depth is a likely indicator of groundwater transport and redox behavior, creating the potential for trace

metal sourcing to surface waters. Given sufficient loading, large metal concentrations in surface water can impact water quality. Further analysis of metal speciation, such as ferrous versus ferric iron, will lend insight to solubility and transportability of metals throughout the soil profile, and may aid with assessing this interpretation (Barker et al. 2023).

For a detailed analysis of the effects of permafrost thaw on mineral weathering, trace metal distribution in soil, and trace metal transport to surface waters, see Barker et al. (2014) and Barker et al. (2023).

3.2.3 Microbial Community Profiling

Microbial communities in soil are structured by many environmental factors such as temperature, moisture, and vegetation (Moyano et al. 2013; Fierer 2017). Microbial community structure and function influence ecosystem-level processes such as soil strength, carbon and nutrient cycling, and plant-microbe interactions (Van Der Heijden et al. 2008; Vishwakarma et al. 2020). Permafrost thaw induced by climatic warming activates microorganisms and subsequently leads microbial communities to rearrange or assemble with new community members (Barbato et al. 2022) with major differences in metabolic processes occurring between frozen and thawed conditions (Messan et al. 2020). By applying assembly theory to the permafrost microbiome, the balance between stochastic (i.e., random) or deterministic (i.e., driven by environmental factors) processes (Ernakovich et al. 2022) can be estimated. In permafrost-affected soils in Abisko, Sweden, stochastic processes dominate immediately following thaw, before deterministic processes eventually become more prevalent (Doherty et al. 2020). This technique combined with microbial characterization of soils enable predictions of microbial community response to disturbance such as thaw. We present here various datasets of microorganism characteristics in Arctic soils.

Microbial communities were profiled at various field sites across Alaska and northern Europe from 2015 to 2023 (Table 4). In general, microbial datasets consist of replicate soil samples where microbial community structure is described as the relative abundance of an individual amplicon sequence variants (ASV) (Callahan et al. 2017) down to a particular taxonomic level depending on the best match to the sequencing database. These data were derived from high throughput marker-gene sequencing data using the 16S rRNA marker gene for profiling bacterial and archaeal communities and the internal transcribed spacer (ITS) gene for profiling

fungal communities. For a limited number of sites (e.g., the Permafrost Tunnel and Storflaket Mire, Sweden), shotgun metagenomics data were collected representing all genes of all organisms present in a soil sample, from which functional annotation of the microbial communities can be inferred. This technique enables characterization of microbial taxonomy and potential function. Microbial abundance measured via quantitative polymerase chain reaction (qPCR) was determined for several sites. Extracellular enzyme activity and soil respiration was measured across different temperatures and moistures for some of the soils collected.

Microbial datasets were often accompanied by measurements of soil properties (e.g., pH, gravimetric water content, and organic matter content). Bulk soil collected from some of the field sites was characterized by generating water retention curves for various lab experiments. These curves describe the relationship between soil water content and the force with which water is held in soil pores.

Geospatial visualization of soil microbial datasets is limited and primarily includes taxonomic identity of community members as static points in time. This is largely due to the limited understanding of microbial community equilibrium through time, resiliency after disturbance, and ability to extrapolate point observations across space. Information regarding microbial community structure and function could provide Army operations with awareness of environmental threats or microbial contributions to physical properties in the terrain. Included in the final section of this report is a conceptualized spatial visualization of a microbial dataset (Figure 21). The relative abundances of the top taxa are shown for a given timepoint that the soil was last analyzed. Similar visualizations of microbial community function could be applied at various locations across the Arctic.

Figure 21. Conceptual diagram of geospatial visualization of microbial community data across field sites.

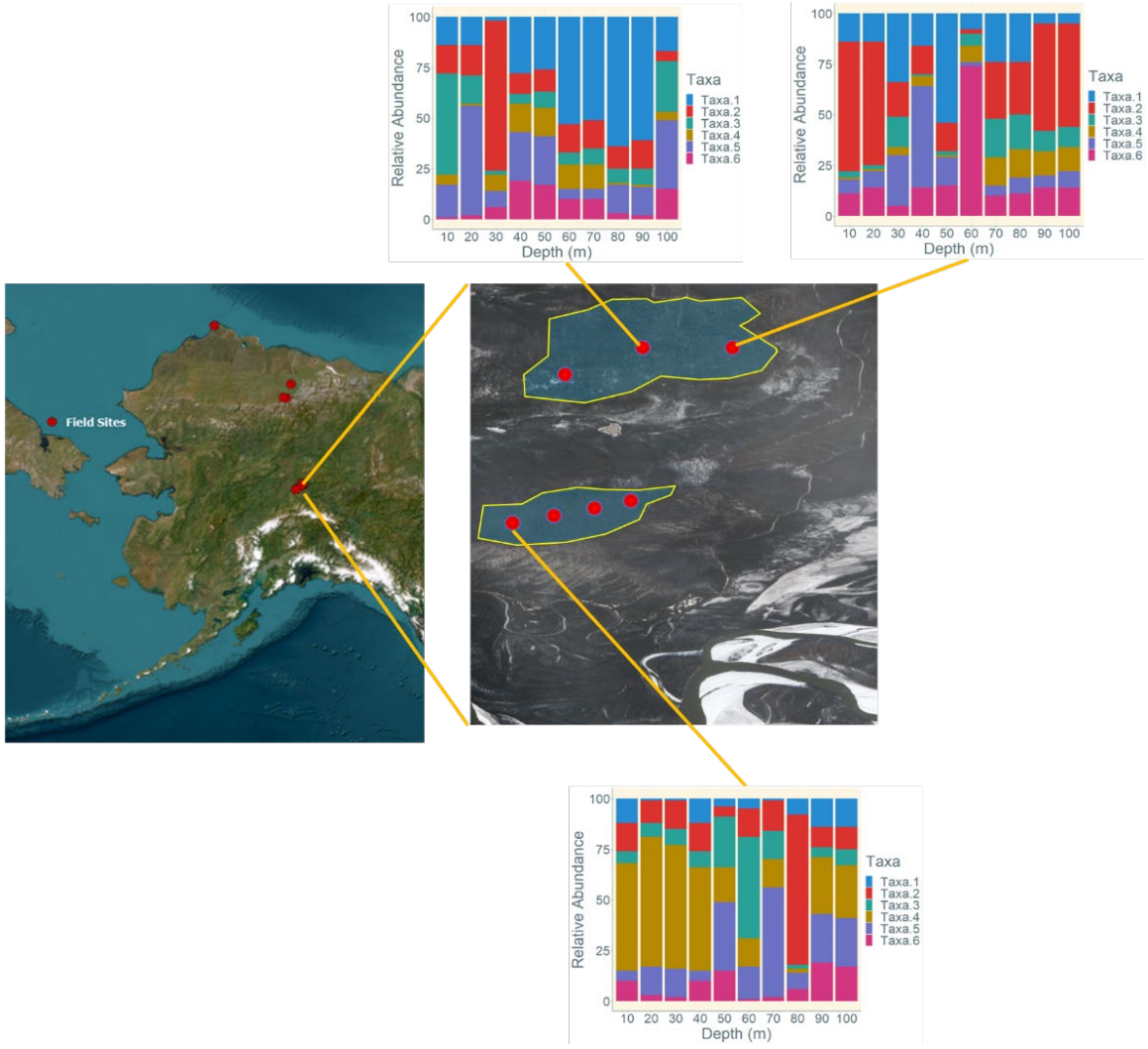

Table 4. Collection of microbiological datasets, sampling efforts, and publications associated with this study.

Sampling Site	Data Category	Sample Type	Dataset Details	Initial Sampling Date	Latest Sampling Date	Related Publication
Utqiagvik, AK	Soil, Microbial	surface soil	amplicon sequencing - bacterial and fungal communties	2015	2018	Barbato et al., 2017
Utqiagvik, AK	Soil, Microbial	surface soil	qPCR - bacteria, fungi, petroleum degradation genes	2015	2018	Barbato et al., 2017
Utqiagvik, AK	Soil	surface soil	soil properties - gravimetric water content, organic matter content, pH	2015	2018	Barbato et al., 2017
Utqiagvik, AK	Soil	surface soil	petroleum chemistry - aromatic, aliphatic, VOC, BTEX, GRO, DRO, RRO*	2015	2018	Barbato et al., 2017
Utqiagvik, AK	Soil, Microbial	surface soil	amplicon sequencing - bacterial and fungal communties	2015	2018	Barbato et al., 2017
Utqiagvik, AK	Soil, Microbial	surface soil	qPCR - bacteria, fungi, petroleum degradation genes	2015	2018	Barbato et al., 2017
Utqiagvik, AK	Soil	surface soil	soil properties - gravimetric water content, organic matter content, pH	2015	2018	Barbato et al., 2017
Utqiagvik, AK	Soil	surface soil	petroleum chemistry - aromatic, aliphatic, VOC, BTEX, GRO, DRO, RRO	2015	2018	Barbato et al., 2017
Utqiagvik, AK	Soil, Microbial	permafrost	amplicon sequencing - bacterial and fungal communties	9/24/2018	9/26/2018	
Utqiagvik, AK	Soil	permafrost	soil properties - gravimetric water content, organic matter content, pH	9/24/2018	9/26/2018	
Interior AK	Soil, Microbial	surface soil	soil heterotrophic respiration from lab incubation	2018	2018	
Interior AK	Soil	surface soil	water retention curve	2018	2018	
Interior AK	Soil	surface soil	soil properties - carbon, nitrogen, particle size, soil texture, pH, phosphorus, potassium, magnesium, GWC, WHC	2018	2018	
Interior AK	Soil, Microbial	surface soil	extracellular enzyme activity	2018	2018	
Interior AK	Soil, Microbial	surface soil	amplicon sequencing - bacterial and fungal communties	2018	2018	

Table 4 (cont.). Collection of microbiological datasets, sampling efforts, and publications associated with this study.

Fairbanks, AK	Peat, Microbial	peat	amplicon sequencing - bacterial and fungal communties	2015	2016	
Fairbanks, AK	Peat, Microbial	peat	extracellular enzyme activity	2015	2017	
Fairbanks, AK	Peat	peat	soil properties - gravimetric water content, pH, Eh	2015	2017	
Fairbanks, AK	Peat, Microbial	peat	amplicon sequencing - bacterial and fungal communties	2015	2016	
Fairbanks, AK	Peat, Microbial	peat	extracellular enzyme activity	2015	2017	
Fairbanks, AK	Peat	peat	soil properties - gravimetric water content, pH, Eh	2015	2017	
Fairbanks, AK	Peat, Microbial	peat	amplicon sequencing - bacterial and fungal communties	2015	2016	
Fairbanks, AK	Peat, Microbial	peat	extracellular enzyme activity	2015	2017	
Fairbanks, AK	Peat	peat	soil properties - gravimetric water content, pH, Eh	2015	2017	
Fairbanks, AK	Soil, Microbial	surface soil	amplicon sequencing - bacterial and fungal communties	2021	2021	
Fairbanks, AK	Soil, Microbial	surface soil	soil heterotrophic respiration from lab incubation	2021	2021	
Fairbanks, AK	Soil	surface soil	water retention curve	2021	2021	
Fairbanks, AK	Soil	surface soil	soil properties - carbon, nitrogen, particle size, soil texture, pH, phosphorus, potassium, magnesium, GWC, WHC	Fall 2020	Fall 2020	
Fairbanks, AK	Soil, Microbial	permafrost	shotgun metagenomes from 5 locations - microbial community and function, frozen and thawed	2017	2017	Barbato et al., 2022
Fairbanks, AK	Soil	permafrost	soil properties from 5 locations - gravimetric water content, organic matter content, pH	2017	2017	Barbato et al., 2022
Fairbanks, AK	Soil, Microbial	surface soil	amplicon sequencing - bacterial and fungal communties	2021	2021	
Fairbanks, AK	Soil, Microbial	surface soil	soil heterotrophic respiration from lab incubation	2021	2021	

Table 4 (cont.). Collection of microbiological datasets, sampling efforts, and publications associated with this study.

Fairbanks, AK	Soil	surface soil	water retention curve	2021	2021	
Fairbanks, AK	Soil	surface soil	soil properties - carbon, nitrogen, particle size, soil texture, pH, phosphorus, potassium, magnesium, GWC, WHC	Fall 2020	Fall 2020	
Abisko, Sweden	Soil, Microbial	1 m depth profile	amplicon sequencing - bacterial and fungal communities, frozen and thawed	2019	2019	Doherty et al., 2020
Abisko, Sweden	Soil	1 m depth profile	soil properties - gravimetric water content, pH, carbon content, nitrogen content	2019	2019	Doherty et al., 2020
Abisko, Sweden	Soil	1 m depth profile	shotgun metagenomes - microbial community and function, frozen and thawed	2019	2019	Doherty et al., 2020
Interior AK	Soil, Microbial	permafrost	amplicon sequencing - bacterial and fungal communties	10/1/2018	10/1/2018	
Interior AK	Soil	permafrost	soil properties - gravimetric water content, organic matter content, pH	10/1/2018	10/1/2018	
Interior AK	Soil, Microbial	permafrost	amplicon sequencing - bacterial and fungal communties	9/28/2018	9/28/2018	
Interior AK	Soil	permafrost	soil properties - gravimetric water content, organic matter content, pH	9/28/2018	9/28/2018	
Fairbanks, AK	Soil, Microbial	permafrost	amplicon sequencing - bacterial and fungal communties	2017	2017	
Fairbanks, AK	Soil, Microbial	permafrost	shotgun metagenomes - microbial community and function, frozen and thawed	2017	2017	
Fairbanks, AK	Soil	permafrost	soil properties - gravimetric water content, organic matter content, pH	2017	2017	
Interior AK	Soil, Microbial	1 m depth profile	amplicon sequencing - bacterial and fungal communties	2019	2019	Baker et al., 2023
Interior AK	Soil	1 m depth profile	soil properties - gravimetric water content, organic matter content, pH	2019	2019	Baker et al., 2023
Interior AK	Soil	1 m depth profile	soil metal concentrations	2019	2019	Baker et al., 2023

*VOC (volatile organic compounds), BTEX (benzene toluene ethylbenzene xylenes), GRO (gasoline range organics), DRO (diesel range organics), RRO (residual range organics), GWC (gravimetric water content), and WHC (water holding capacity).

3.2.4 Root Strength

The preceding subsections explored biogeochemical variables associated with permafrost conditions that can be indicative of change over time. This section instead summarizes the results on vegetation root strength as a control on soil strength of permafrost soils in the boreal forest region of Alaska.

Shear vane samples were tested for the various ecotypes of the Farmer's Loop and Creamer's Field study sites to represent variability in the boreal forest biome. 905 shear vane samples from conifer forest cover produced a mean of 30.58 KPa (standard error = 3.95), while 700 samples for mixed canopy forest averaged at 46.07 KPa (standard error = 6.03), potentially due to the greater presence of woody shrub and grass understory in mixed canopy taiga versus coniferous canopy understory. The highest root strength values observed were in tussock tundra, where 420 shear vane samples were collected between tussock mounds, producing a mean of 47.91 KPa (standard error = 8.12). Together, these results suggest greatest ground surface integrity in tussock fields, although the rugged microtopography of these ecotypes makes them nearly impassible. Among the forested taiga ecotypes, ground surface strength is likely greater under mixed canopies, due to higher shear vane values.

The shear vane data are important parameters to consider when informing models of surface stability in each of these ecotypes, ultimately assisting with terrain condition projections in the future. The last environmental control on surface conditions discussed in this study, is snowpack depth, as snow can create immediate challenges to ground mobility during winter months at boreal latitudes, and over longer periods in the Arctic.

3.3 Temporal and Spatial Trends in Snowpack Depth

Snowpack can be highly variable in boreal forest ecosystems, largely due to vegetation cover (Douglas and Zhang 2021), causing spatially heterogenous challenges to ground transportation. The depth and distribution of snowpack also relates to snow water equivalent (SWE) which is not only used to project water resources (Jonas et al. 2009; Sturm et al. 2010; Hill et al. 2019) but may assist in anticipating areas prone to surface saturation upon spring runoff, with ramifications for assessing spring-time operations. Understanding the distribution of snowpack and potential controls can

therefore enhance both operations planning and water resource studies in northern regions.

Repeat annual snow depth measurements at long-term CRREL survey transects have produced 9–10 years of data for the Interior Alaska sites to date. Temporal variability in transect-averaged snow depths throughout this period follow similar patterns across the sites (Figure 22) which is expected given meteorological controls on snow accumulation versus loss at the regional scale. As discussed in Douglas and Zhang (2021), Fairbanks experienced the warmest winter on record in 2015–2016 which currently remains true and correlates with the lowest measured snow depths across the sites. Conversely, the 2017–2018 winter temperatures fell below the 2013–2022 mean of –11°C, and snow depths were approximately 40 cm greater than the preceding winter (nearly double) across sites. From the 2019–2020 winter to March 2023, winter temperatures remained at or below the mean minimum temperature of –13°C for the study period and total snowfall averaged above the period of study mean of 237 mm. During this timeframe the transect-averaged snow depth exceeded the local averages in Creamer's Field (mean = 60 cm, exceeded 2019-2020 and 2020–2021), Farmer's Loop (mean = 67 cm, exceeded 2019–2020, 2020–2021, and 2021–2022), and at the Permafrost Tunnel (mean = 62 cm, exceeded 2021–2022 and 2022–2023), together demonstrating a general increase in snowpack thickness over the last 10 years. However, given the century-scale trend in increased winter temperatures for Fairbanks (Wendler and Shulski 2009), a trend towards shorter and milder winters is expected to continue (Littell et al. 2018; Lader et al. 2020) with the potential for increased ablation or altogether altered snow accumulation patterns (McAfee et al. 2014; Winski et al. 2017).

While annual weather strongly influences the mean snowpack thickness across sites interannually, spatial variability in snow depth within sites tends to correlate with ecotypes present along the transects (Douglas and Zhang 2021). Figure 23 displays these ecotype-snow depth relationships that continue to support the patterns identified in Douglas and Zhang (2021), with the deepest snowpacks generally observed in tussock tundra that lacks continuous canopy cover to intercept snow. Coniferous forest, mainly dominated by spruce, supports nearly comparable snowpack to tussock tundra, with prior studies relating small-scale variability in the coniferous forest snowpack to tree density as a barrier to wind redistribution (Hedstrom and Pomeroy 1998; Pugh and Small 2013). In

these environments troop mobility can undergo significant hinderance by the combination of dense tree cover with deep snow.

Figure 22. Transect-averaged snow depths along the interior-Alaska survey transects for the period of record (*top*) and meteorological data from Fairbanks, Alaska. (Data from Alaska Climate Research Center 2023.)

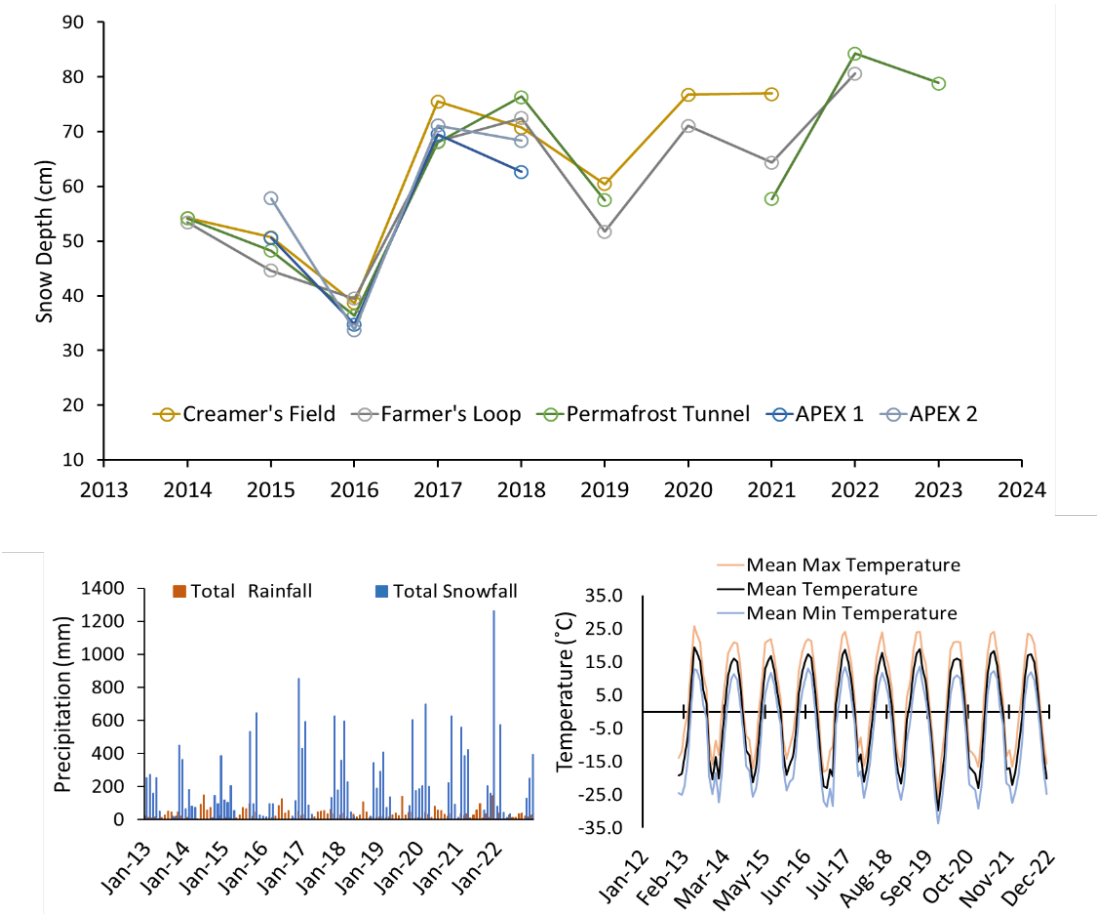

Transect extents passing through wetland had slightly lower snow depths than those passing through tussock fields and spruce forest (Figure 23), likely due to their sporadic cover of black spruce (*P. mariana*), tamarack (*Larix laricina*), and various shrubs (*Rhododendron* sp. *Vaccinium uliginosum*) creating inconsistent cover for wind protection and canopy interception across space. Overall, mixed canopy forest supported the shallowest snowpack as multiple levels of tree and shrub canopy and dense shrub cover beneath deciduous trees may store intercepted snow for long periods, where it may sublimate instead of contributing to the snowpack (Essery et al. 2003; Pomeroy et al. 2012; Douglas and Zhang, 2021).

In addition to impacting surface trafficability, the seasonal snowpack can influence the thermal regime of underlying soil (Zhang et al. 2001; Stieglitz et al. 2003), as early-season snowpack can affect shallow permafrost temperatures during winter months (Yi et al. 2019; Jan and Painter 2020). Early winter snowpack can reduce winter refreeze of active layer soils and has been identified as a control on microbial decomposition potentials through arctic winters (Ricketts et al. 2016). Therefore, the anticipated alterations to winter precipitation patterns across Alaska and the global Arctic hold the potential of impacting active layer refreeze and high-latitude carbon storage.

Snowpack thickness is furthermore an essential consideration for water resource studies as SWE calculations from remote sensing radar platforms require accurate snow depths (Deeb et al. 2011). Depending on the densities of snowpack layers, SWE is expected to be highest for deeper snow depths in the boreal biome (Sturm et al. 2010), which may result in the greatest surface water content in tussock tundra and conifer forest following spring melt, potentially degrading the integrity and particle cohesion of surface soils in these ecotypes seasonally.

Various methods are in development for measuring snowpack thickness and SWE, including various satellite-based remote detection instruments (e.g., Liu et al. 2013; Wang et al. 2020), airborne systems (NASA SnowEx Alaska campaign), and GPS reflectometry (Boniface et al. 2015; Jin et al. 2016; Larson 2016). Continued manual measurements of snowpack thickness along these transects will allow for robust ground truth information for developing snow depth algorithms and will allow for refined modeling of the controls on snow depth in boreal forest environments. Furthermore, the spatial relationships between snowpack depth and biophysical settings have been exploited to upscale these manual point measurements. For recent applications of machine learning in upscaling these point measurements of snow depth to the landscape scale, see Douglas and Zhang, (2021).

Figure 23. Snow depths along the CRREL transects at Farmer's Loop (*a* and *b*) and Creamer's Field (*c*) from 2014 to 2020.

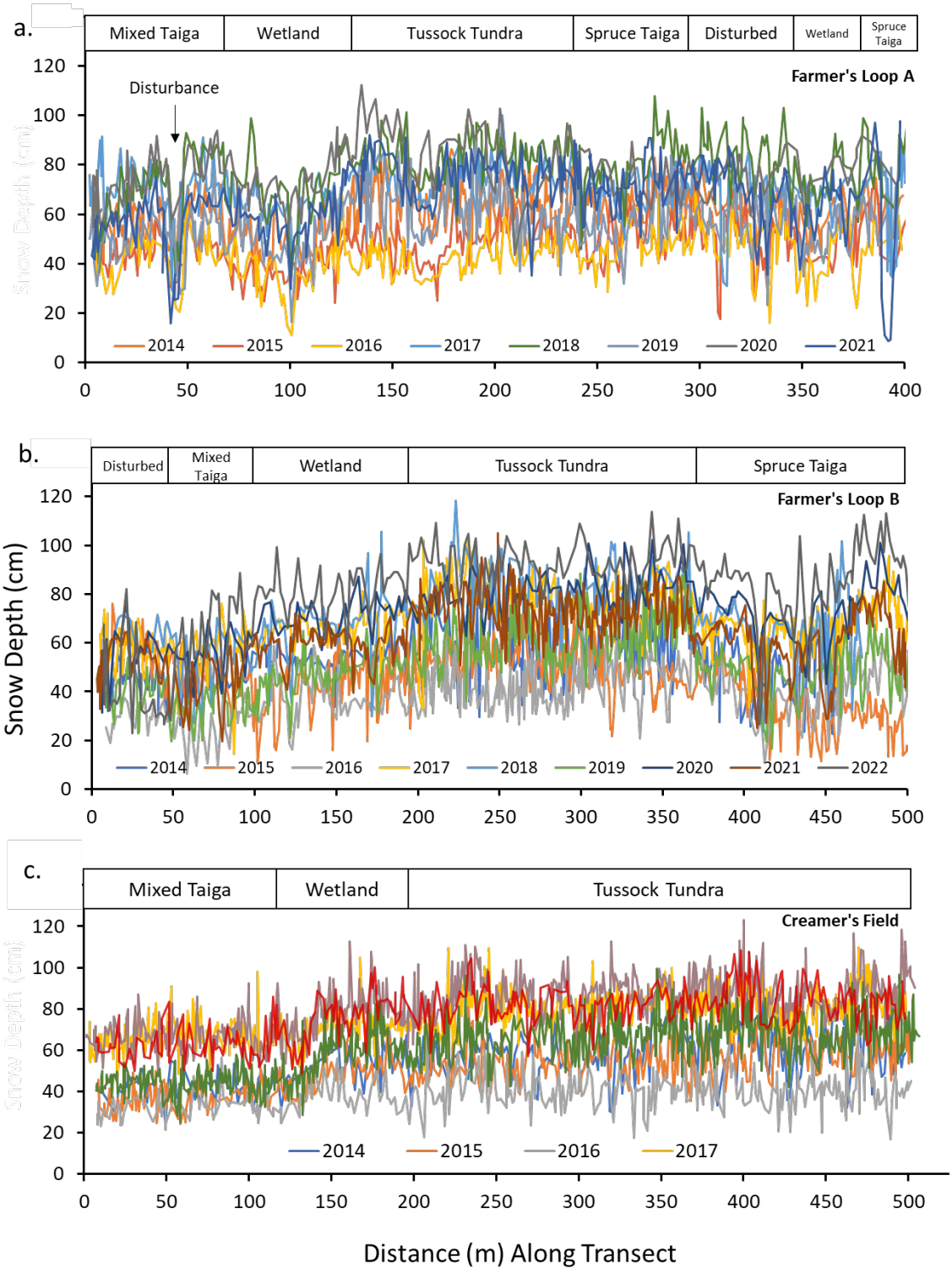

3.4 Data Visualization and Management for Arctic Field Site Collaboration

Geospatial data visualization has proven useful in all stages of the project timeline, from early site scouting to field-based digital data recording late in the iteration stages. The logistical challenges involved with reaching arctic and boreal field sites necessitates well-planned field campaigns, including the review of accurate geospatial information when selecting field sites and the capability to access this information when in the field. This allows researchers to make changes when necessary, or even to digitally record spatial observations in a geospatially explicit format. Additionally, in collaborative studies, managing spatial data as shapefiles makes sharing and updating files in collective access possible.

Offline access to shapefiles in the field has proven particularly useful as it offers conveniences that enhance field work efficiency and sampling accuracy. In site scouting and planning stages, polygon shapefiles containing information about land administration agencies (USDOI 2022) and soil taxonomic groups (USDA, n.d.) were acquired from the respective agency geospatial hubs and made available for offline use in AGOL prior to field sampling. This allowed researchers to refer to maps of land ownership and soil types when choosing sampling locations. The built-in GPS capability of mobile devices allowed for real-time positioning within the shapefiles for accurate reference to the polygon units. During the field sampling stage, the field-based mapping capability of ArcGIS mobile apps is useful for simultaneously recording the location of survey points as vector features while digitally recording observations as attribute text. This saves the steps of digitizing hand-written field notes and transferring GPS coordinates into map points.

In addition to collecting spatial data in real time as noted above, results from lab analyses may be entered into the geospatial environment through file conversion from tabular results to attribute information. Subsequent spatial visualization of analytical results can then be viewed in the field to inform sampling or to supplement new observations. For example, a conceptualized microbial community composition demonstrated in Figure 21 is linked to survey locations to make spatial trends and relationships clear. In the case of this example, multiple vector files representing multiple sampling dates and their respective community profiles would allow for easier comparisons of community structure and distribution

through time. Viewing this data in remote field settings would allow an operator to refer to the distribution of microbial communities for a greater awareness of microbial contributions to physical terrain properties such as soil strength.

Shapefiles linking spatial information to survey or potentially analytical results are easily shared amongst collaborators for geospatial visualization in GIS and export to tabular formats for use in other programs. However, the benefits of these digital methods are met with the limitations of operating mobile devices in field settings, such as battery life, processing speed, storage capacity, and device durability. Therefore, these limitations should be recognized and accounted for (external batteries, waterproof cases, etc.) before preparing to rely on mobile mapping and data collection platforms.

4 Recommendations and Conclusions

4.1 Recommendations

The accuracy and reliability of terrain predictions depend closely on the diversity of field observations and their linkage to controls. Due to logistical challenges and time constraints, not all methods were performed for each site, inhibiting straight across comparisons of all methods for each region. A standardization of repeat measurement parameters across sites may prove necessary in order to enhance comparisons across regions.

Continuation of long-term monitoring and enhanced spatial coverage of sites in future studies will allow for better isolation of controls on terrain conditions and illustration of trends, ultimately improving projections of land conditions to unknown areas. Recommended work for the future includes the following:

- Continued monitoring of ALT and snow depth on long-term CRREL survey transects
- Linkage of ALT with surface moisture conditions in various geological, topographical, biological, and hydrological settings
- Development of repeat GPR surveys of ALT at the catchment scale in representative boreal and tundra study sites
- Laboratory experiments to determine the effect of site-specific soil organic content and redox state on soil dielectric permittivity and resistivity
- Time-lapse implementation of ERT to monitor changes in subsurface water phases in permafrost regions
- Further exploration of the implementation of TLS and other lidar platforms in accurately characterizing surface change
- Continued monitoring of surface elevation above the Permafrost Tunnel and in other Army training lands with TLS to characterize change over time
- Modeling of soil biogeochemical processes that impact terrain state
- Monitor soil and freshwater biogeochemistry in permafrost catchments to visualize changes over time and evaluating relationships between freshwater geochemistry and permafrost degradation
- Model terrain conditions based on observations made in this study, followed by field validation of their accuracy

- Enhance projections of how, where, when, and at what rates future climate change will affect terrain state conditions
- Test the applicability of detailed datasets from Interior and Arctic Alaska to serve as analogs for other boreal and arctic regions
- Develop geospatial analyses and machine learning frameworks that can allow ingestion of new datasets, particularly where repeat measurements are made annually
- Broad application of aerial-based remote sensing measurements in all seasons
- Develop a streamlined integration of remotely sensed and ground-based measurements into near real-time geospatial displays for warfighter and land manager use

4.2 Conclusions

As US Army operations continue to evolve in cold regions, the importance of terrain analysis will grow in suit. Applications of satellite, manned aircraft, and unmanned aerial systems, and remote sensing are leading to near real-time assessment of terrain surface conditions. However, before recently acquired data can be used to project terrain conditions over space and time, the relationships between remotely sensed and field-based measurements must be well synthesized. This report highlights methods for characterizing critical parameters that are influential on terrain conditions including permafrost characteristics, ground surface topography, and snowpack thickness. The primary focus is directed to Interior and Arctic Alaska permafrost terrains that are experiencing increased interest for Department of Defense training and infrastructure development. As high latitudes continue to warm, the seasonal uncertainties in terrain state conditions will continue to pose new challenges. In response, this report identifies a variety of field and laboratory measurements that establish a broad baseline for translating remote assessments into high-resolution understanding of local permafrost, vegetation, and snow conditions.

Temporal trends in ALT were noticeable at the regional scale while spatial trends were identified at the local scale and are likely influenced by land cover. A long-term trend of ALT deepening was noticeable for warmer soils of the Interior Alaska sites, but colder soils of Alaska's North Slope demonstrated little ALT change over the study period. In the warm and nearly sporadic permafrost of the Abisko Valley, Sweden, GPR surveys

near the research station demonstrated a snapshot of potential permafrost distribution in the area, with possible signal reflections from frost tables generally restricted to topographically higher areas. Alterations to surface elevation related to permafrost degradation were explored through TLS surveys which demonstrates potential for characterizing surface change over various spatial scales and identifying thermokarst hot spots such as the actively subsiding trough above the CRREL Permafrost Tunnel. Snowpack depths demonstrated a consistent temporal variability across Interior Alaska sites and spatial variability with relationship to land cover types, likely as a control on canopy interception of falling snow and barriers to wind redistribution. Each of these observations can inform models of terrain conditions in boreal and tundra environments to aid in the success of troop operations in these highly diverse settings.

Bibliography

Åkerman, H. J., and M. Johansson. 2008. "Thawing Permafrost and Thicker Active Layers in Sub-arctic Sweden." *Permafrost and Periglacial Processes* 19 (3): 279–292. http://dx.doi.org/10.1002/ppp.626.

Alam, S., A. Banjara, J. Wang, W. B. Patterson, and S. Baral. 2018. "Novel Approach in Sampling and Tensile Strength Evaluation of Roots to Enhance Soil for Preventing Erosion." *Open Journal of Soil Science* 8 (12): 330. https://doi.org/10.4236/ojss.2018.812024.

Alaska Climate Research Center. n.d. The Alaska State Climate Center Database. Accessed May 2023. https://akclimate.org/data/.

Alaska.gov. n.d. "Creamer's Field—Migratory Waterfowl Refuge." Alaska Department of Fish and Game. Accessed February 3, 2023. https://www.adfg.alaska.gov/index.cfm?adfg=creamersfield.main.

Almeida, I. C. C., C. Ernesto, G. R. Schaefer, R. B. A. Fernandes, T. T. C. Pereira, Al. Nieuwendam, and A. B. Pereira. 2014. "Active Layer Thermal Regime at Different Vegetation Covers at Lions Rump, King George Island, Maritime Antarctica." *Geomorphology* 225: 36–46. https://doi.org/10.1016/j.geomorph.2014.03.048.

Anders, K., S. Marx, J. Boike, B. Herfort, E. J. Wilcox, M. Langer, P. Marsh, and B. Höfle. 2020. "Multitemporal Terrestrial Laser Scanning Point Clouds for Thaw Subsidence Observation at Arctic Permafrost Monitoring Sites." *Earth Surface Processes and Landforms* 45 (7): 1589–1600. https://doi.org/10.1016/j.geomorph.2014.03.048.

Anderson, J. E., T. A. Douglas, R. A. Barbato, Stephanie Saari, Jarrod D. Edwards, and Robert M. Jones. 2019. "Linking Vegetation Cover and Seasonal Thaw Depths in Interior Alaska Permafrost Terrains Using Remote Sensing." *Remote Sensing of Environment* 233: 111363. https://doi.org/10.1016/j.ecolind.2017.09.034.

Anderson, K. E., N. F. Glenn, L. P. Spaete, D. J. Shinneman, D. S. Pilliod, R. S. Arkle, S. K. McIlroy, and D. R. Derryberry. 2018. "Estimating Vegetation Biomass and Cover Across Large Plots in Shrub and Grass Dominated Drylands using Terrestrial Lidar And Machine Learning." *Ecological Indicators* 84:793–802. https://doi.org/10.1016/j.ecolind.2017.09.034.

Arcone, Steven A., and Allan J. Delaney. 1982. "Dielectric Properties of Thawed Active Layers Overlying Permafrost Using Radar at VHF." *Radio Science* 17 (03): 618–626. https://doi.org/10.1029/RS017i003p00618.

Arp, Christopher D., Benjamin M. Jones, Frank E. Urban, and Guido Grosse. 2011. "Hydrogeomorphic Processes of Thermokarst Lakes with Grounded-ice and Floating-ice Regimes on the Arctic Coastal Plain, Alaska." *Hydrological Processes* 25 (15): 2422–2438. https://doi.org/10.1002/hyp.8019.

Avian, M., A. Kellerer-Pirklbauer, and A. Bauer. 2008. "Remote Sensing Data for Monitoring Periglacial Processes in Permafrost Areas: Terrestrial Laser Scanning at the Rock Glacier Hinteres Langtalkar, Austria." In *Proceedings of the Ninth International Conference on Permafrost*, 77–82.

Baker, C. M., A. J. Barker, T. A. Douglas, S. J. Doherty, and R. A. Barbato. 2023 "Seasonal Variation in Near-Surface Seasonally Thawed Active Layer and Permafrost Soil Microbial Communities." *Environmental Research Letters* 18 (5): 1–14. https://doi.org/10.1088/1748-9326/acc542.

Bakian-Dogaheh, Kazem, Richard H. Chen, Mahta Moghaddam, and Alireza Tabatabaeenejad. 2019. "Experimental Investigation of the Coupled Hydraulic and Low-Frequency Dielectric Behavior of the Arctic Permafrost Active Layer Organic Soil." In *IGARSS 2019-2019 IEEE International Geoscience and Remote Sensing Symposium*, 7104–7107. https://doi.org/10.1109/IGARSS.2019.8897872.

Barbato, R. A., K. L. Foley, C. M. Reynolds. 2015. *Soil Temperature and Moisture Effects on Soil Respiration and Microbial Community Abundance*. ERDC-CRREL TR-15-6. Hanover, NH: ERDC-CRREL. http://hdl.handle.net/11681/5549.

Barbato, R. A., R. M. Jones, T. A. Douglas, S. J. Doherty, K. Messan, K. L. Foley, E. J. Perkins, A. K. Thurston, and N. Garcia-Reyero. 2022. "Not All Permafrost Microbiomes Are Created Equal: Influence of Permafrost Thaw on the Soil Microbiome in a Laboratory Incubation Study." *Soil Biology and Biochemistry*, 167. https://doi.org/10.1016/j.soilbio.2022.108605.

Barker, A. J., T. A. Douglas, A. D. Jacobson, J. W. McClelland, A. G. Ilgen, M. S. Khosh, G. O. Lehn, and T. P. Trainor. 2014. "Late Season Mobilization of Trace Metals in Two Small Alaskan Arctic Watersheds as a Proxy for Land-Scape Scale Permafrost Active Layer Dynamics." *Chemical Geology* 381:180–193. https://doi.org/10.1016/j.chemgeo.2014.05.012.

Barker, A. J., T. D. Sullivan, W. B. Baxter, R. A. Barbato, S. Gallaher, G. E. Patton, J. P. Smith, and T. A. Douglas. 2023. "Redox and Geophysical Controls Across a Small Alaskan Arctic Watershed." ACS Earth and Space Reviews, unpublished report.

Barnhart, Theodore B., and Benjamin T. Crosby. 2013. "Comparing Two Methods of Surface Change Detection on an Evolving Thermokarst Using High-Temporal-Frequency Terrestrial Laser Scanning, Selawik River, Alaska." *Remote Sensing* 5 (6): 2813–2837. https://doi.org/10.3390/rs5062813.

Bartsch, Annett, Marina Leibman, Tazio Strozzi, Artem Khomutov, Barbara Widhalm, Elena Babkina, Damir Mullanurov, Ksenia Ermokhina, Christine Kroisleitner, and Helena Bergstedt. 2019. "Seasonal Progression of Ground Displacement Identified with Satellite Radar Interferometry and the Impact of Unusually Warm Conditions on Permafrost at the Yamal Peninsula in 2016." *Remote Sensing,* 11 (16). https://doi.org/10.3390/rs11161865.

Bense, V. F.,. G. Ferguson, and H. Kooi. 2009. "Evolution of Shallow Groundwater Flow Systems in Areas of Degrading Permafrost." *Geophysical Research Letters* 36 (22): 1–6. https://dx.doi.org/10.1029/2009GL039225.

Berglund, Björn E., Lena Barnekow, Dan Hammarlund, Per Sandgren, and Ian F. Snowball. 1996. "Holocene Forest Dynamics and Climate Changes in the Abisko Area, Northern Sweden: the Sonesson Model of Vegetation History Reconsidered and Confirmed." *Ecological Bulletins* 45:15–30. http://www.jstor.org/stable/20113180.

Bockheim, J. G., and K. M. Hinkel. 2005 "Characteristics and Significance of the Transition Zone in Drained Thaw-Lake Basins of the Arctic Coastal Plain, Alaska." *Arctic*, 58 (4): 406–417. http://www.jstor.org/stable/20113180.

Boniface, K., J. J. Braun, J. L. McCreight, and F. G. Nievinski. 2015. "Comparison of Snow Data Assimilation System with GPS Reflectometry Snow Depth in the Western United States." *Hydrological Processes*, 29 (10): 2425–2437. https://doi.org/10.1002/hyp.10346.

Brown, D. R. N., M. T. Jorgenson, T. A. Douglas, V. E. Romanovsky, K. Kielland, C. Hiemstra, E. S. Euskirchen, and R. W. Ruess. 2015. "Interactive Effects of Wildfire and Climate on Permafrost Degradation in Alaskan Lowland Forests." *Journal of Geophysical Research: Biogeosciences*, 120 (8): 1619–1637. https://doi.org/10.1002/2015JG003033.

Brown, J., K. Muc Hinkel, and F. E. Nelson. 2000. "The Circumpolar Active Layer Monitoring (CALM) Program: Research Designs and Initial Results." *Polar Geography* 24 (3): 166–258. https://doi.org/10.1080/10889370009377698.

Callahan, Benjamin J., Paul J. McMurdie, and Susan P. Holmes. 2017. "Exact Sequence Variants Should Replace Operational Taxonomic Units in Marker-Gene Data Analysis." *The ISME Journal* 11 (12): 2639–2643. https://doi.org/10.1038/ismej.2017.119.

Cifuentes, Renato, Dimitry Van der Zande, Jamshid Farifteh, Christian Salas, and Pol Coppin. 2014. "Effects of Voxel Size and Sampling Setup on the Estimation of Forest Canopy Gap Fraction from Terrestrial Laser Scanning Data." *Agricultural and Forest Meteorology* 194: 230–240. https://doi.org/10.1016/j.agrformet.2014.04.013.

Deeb, Elias J., Richard R. Forster, and Douglas L. Kane. 2011. "Monitoring Snowpack Evolution Using Interferometric Synthetic Aperture Radar on the North Slope of Alaska, USA." *International Journal of Remote Sensing* 32 (14): 3985–4003. https://doi.org/10.1080/01431161003801351.

Doherty, Stacey Jarvis, Robyn A. Barbato, A. Stuart Grandy, W. Kelley Thomas, Sylvain Monteux, Ellen Dorrepaal, Margareta Johansson, and Jessica G. Ernakovich. 2020. "The Transition from Stochastic to Deterministic Bacterial Community Assembly During Permafrost Thaw Succession." *Frontiers in Microbiology*, 11. https://doi.org/10.3389/fmicb.2020.596589.

Douglas, Thomas A., D. Fortier, Y. L. Shur, M. Z. Kanevskiy, L. Guo, Y. Cai, and M. T. Bray. 2011 "Biogeochemical and Geocryological Characteristics of Wedge and Thermokarst-Cave Ice in the CRREL Permafrost Tunnel, Alaska." *Permafrost and Periglacial Processes* 22 (2): 120–128. https://doi.org/10.1002/ppp.709.

Douglas, T. A., C. A. Hiemstra, J. E. Anderson, R. A. Barbato, K. L. Bjella, E. J. Deeb, A. B. Gelvin et al. 2021. "Recent Degradation of Interior Alaska Permafrost Mapped with Ground Surveys, Geophysics, Deep Drilling, and Repeat Airborne Lidar." *The Cryosphere* 15 (8): 3555–3575. https://doi.org/10.5194/tc-15-3555-2021.

Douglas, T. A., C. A. Hiemstra, M. C. Jones, and J. R. Arnold. 2014. "Sources and Sinks of Carbon in Boreal Ecosystems of Interior Alaska: A Review." *Elementa: Science of the Anthropocene* 2(000032). https://doi.org/10.12952/journal.elementa.000032.

Douglas, T. A., M. Torre Jorgenson, D. R. N. Brown, S. W. Campbell, C. A. Hiemstra, S. P. Saari, K. Bjella, and A. K. Liljedahl. 2016. "Degrading Permafrost Mapped with Electrical Resistivity Tomography, Airborne Imagery and LiDAR, and Seasonal Thaw Measurements." *Geophysics* 81 (1): WA71–WA85. https://doi.org/10.1190/geo2015-0149.1.

Douglas, T. A., M. Torre Jorgenson, M. Z. Kanevskiy, V. E. Romanovsky, Y. Shur, and K. Yoshikawa. 2008. "Permafrost Dynamics at the Fairbanks Permafrost Experimental Station Near Fairbanks, Alaska." *Proceedings of the Ninth International Conference on Permafrost, University of Alaska, Fairbanks*, 373–378. https://citeseerx.ist.psu.edu/document?repid=rep1&type=pdf&doi=8fc4c128e86bee153729e158b3f60278baa0bc51.

Douglas, Thomas A., Merritt R. Turetsky, and Charles D. Koven. 2020. "Increased Rainfall Stimulates Permafrost Thaw Across a Variety of Interior Alaskan Boreal Ecosystems." *NPJ Climate and Atmospheric Science*, 3 (1): 28. https://doi.org/10.1038/s41612-020-0130-4.

Douglas, T. A., and C. Zhang. 2021. "Machine Learning Analyses of Remote Sensing Measurements Establish Strong Relationships Between Vegetation and Snow Depth in the Boreal Forest of Interior Alaska." *Environmental Research Letters* 16, (6): 065014. https://doi.org/10.1088/1748-9326/ac04d8.

Eitel, Jan U. H., Bernhard Höfle, Lee A. Vierling, Antonio Abellán, Gregory P. Asner, Jeffrey S. Deems, Craig L. Glennie et al. 2016. "Beyond 3-D: The New Spectrum of Lidar Applications for Earth and Ecological Sciences." *Remote Sensing of Environment* 186:372–392. https://doi.org/10.1016/j.rse.2016.08.018.

Environmental Data Center Team. 2023. Meteorological monitoring program at Toolik, Alaska. Toolik Field Station, Institute of Arctic Biology, University of Alaska Fairbanks, Fairbanks, AK 99775. https://toolik.alaska.edu/edc/monitoring/abiotic/met-data-query.php.

Ernakovich, J. G., R. A. Barbato, V. I. Rich, C. Schädel, R. E. Hewitt, S. J. Doherty, E. D. Whalen, et al. 2022. "Microbiome Assembly in Thawing Permafrost and Its Feedbacks to Climate." *Global Change Biology* 28 (17): 5007–5026. https://doi.org/10.1111/gcb.16231.

Essery, R., J. Pomeroy, J. Parviainen, and P. Storck. 2003. "Sublimation of Snow from Coniferous Forests in a Climate Model." *Journal of Climate* 16 (1): 1855–1864. https://doi.org/10.1175/1520-0442(2003)016%3C1855:SOSFCF%3E2.0.CO;2.

Fan, L., W. Powrie, J. Smethurst, P. M. Atkinson, and H. Einstein. 2014. "The Effect of Short Ground Vegetation on Terrestrial Laser Scans at a Local Scale." *ISPRS Journal of Photogrammetry and Remote Sensing* 95: 42–52. https://doi.org/10.1111/gcb.12041.

Fan, Z., A. D. McGuire, M. R. Turetsky, J. W. Harden, J. M. Waddington, and E. S. Kane. 2013. "The Response of soil Organic Carbon of a Rich Fen Peatland in Interior Alaska to Projected Climate Change." *Global Change Biology* 19 (2): 604–620. https://doi.org/10.1111/gcb.12041.

Fierer, N. 2017. "Embracing the Unknown: Disentangling the Complexities of the Soil Microbiome." *Nature Reviews Microbiology* 15 (10): 579–590. https://doi.org/10.1038/nrmicro.2017.87.

Finnish Meteorological Institute. n.d. "Temperature and Precipitation Statistics from 1961 Onwards." Finnish Meteorological Institute. Accessed February 7, 2023. https://en.ilmatieteenlaitos.fi/statistics-from-1961-onwards.

Fisher, J. P., C. Estop-Aragonés, A. Thierry, D. J. Charman, S. A. Wolfe, I. P. Hartley, J. B. Murton, M. Williams, and G. K. Phoenix. 2016. "The Influence of Vegetation and Soil Characteristics on Active-Layer Thickness of Permafrost Soils in Boreal Forest." *Global Change Biology* 22 (9): 3127–3140. https://doi.org/10.1111/gcb.13248.

Fox, J., and S. Weisberg. 2018. *An R Companion to Applied Regression*. 3rd ed. Thousand Oaks, CA: Sage Publications. https://us.sagepub.com/en-us/nam/an-r-companion-to-applied-regression/book246125.

Genet, M. A. Stokes, F. Salin, S. B. Mickovski, T. Fourcaud, J.-F. Dumail, and R. Van Beek. 2005. "The Influence of Cellulose Content on Tensile Strength in Tree Roots." *Plant and Soil* 278:1–9. https://doi.org/10.1007/s11104-005-8768-6.

Gittleman, J. L., and M. Kot. 1990. "Adaptation: Statistics and a Null Model for Estimating Phylogenetic Effects." *Systematic Zoology* 39:227–241. https://doi.org/10.2307/2992183.

Green, A. A., M. Berman, P. Switzer, and M. D. Craig. 1988. "A Transformation for Ordering Multispectral Data in Terms of Image Quality with Implications for Noise Removal." *IEEE Transactions on Geoscience and Remote Sensing* 26 (1): 65–74. https://doi.org/10.1109/36.3001.

Guglielmin, M., M. R. Worland, and N. Cannone. 2012. "Spatial and Temporal Variability of Ground Surface Temperature and Active Layer Thickness at the Margin of Maritime Antarctica, Signy Island." *Geomorphology* 155: 20–33. https://doi.org/10.1016/j.geomorph.2011.12.016.

Hall, M., E. Frank, G. Holmes, B. Pfahringer, P. Reutemann, and I. H. Witten. 2009. "The WEKA Data Mining Software: An Update." *ACM SIGKDD Explorations Newsletter* 11 (1): 10–18. https://doi.org/10.1145/1656274.1656278.

Hamilton, T. D., J. L. Craig, and P. V. Sellmann. 1988. "The Fox Permafrost Tunnel: A Late Quaternary Geologic Record in Central Alaska." *Geological Society of America Bulletin* 100 (6): 948–969. https://doi.org/10.1130/0016-7606(1988)100%3C0948:TFPTAL%3E2.3.CO;2.

Hedstrom, N. R., and J. W. Pomeroy. 1998. "Measurements and Modelling of Snow Interception in the Boreal Forest." *Hydrological Processes* 12 (10-11): 1611–1625. https://doi.org/10.1002/(SICI)1099-1085(199808/09)12:10/11%3C1611::AID-HYP684%3E3.0.CO;2-4.

Heijmans, M. M. P. D., W. J. Arp, and F. S. Chapin III. 2004. "Carbon Dioxide and Water Vapour Exchange from Understory Species in Boreal Forest." *Agricultural and Forest Meteorology* 123 (3-4): 135–147. https://doi.org/10.1016/j.agrformet.2003.12.006.

Hill, D. F., E. A. Burakowski, R. L. Crumley, J. Keon, J. M. Hu, A. A. Arendt, K. W. Jones, and G. J. Wolken. 2019. "Converting Snow Depth to Snow Water Equivalent Using Climatological Variables." *The Cryosphere* 13 (7): 1767–1784. https://doi.org/10.5194/tc-13-1767-2019.

Hinkel, K. M., and F. E. Nelson. 2003. "Spatial and Temporal Patterns of Active Layer Thickness at Circumpolar Active Layer Monitoring (CALM) Sites in Northern Alaska, 1995–2000." *Journal of Geophysical Research: Atmospheres* 108 (D2). https://doi.org/10.1029/2001JD000927.

Hinzman, L. D., and L. A. Viereck. 2006. "Climate and Permafrost Dynamics of the Alaskan Boreal Forest." In *Alaska's Changing Boreal Forest*, eds. F. S. Chapin III, M. W. Oswood, K. Van Cleve, L. A. Viereck, and D. L. Verbyla. New York, NY: Oxford University Press. https://doi.org/10.1093/oso/9780195154313.002.0002.

Hugelius, G., J. G. Bockheim, P. Camill, B. Elberling, G. Grosse, J. W. Harden, K. Johnson, et al. 2013. "A New Data Set for Estimating Organic Carbon Storage to 3 m Depth in Soils of the Northern Circumpolar Permafrost Region." *Earth System Science Data* 5 (2): 393–402. https://doi.org/10.5194/essd-5-393-2013.

Hugelius, G., J. Strauss, S. Zubrzycki, J. W. Harden, E. A. G. Schuur, C-L. Ping, L. Schirrmeister, et al. 2014. "Estimated Stocks of Circumpolar Permafrost Carbon with Quantified Uncertainty Ranges and Identified Data Gaps." *Biogeosciences* 11 (23): 6573–6593. https://doi.org/10.5194/bg-11-6573-2014.

Jan, A., and S. L. Painter. 2020. "Permafrost Thermal Conditions are Sensitive to Shifts in Snow Timing." *Environmental Research Letters* 15 (8): 084026. https://doi.org/10.1088/1748-9326/ab8ec4.

Jin, S., X. Qian, and H. Kutoglu. 2016. "Snow Depth Variations Estimated from GPS-Reflectometry: A Case Study in Alaska from L2P SNR Data." *Remote Sensing* 8 (1): 63. https://doi.org/10.3390/rs8010063.

Johansson, M., J. Åkerman, F. Keuper, T. R. Christensen, H. Lantuit, and T. V. Callaghan. 2011. "Past and Present Permafrost Temperatures in the Abisko Area: Redrilling of Boreholes." *Ambio* 40: 558–565. https://doi.org/10.1007/s13280-011-0163-3.

Jonas, T., C. Marty, and J. Magnusson. 2009. "Estimating the Snow Water Equivalent from Snow Depth Measurements in the Swiss Alps." *Journal of Hydrology* 378 (1-2)): 161–167. https://doi.org/10.1016/j.jhydrol.2009.09.021.

Jonasson, C., M. Sonesson, T. R. Christensen, and T. V. Callaghan. 2012. "Environmental Monitoring and Research in the Abisko Area—An Overview." *Ambio* 41: 178–186. https://doi.org/10.1016/j.jhydrol.2009.09.021.

Jones, B. M., J. M. Stoker, A. E. Gibbs, G. Grosse, V. E. Romanovsky, T. A. Douglas, N. E. M. Kinsman, and B. M. Richmond. 2013. "Quantifying Landscape Change in an Arctic Coastal Lowland Using Repeat Airborne LiDAR." *Environmental Research Letters* 8 (4): 045025. https://dx.doi.org/10.1088/1748-9326/8/4/045025.

Jorgenson, M. T., T. A. Douglas, A. K. Liljedahl, J. E. Roth, T. C. Cater, W. A. Davis, G. V. Frost, P. F. Miller, and C. H. Racine. 2020. "The Roles of Climate Extremes, Ecological Succession, and Hydrology in Repeated Permafrost Aggradation and Degradation in Fens on the Tanana Flats, Alaska." *Journal of Geophysical Research: Biogeosciences* 125 (12): e2020JG005824. http://dx.doi.org/10.1029/2020JG005824.

Jorgenson, M. T., C. H. Racine, J. C. Walters, and T. E. Osterkamp. 2001. "Permafrost Degradation and Ecological Changes Associated with a Warming Climate in central Alaska." *Climatic Change* 48 (4): 551–579. https://doi.org/10.1023/A:1005667424292.

Jorgenson, M. T., K. Yoshikawa, M. Kanevskiy, Y. Shur, V. Romanovsky, S. Marchenko, G. Grosse, J. Brown, and B. Jones. 2008. "Permafrost Characteristics of Alaska." In *Proceedings of the Ninth International Conference on Permafrost* vol. 3. Fairbanks, AK: University of Alaska. https://www.researchgate.net/profile/Sergey-Marchenko-3/publication/334524021_Permafrost_Characteristics_of_Alaska_Map/links/5d2f7672a6fdcc2462e86fae/Permafrost-Characteristics-of-Alaska-Map.pdf.

Kääb, A. 2008. "Remote Sensing of Permafrost-Related Problems and Hazards." *Permafrost and Periglacial Processes* 19 (2): 107–136. https://doi.org/10.1002/ppp.619.

Kanevskiy, M., D. Fortier, Y. Shur, M. Bray, and T. Jorgenson. 2008. "Detailed Cryostratigraphic Studies of Syngenetic Permafrost in the Winze of the CRREL Permafrost Tunnel, Fox, Alaska." In *Proceedings of the Ninth International Conference on Permafrost*, vol. 1. Fairbanks, AK: Institute of Northern Engineering University of Alaska. https://www.researchgate.net/profile/Mikhail-Kanevskiy/publication/270219066_Detailed_cryostratigraphic_studies_of_syngenetic_permafrost_in_the_winze_of_the_CRREL_permafrost_tunnel_Fox_Alaska/links/54a327410cf267bdb9042f7f/Detailed-cryostratigraphic-studies-of-syngenetic-permafrost-in-the-winze-of-the-CRREL-permafrost-tunnel-Fox-Alaska.pdf.

Kejonen, A. I. M. O. 1997. "Permafrost and Patterned Ground in Finland-Periglacial or Something Else." *Bulletin-Geological Society Of Finland* 69: 97–108. https://pdfs.semanticscholar.org/b5b9/374f64dffaef86ac6fc424301c53a26ea759.pdf.

Kociuba, W., W. Kubisz, and P. Zagórski. 2014. "Use of Terrestrial Laser Scanning (TLS) for Monitoring and Modelling of Geomorphic Processes and Phenomena at a Small and Medium Spatial Scale in Polar Environment (Scott River—Spitsbergen)." *Geomorphology* 212: 84–96. https://doi.org/10.1016/j.geomorph.2013.02.003.

Kohler, J. O. Brandt, M. Johansson, and T. Callaghan. 2006. "A Long-Term Arctic Snow Depth Record from Abisko, Northern Sweden, 1913–2004." *Polar Research* 25 (2): 91–113. https://doi.org/10.3402/polar.v25i2.6240.

Kokelj, S. V., and M. T. Jorgenson. 2013. "Advances in Thermokarst Research." *Permafrost and Periglacial Processes* 24 (2): 108–119. https://doi.org/10.1002/ppp.1779.

Köster, E., K. Köster, M. Aurela, T. Laurila, F. Berninger, A. Lohila, and J. Pumpanen. 2013. "Impact of Reindeer Herding on Vegetation Biomass and Soil Carbon Content: A Case Study from Sodankylä, Finland." *Boreal Environment Research* 18 (6). https://go.gale.com/ps/i.do?id=GALE%7CA356354219&sid=googleScholar&v=2.1&it=r&linkaccess=abs&issn=12396095&p=AONE&sw=w&userGroupName=anon%7Eb2e23ec6&aty=open+web+entry.

Lader, R., J. E. Walsh, U. S. Bhatt, and P. A. Bieniek. 2020. "Anticipated Changes to the Snow Season in Alaska: Elevation Dependency, Timing and Extremes." *International Journal of Climatology* 40 (1): 169–187. https://doi.org/10.1002/joc.6201.

Larson, K. M. 2016. "GPS Interferometric Reflectometry: Applications to Surface Soil Moisture, Snow Depth, and Vegetation Water Content in the Western United States." *Wiley Interdisciplinary Reviews: Water* 3 (6): 775–787. https://doi.org/10.1002/wat2.1167.

Li, H., F. Santos, K. Butler, and E. Herndon. 2021. "A Critical Review on the Multiple Roles of Manganese in Stabilizing and Destabilizing Soil Organic Matter." *Environmental Science & Technology* 55 (18): 12136–12152. https://doi.org/10.1021/acs.est.1c00299.

Liston, G. E.,. and C. A. Hiemstra. 2011. "The Changing Cryosphere: Pan-Arctic Snow Trends (1979–2009)." *Journal of Climate* 24 (21): 5691–5712. https://doi.org/10.1175/JCLI-D-11-00081.1.

Littell, J. S., S. A. McAfee, and G. D. Hayward. 2108. "Alaska Snowpack Response to Climate Change: Statewide Snowfall Equivalent and Snowpack Water Scenarios." *Water* 10 (5): 668. https://www.mdpi.com/2073-4441/10/5/668#.

Liu, Y., C. D. Peters-Lidard, S. Kumar, J. L. Foster, M. Shaw, Y. Tian, and G.M. Fall. 2013. "Assimilating Satellite-Based Snow Depth and Snow Cover Products for Improving Snow Predictions in Alaska." *Advances in Water Resources* 54: 208–227. https://doi.org/10.1016/j.advwatres.2013.02.005.

Loke, M. Heng, and R. D. Barker. 1996. "Rapid Least-Squares Inversion of Apparent Resistivity Pseudosections by a Quasi-Newton Method." *Geophysical Prospecting* 44 (1): 131–152. https://doi.org/10.1111/j.1365-2478.1996.tb00142.x.

Loranty, M. M., B. W. Abbott, D. Blok, T. A. Douglas, H. E. Epstein, B. C. Forbes, B. M. Jones, et al. 2018. "Reviews and Syntheses: Changing Ecosystem Influences on Soil Thermal Regimes in Northern High-Latitude Permafrost Regions." *Biogeosciences* 15 (17): 5287–5313. https://doi.org/10.5194/bg-15-5287-2018.

Luo, D., Q. Wu, H. Jin, S. S. Marchenko, L. Lü, and S. Gao. 2016. "Recent Changes in the Active Layer Thickness Across the Northern Hemisphere." *Environmental Earth Sciences* 75: 1–15. https://doi.org/10.1007/s12665-015-5229-2.

Mackay, J. R. 1983. "Downward Water Movement Into Frozen Ground, Western Arctic Coast, Canada." *Canadian Journal of Earth Sciences* 20 (1): 120–134. https://doi.org/10.1139/e83-012.

Marx, S., K. Anders, S. Antonova, I. Beck, J. Boike, P. Marsh, M. Langer, and B. Höfle. 2017. "Terrestrial Laser Scanning for Quantifying Small-Scale Vertical Movements of the Ground Surface in Artic Permafrost Regions." *Earth Surface Dynamics Discussions* 1–31. https://doi.org/10.5194/esurf-2017-49.

McAfee, S. A., J. Walsh, and T. S. Rupp. 2104. "Statistically Downscaled Projections of Snow/Rain Partitioning for Alaska." *Hydrological Processes* 28 (12): 3930–3946. https://doi.org/10.1002/hyp.9934.

McNamara, J. P., D. L. Kane, and L. D. Hinzman. 1997. "Hydrograph Separations in an Arctic Watershed Using Mixing Model and Graphical Techniques." *Water Resources Research* 33 (7): 1707–1719. https://doi.org/10.1029/97WR01033.

Messan, K. S., R. M. Jones, S. J. Doherty, K. Foley, T. A. Douglas, and R. A. Barbato. 2020. "The Role of Changing Temperature in Microbial Metabolic Processes During Permafrost Thaw." *PloS One* 15 (4): e0232169. https://doi.org/10.1371/journal.pone.0232169.

Moyano, F. E., S. Manzoni, and C. Chenu. 2013. "Responses of Soil Heterotrophic Respiration to Moisture Availability: An Exploration of Processes and Models." *Soil Biology and Biochemistry* 59: 72–85. https://doi.org/10.1016/j.soilbio.2013.01.002.

Neal, A. 2004. "Ground-Penetrating Radar and its use in Sedimentology: Principles, Problems and Progress" *Earth-Science Reviews* 66 (3-4): 261–330. https://doi.org/10.1016/j.earscirev.2004.01.004.

Nelson, F. E., S. I. Outcalt, J. Brown, N. I. Shiklomanov, and K. M. Hinkel. 1998. "Spatial and Temporal Attributes of the Active Layer Thickness Record, Barrow, Alaska, USA." In *Proceedings of the Seventh International Conference on Permafrost*. Yellowknife: NWT. https://www.arlis.org/docs/vol1/ICOP/40770716/CD-ROM/Proceedings/PDF001189/122280.pdf.

Nelson, F. E., N. I. Shiklomanov, G. R. Mueller, K. M. Hinkel, D. A. Walker, and J. G. Bockheim. 1997. "Estimating Active-Layer Thickness Over a Large Region: Kuparuk River basin, Alaska, USA." *Arctic and Alpine Research* 29 (4): 367–378. https://doi.org/10.1080/00040851.1997.12003258.

Osterkamp, T. E., L. Viereck, Y. Shur, M. T. Jorgenson, Charles Racine, A. Doyle, and R. D. Boone. 2000. "Observations of Thermokarst and its Impact on Boreal Forests in Alaska, USA." *Arctic, Antarctic, and Alpine Research* 32 (3): 303–315. https://doi.org/10.1080/15230430.2000.12003368.

Parsekian, A. D., R. H. Chen, R. J. Michaelides, T. D. Sullivan, L. K. Clayton, L. Huang, Y. Zhao, et al. 2021. "Validation of Permafrost Active Layer Estimates from Airborne SAR Observations." *Remote Sensing* 13 (15): 2876. https://www.mdpi.com/2072-4292/13/15/2876#.

Péwé, T. L. 1975. *Quaternary Stratigraphic Nomenclature in Unglaciated Central Alaska*. No. 862. Reston, VA: USGS. https://doi.org/10.3133/pp862.

Philipp, M., A. Dietz, S. Buchelt, and C. Kuenzer. 2021. "Trends in Satellite Earth Observation for Permafrost Related Analyses—A Review." *Remote Sensing* 13 (6): 1217. https://www.mdpi.com/2072-4292/13/6/1217#.

Ping, C. L., J. D. Jastrow, M. T. Jorgenson, G. J. Michaelson, Y. L. Shur. 2015. "Permafrost Soils and Carbon Cycling." *Soil* 1: 147–171. https://doi.org/10.5194/soil-1-147-2015.

Ping, C.-L., J. G. Bockheim, J. M. Kimble, G. J. Michaelson, and D. A. Walker. 1998. "Characteristics of Cryogenic Soils Along a Latitudinal Transect in Arctic Alaska." *Journal of Geophysical Research: Atmospheres* 103 (D22): 28917–28928. https://doi.org/10.1029/98JD02024.

Pomeroy, J., X. Fang, and C. Ellis. 2012. "Sensitivity of Snowmelt Hydrology in Marmot Creek, Alberta, to Forest Cover Disturbance." *Hydrological Processes* 26 (12): 1891–1904. https://doi.org/10.1002/hyp.9248.

Pugh, E. T., and E. E. Small. 2013. "The Impact of Beetle-Induced Conifer Death on Stand-Scale Canopy Snow Interception." *Hydrology Research* 44 (4): 644–657. https://doi.org/10.2166/nh.2013.097.

QGIS.org. 2023. "QGIS Geographic Information System." QGIS Association. http://www.qgis.org.

R Development Core Team. 2021. "R: A Language and Environment for Statistical Computing." R Foundation for Statistical Computing, Vienna, Austria. https://www.R-project.org/.

Rousset, F., and J.-B. Ferdy. 2014. "Testing Environmental and Genetic Effects in the Presence of Spatial Autocorrelation." *Ecography* 37: 781–790. https://doi.org/10.1111/ecog.00566.

Rowland, J. C., and E. T. Coon. 2015. "From Documentation to Prediction: Raising the Bar for Thermokarst Research." *Hydrogeology Journal* 24: 645–648. https://doi.org/10.1007/s10040-015-1331-5.

Sandmeier, K. J. 2016. "ReflexW: 32 and 64 Bit." *Windows™ 7/8/10/11-program for the processing of seismic, acoustic or electromagnetic reflection, refraction and transmission data,* V. 8.1. https://www.sandmeier-geo.de/Download/reflexw_manual.pdf.

Schaefer, K., L. Liu, A. Parsekian, E. Jafarov, A. Chen, T. Zhang, A. Gusmeroli, Santosh Panda, Howard A. Zebker, and Tim Schaefer. 2015. "Remotely Sensed Active Layer Thickness (ReSALT) at Barrow, Alaska Using Interferometric Synthetic Aperture Radar." *Remote Sensing*, 7 (4): 3735–3759. https://www.mdpi.com/2072-4292/7/4/3735#.

Schuur, Edward A. G., A. David McGuire, Christina Schädel, Guido Grosse, Jennifer W. Harden, Daniel J. Hayes, Gustaf Hugelius et al. 2015. "Climate Change and the Permafrost Carbon Feedback." ,*Nature* 520 (7546): 171–179. https://doi.org/10.1038/nature14338.

Sellmann, P. V., J. Brown, R. I. Lewellen, H. L. McKim, and C. J. Merry. 1975. *The Classification and geomorphic implications of thaw lakes on the Arctic Coastal Plain, Alaska*. CRREL Research Report 344. Hanover, NH: CRREL-ERDC. http://hdl.handle.net/11681/5852.

Serreze, M. C., and R. G. Barry. 2011. "Processes and Impacts of Arctic Amplification: A Research Synthesis." *Global and Planetary Change* 77 (1-2): 85–96. https://doi.org/10.1016/j.gloplacha.2011.03.004.

Shiklomanov, N. I., D. A. Streletskiy, J. D. Little, and F. E. Nelson. 2013. "Isotropic Thaw Subsidence in Undisturbed Permafrost Landscapes." *Geophysical Research Letters* 40 (24): 63566361. https://doi.org/10.1002/2013GL058295.

Shiklomanov, N. I., D. A. Streletskiy, F. E. Nelson, R. D. Hollister, V. E. Romanovsky, C. E. Tweedie, J. G. Bockheim, and J. Brown. 2010. "Decadal Variations of Active-Layer Thickness in Moisture-Controlled Landscapes, Barrow, Alaska." *Journal of Geophysical Research: Biogeosciences*, 115. https://doi.org/10.1029/2009JG001248.

Shur, Y., K. M. Hinkel, and F. E. Nelson. 2005. "The Transient Layer: Implications for Geocryology and Climate-Change Science." *Permafrost and Periglacial Processes* 16 (1): 5–17. https://doi.org/10.1002/ppp.518.

Shur, Y. L., and M. T. Jorgenson. 2007. "Patterns of Permafrost Formation and Degradation in Relation to Climate and Ecosystems." *Permafrost and Periglacial Processes* 18 (1): 7–19. https://doi.org/10.1002/ppp.582.

Stein, M. L. 1999. *Interpolation of Spatial Data: Some Theory for Kriging*. New York, NY: Springer. https://doi.org/10.1007/978-1-4612-1494-6.

Stieglitz, M., S. J. Déry, V. E. Romanovsky, and T. E. Osterkamp. 2003. "The Role of Snow Cover in the Warming of Arctic Permafrost." *Geophysical Research Letters* 30(13). https://doi.org/10.1029/2003GL017337.

Stocker, T. F., D. Qin, G.-K. Plattner, M. Tignor, S. K. Allen, J. Boschung, A. Nauels, Y. Xia, V. Bex, and P. M. Midgley, eds. 2013. "Climate Change 2013: The Physical Science Basis. Contribution of Working Group I to the Fifth Assessment Report of the Intergovernmental Panel on Climate Change." Cambridge, United Kingdom: Cambridge University Press. https://www.ipcc.ch/report/ar5/wg1/.

Streletskiy, D. A., N. I. Shiklomanov, J. D. Little, F. E. Nelson, J. Brown, K. E. Nyland, and A. E. Klene. 2017. "Thaw Subsidence in Undisturbed Tundra Landscapes, Barrow, Alaska, 1962–2015." *Permafrost and Periglacial Processes* 28 (3): 566–572. https://doi.org/10.1002/ppp.1918.

Sturm, M., and J. Holmgren. 2018. "An automatic Snow Depth Probe for Field Validation Campaigns." *Water Resources Research* 54 (11): 9695–9701. https://doi.org/10.1029/2018WR023559.

Sturm, M., B. Taras, G. E. Liston, C. Derksen, T. Jonas, and J. Lea. 2010. "Estimating Snow Water Equivalent Using Snow Depth Data and Climate Classes." *Journal of Hydrometeorology* 11 (6): 1380–1394. https://doi.org/10.1175/2010JHM1202.1.

Tosi, M. 2007. "Root Tensile Strength Relationships and Their Slope Stability Implications of Three Shrub Species in the Northern Apennines (Italy)." *Geomorphology* 87 (4): 268–283. https://doi.org/10.1016/j.geomorph.2006.09.019.

Trimble. 2014. *eCognition Developer 9.0. 1 Reference Book*. Munich: Trimble Germany GmbH. https://www.scribd.com/document/332173213/Reference-Book#.

Turetsky, M. R., C. C. Treat, M. P. Waldrop, J. M. Waddington, Jennifer W. Harden, and A. David McGuire. 2008. "Short-Term Response of Methane Fluxes and Methanogen Activity to Water Table and Soil Warming Manipulations in an Alaskan Peatland." *Journal of Geophysical Research: Biogeosciences* 113 (G3). https://doi.org/10.1029/2007JG000496.

USDA. n.d. *Soil Survey Geographic Database (SSURGO)* Natural Resources Conservation Service: Web Soil Survey. Accessed December 2022. https://www.nrcs.usda.gov/resources/data-and-reports/soil-survey-geographic-database-ssurgo.

USDOI (US Department of the Interior). 2022. *BLM AK Administered Lands Dataset* (November 23, 2022). Bureau of Land Management Geospatial Business Platform. Accessed December 2022. https://gbp-blm-egis.hub.arcgis.com/datasets/blm-ak-administered-lands/explore.

Van Der Heijden, M. G. A., R. D. Bardgett, and N. M. Van Straalen. 2008. "The Unseen Majority: Soil Microbes as Drivers of Plant Diversity and Productivity in Terrestrial Ecosystems." *Ecology Letters* 11 (3): 296–310. https://doi.org/10.1111/j.1461-0248.2007.01139.x.

Van Rossum, G., and Drake, F. L. 2009. *Python 3 Reference Manual*. Scotts Valley, CA: CreateSpace. https://dl.acm.org/doi/book/10.5555/1593511.

Vishwakarma, K., N. Kumar, C. Shandilya, S. Mohapatra, S. Bhayana, and A. Varma. 2020. "Revisiting Plant-Microbe Interactions and Microbial Consortia Application for Enhancing Sustainable Agriculture: A Review." *Frontiers in Microbiology*, 11. https://doi.org/10.3389/fmicb.2020.560406.

Waldron, L. J. 1977. "The Shear Resistance of Root-Permeated Homogeneous and Stratified Soil." *Soil Science Society of America Journal* 41 (5): 843–849. https://doi.org/10.2136/sssaj1977.03615995004100050005x.

Wang, B., C. P. Hults, D. D. Eberl, L. G. Woodruff, W. F. Cannon, and L. P. Gough. 2019. *Soil Mineralogy and Geochemistry Along a North-South Transect in Alaska and the Relation to Source-Rock Terrane*. No. 1814-E. Reston, VA: USGS. https://doi.org/10.3133/pp1814E.

Wang, G., L. Liu, G. Liu, H. Hu, and T. Li. 2010. "Impacts of Grassland Vegetation Cover on the Active-Layer Thermal Regime, Northeast Qinghai-Tibet Plateau, China." *Permafrost and Periglacial Processes* 21 (4): 335–344. https://doi.org/10.1002/ppp.699.

Wang, J., Q. Yuan, H. Shen, T. Liu, T. Li, L. Yue, X. Shi, and L. Zhang. 2020. "Estimating Snow Depth by Combining Satellite Data and Ground-Based Observations Over Alaska: A Deep Learning Approach." *Journal of Hydrology*, 585. https://doi.org/10.1016/j.jhydrol.2020.124828.

Wang, C., Z. Zhang, H. Zhang, B. Zhang, Y. Tang, and Q. Wu. 2018. "Active Layer Thickness Retrieval of Qinghai–Tibet Permafrost Using the TerraSAR-X InSAR Technique." *IEEE Journal of Selected Topics in Applied Earth Observations and Remote Sensing* 11 (11): 4403–4413. https://doi.org/10.1109/JSTARS.2018.2873219.

Wendler, G., and M. Shulski. 2009. "A Century of Climate Change for Fairbanks, Alaska." *Arctic,* 295–300. https://www.jstor.org/stable/40513307.

Winski, D., E. Osterberg, D. Ferris, K. Kreutz, C. Wake, S. Campbell, R. Hawley, et al. 2017. "Industrial-Age Doubling of Snow Accumulation in the Alaska Range Linked to Tropical Ocean Warming." *Scientific Reports* 7 (1). https://doi.org/10.1038/s41598-017-18022-5.

WRCC (Western Regional Climate Center). n.d. WRCC Database, accessed May 2023. https://wrcc.dri.edu/.

Zhang, T., R. G. Barry, and W. Haeberli. 2001. "Numerical Simulations of the Influence of the Seasonal Snow Cover on the Occurrence of Permafrost at High Latitudes." *Norsk Geografisk Tidsskrift-Norwegian Journal of Geography* 55 (4): 261–266. https://doi.org/10.1080/00291950152746621.

Zhang, C., S. Denka, H. Cooper, and D. R. Mishra. 2018. "Quantification of Sawgrass Marsh Aboveground Biomass in the Coastal Everglades Using Object-Based Ensemble Analysis and Landsat Data." *Remote Sensing of Environment*, 204: 366–379. https://doi.org/10.1016/j.rse.2017.10.018.

Zhang, C., T. A. Douglas, and J. E. Anderson. 2021. "Modeling and Mapping Permafrost Active Layer Thickness Using Field Measurements and Remote Sensing Techniques." *International Journal of Applied Earth Observation and Geoinformation*, 102. https://doi.org/10.1016/j.jag.2021.102455.

Zhang, X., J. He, J. Zhang, I. Polyakov, R. Gerdes, J. Inoue, and P. Wu. 2013. "Enhanced Poleward Moisture Transport and Amplified Northern High-Latitude Wetting Trend." *Nature Climate Change* 3 (1): 47–51. https://doi.org/10.1038/nclimate1631.

Zwieback, S., and F. J. Meyer. 2021. "Top-of-Permafrost Ground Ice Indicated by Remotely Sensed Late-Season Subsidence." *The Cryosphere* 15 (4): 2041–2055. https://doi.org/10.5194/tc-15-2041-2021.

Abbreviations

AGOL	ArcGIS Online
ALS	Aerial laser scan
ALT	Active layer thickness
APEX	Alaska Peatland Experiment
ASV	Amplicon sequence variants
BTEX	Benzene toluene ethylbenzene xylenes
CALM	Circumpolar Active Layer Monitoring
CERL	Construction Engineering Research Laboratory
CRREL	Cold Regions Research and Engineering Laboratory
DEM	Digital elevation model
DRO	Diesel range organics
ERDC	US Army Engineer Research and Development Center
ERT	Electrical resistivity tomography
GIS	Geographic information systems
GPR	Ground-penetrating radar
GRO	Gasoline range organics
GWC	Gravimetric water content
HDS	High-Definition survey
ITS	Internal transcribed spacer
LRT	Likelihood Ratio Test
LTER	Long-Term Ecological Research
MLR	Multiple linear regression

NAVD88	North American Vertical Datum of 1988
OBIA	Object-Based Image Analysis
OPUS	Online Positioning User Service
qPCR	Quantitative polymerase chain reaction
RF	Random forest
RGB	Red green blue
RMAE	Registration mean absolute error
RRO	Residual range organics
RTK	Real-Time kinematic
SIPRE	Snow Ice and Permafrost Research Establishment
SOC	Soil organic carbon
SVM	Support vector machine
SWE	Snow water equivalent
TLS	Terrestrial laser scan
USDOI	US Department of the Interior
UTM	Universal Transverse Mercator
VOC	Volatile organic compounds
WHC	Water holding capacity
WRCC	Western Regional Climate Center

REPORT DOCUMENTATION PAGE

1. REPORT DATE	2. REPORT TYPE	3. DATES COVERED	
February 2024	Final	START DATE FY23	END DATE FY23

4. TITLE AND SUBTITLE

A Comprehensive Approach to Data Collection, Management, and Visualization for Terrain Characterization in Cold Regions

5a. CONTRACT NUMBER	5b. GRANT NUMBER	5c. PROGRAM ELEMENT
5d. PROJECT NUMBER	**5e. TASK NUMBER**	**5f. WORK UNIT NUMBER**

6. AUTHOR(S)

W. Brad Baxter, Amanda J. Barker, Samuel A. Beal, Lauren V. Bosche, Ryan R. Busby, Zoe R. Courville, Eli J. Deeb, Stacey J. Doherty, Thomas A. Douglas, Arthur B. Gelvin, Robert M. Jones, Taylor D. Sullivan, Dragos A. Vas, and Robyn A. Barbato

7. PERFORMING ORGANIZATION NAME(S) AND ADDRESS(ES)

US Army Engineer Research and Development Center (ERDC)
Cold Regions Research and Engineering Laboratory (CRREL)
72 Lyme Road
Hanover, NH 03755-1290

8. PERFORMING ORGANIZATION REPORT NUMBER

ERDC TR-24-4

9. SPONSORING/MONITORING AGENCY NAME(S) AND ADDRESS(ES)	10. SPONSOR/MONITOR'S ACRONYM(S)	11. SPONSOR/MONITOR'S REPORT NUMBER(S)
US Army Futures Command, the Assistant Secretary for the Army Acquisition, Logistics, and Technology Basic and Applied Research Programs,		

12. DISTRIBUTION/AVAILABILITY STATEMENT

Distribution Statement A. Approved for public release: distribution is unlimited.

13. SUPPLEMENTARY NOTES

MIPR 0642384626

14. ABSTRACT

As global focus shifts to northern latitudes for their enhanced access to newly viable resources, US Army operational readiness in these extreme environments is increasingly important. Rapid and accurate intelligence on the conditions influencing operations in these regions is essential to mission success and warfighter safety. Arctic and boreal environments are highly heterogeneous, including changing extents of frozen versus thawing ground, snow, and ice that affect ground trafficability and visibility, terrain physics, and physicochemical properties of water and soil. Further-more, projected climatic warming in these regions makes the timing of seasonal transitions increasingly uncertain. Broad coverage of long-term datasets is critical for assessing spatial and temporal variability in these northern environments at the landscape-scale. However, decadal measurements are difficult to acquire, manage, and visualize in the field set-ting. Here, we present a synopsis of data collection, management, and visualization for long-term permafrost, snow, vegetation, geophysics, and biogeochemical data from Alaska and review related literature. We also synthesize short-term data from various permafrost affected sites in the US and northern Europe to further assess the state of northern landscapes. Altogether, this work provides a comprehensive approach for high-latitude field site management to accurately inform mission-related operations in extreme northern environments.

15. SUBJECT TERMS

Arctic operations; Geophysics; Landscape monitoring; Long-Term datasets; Permafrost; Snow; Terrain characterization; Terrestrial LiDAR

16. SECURITY CLASSIFICATION OF:			17. LIMITATION OF ABSTRACT	18. NUMBER OF PAGES
a. REPORT	b. ABSTRACT	C. THIS PAGE		
Unclassified	Unclassified	Unclassified	SAR	92

19a. NAME OF RESPONSIBLE PERSON	19b. TELEPHONE NUMBER (include area code)
William B. Baxter	William.B.Baxter@usace.army.mil

7. PERFORMING ORGANIZATION NAME(S) AND ADDRESS(ES) (concluded)
US Army Engineer Research and Development Center (ERDC)
Construction Engineering Research Laboratory (CERL)
2902 Newmark Drive
Champaign, IL 61824